CALCULATION OF PHASE DIAGRAMS AND THE THERMODYNAMIC QUANTITIES FROM THE MEAN FIELD MODELS CLOSE TO PHASE TRANSITIONS IN MOLECULAR AND LIQUID CRYSTALS

A THESIS SUBMITTED TO
THE GRADUATE SCHOOL OF NATURAL AND APPLIED SCIENCE
OF
MIDDLE EAST TECHNICAL UNIVERSITY

BY

SEMA ŞEN

IN PARTIAL FULFILLMENT OF THE REQUIREMENTS

FOR

THE DEGREE OF DOCTOR OF PHILOSOPHY

IN

PHYSICS

FEBRUARY 2009

Approval of the thesis:

CALCULATION OF PHASE DIAGRAMS AND THE THERMODYNAMIC QUANTITIES FROM THE MEAN FIELD MODELS CLOSE TO PHASE TRANSITIONS IN MOLECULAR AND LIQUID CRYSTALS

submitted by **SEMA ŞEN** in partial fulfillment of the requirements for the degree of **Doctor of Philosophy in Physics Department, Middle East Technical University** by,

Prof. Dr. Canan Özgen _____
Dean, Graduate School of **Natural and Applied Sciences**

Prof. Dr. Sinan Bilikmen _____
Head of Department, **Physics**

Prof. Dr. Hamit Yurtseven _____
Supervisor, **Physics Dept., METU**

Examining Committee Members:

Prof. Dr. Tacettin Altanhan _____
Physics Dept., Ankara University

Prof. Dr. Hamit Yurtseven _____
Physics Dept., METU

Prof. Dr. Nizami Hasanli _____
Physics Dept., METU

Prof. Dr. Selahattin Özdemir _____
Physics Dept., METU

Assoc. Prof. Dr. Hatice Kökten _____
Physics Dept., METU

Date: _____

I hereby declare that all information in this document has been obtained and presented in accordance with academic rules and ethical conduct. I also declare that, as required by these rules and conduct, I have fully cited and referenced all material and results that are not original to this work.

Name, Last name: Sema Şen

Signature :

ABSTRACT

CALCULATION OF PHASE DIAGRAMS AND THE THERMODYNAMIC QUANTITIES FROM THE MEAN FIELD MODELS CLOSE TO PHASE TRANSITIONS IN MOLECULAR AND LIQUID CRYSTALS

Şen, Sema

Ph.D., Depatment of Physics

Supervisor : Prof. Dr. Hamit Yurtseven

February 2009, 121 pages

This study gives our calculations for the temperature-pressure and temperature-concentration phase diagrams using the mean field models applied to ammonium halides (NH_4Cl, ND_4Cl), ammonium sulfate ($(NH_4)_2SO_4/H_2O$), lithium potassium rubidium sulfate ($LiK_{1-x}Rb_xSO_4$), potassium pyrosulfate-potassium hydrogensulfate ($K_2S_2O_7$-$KHSO_4$), cholestanyl myristate-cholesteryl myristate (CnM-CrM), cholestanyl myristate-cholesteryl oleate (CnM-CO), benzene (C_6H_6) and ice. The phase line equations are derived from the free energies expanded in terms of the order parameters and they are fitted to the experimental data. Some thermodynamic quantities are calculated close to phase transitions in these crystalline systems.

We also calculate the specific heat C_V using the Raman frequency shifts for NH_4Br on the basis of an Ising model close to the λ-phase transition. A linear

relationship is obtained between the specific heat C_P and the frequency shifts $(1/\nu)(\partial\nu/\partial T)_P$ near the λ-point in NH_4Br.

Keywords**:** Phase Transition, Mean Field Models, Thermodynamic Quantities, Pippard Relation.

ÖZ

MOLEKÜLER VE SIVI KRİSTALLERDE ORTALAMA ALAN MODELLERİYLE FAZ DİYAGRAMLARININ VE TERMODİNAMİK NİCELİKLERİNİN HESAPLANMASI

Şen, Sema

Doktora, Fizik Bölümü

Tez Yöneticisi : Prof. Dr. Hamit Yurtseven

Şubat 2009, 121 sayfa

Bu çalışma amonyum bileşiklerine (NH_4Cl, ND_4Cl), amonyum sülfata ($(NH_4)_2SO_4/H_2O$), lityum potasyum rubidyum sülfat ($LiK_{1-x}Rb_xSO_4$), potasyum pirosülfat-potasyum hidrojensülfata ($K_2S_2O_7$-$KHSO_4$), kolestanil miristat-kolesteril miristata (CnM-CrM), kolestanil miristat-kolesteril oleata (CnM-CO), benzene (C_6H_6) ve buza uygulanan ortalama alan modellerini kullanarak sıcaklık-basınç ve sıcaklık-konsantrasyon faz diyagramlarının hesaplanmasını vermektedir. Faz eğrisi denklemleri, düzen parametrelerinde açılan serbest enerjilerden türetilmiş ve deneysel verilere uydurulmuştur. Bu kristal sistemlerde faz geçişleri yakınında bazı termodinamik nicelikler hesaplanmıştır.

Ayrıca λ-faz geçişi yakınında Ising model temelinde NH_4Br için Raman frekansı kaymaları kullanarak öz ısı C_V hesaplanmıştır. NH_4Br'de λ noktası

yakınında öz ısı C_P ile frekans kaymaları $(1/\nu)(\partial\nu/\partial T)_P$ arasında doğrusal bir bağıntı elde edilmiştir.

Anahtar Kelimeler: Faz Geçişleri, Ortalama Alan Modelleri, Termodinamik Nicelikler, Pippard Bağıntıları.

TO MY FAMILY

ACKNOWLEDGMENTS

I would like to express my deepest gratitude to my advisor Prof. Dr. Hamit Yurtseven. Without his excellent supervision, encouragement, invaluable comments and helps, friendly attitude, patience and continuous support I would never have been able to undertake and carry out this work.

Many great thanks are also due to my husband Şener, my daughter Hande İlknur, my mother, my father and all other members of my family for their continuous support and understanding.

TABLE OF CONTENTS

ABSTRACT iv

ÖZ vi

ACKNOWLEDGMENTS ix

TABLE OF CONTENTS x

LIST OF TABLES xii

LIST OF FIGURES xv

CHAPTER

1. INTRODUCTION 1
   - 1.1 Phase Transitions 1
   - 1.2 Properties of Ammonium Halides 2
     - 1.2.1 Ammonium Bromide 2
     - 1.2.2 Ammonium and Deutero-Ammonium Chloride 2
     - 1.2.3 Ammonium Sulphate 3
   - 1.3 Properties of Lithium Potassium Rubidium Sulfate 4
   - 1.4 Properties of Potassium Pyrosulfate-Potassium Hydrogensulfate (Potassium Bisulfate) 5
   - 1.5 Properties of Cholesteryl Myristate-Cholestanyl Myristate and Cholestanyl Myristate-Cholesteryl Oleate Binary Systems 6
   - 1.6 Properties of Benzene 6
   - 1.7 Properties of Ice 8
2. THEORY 9
   - 2.1 Classification of Phase Transition 9
   - 2.2 Pippard Relations 10
   - 2.3 Ising Model 11
   - 2.4 Mean Field Model 12

2.5 Ferroelectiricity ..……...…….. 13
3. CALCULATIONS AND RESULTS …….. 17
3.1 Lambda Phase Transition in Ammonium Bromide ……...……. 17
3.1.1 Critical Behaviour of the Specific Heat Calculated Using the Raman Frequencies of the Lattice and Internal Modes Near the Lambda-Phase Transition in Ammonium Bromide …….…... 17
3.1.2 Pippard Relations Applied to the Lambda Phase Transition in NH_4Br ……..…… 26
3.2 Calculation of the Phase Diagram Using the Mean Field Theory ….. 31
3.2.1 Ammonium and Deutero-Ammonium Chloride ……..... 32
3.2.2 Ammonium Sulphate ..……...……. 37
3.2.3 Lithium Potassium Rubidium Sulfate ...……..… 41
3.2.4 Potassium Pyrosulfate-Potassium Hydrogensulfate (Potassium Bisulfate) ……. 47
3.2.5 Cholestanyl Myristae (CnM)-Cholesteryl Myristate (CrM) and Cholestanyl Myristate (CnM)-Cholesteryl Oleate (CO) ……. 52
3.2.6 Benzene …...…… 66
3.2.7 Ice …...……. 76
3.3 Calculation of the Spontaneous Polarization and the Dielectric Constant Using a Mean Field Model Close to the Paraelectric-Ferroelectric Phase Transition in Ammonium Sulphate ……..... 95
4. DISCUSSION ……..… 106
5. CONCLUSIONS ……...… 111

REFERENCES ……..… 114

LIST OF TABLES

3.1 Values of the critical exponent α and the amplitude A for the Raman frequency shifts $\frac{1}{\nu}\left(\frac{\partial \nu}{\partial T}\right)_P$ of the frequency ν_7 (56 cm^{-1}) mode in NH_4Br (P=0) within the interval of the reduced temperature ε according to Eq. (3.4). ν_C indicates the critical frequency of this mode (T_C=234 K) ……...……. 19

3.2 Values of the critical exponent α and the amplitude A for the Raman frequency shifts $\frac{1}{\nu}\left(\frac{\partial \nu}{\partial T}\right)_P$ of the frequency ν_2 (1684 cm^{-1}) mode within the interval of the reduced temperature ε in NH_4Br (P=0, T_C=234 K) according to Eq. (3.4). Our values of C_0 and J^2A_1 below and above T_C are also given …….. 21

3.3 Values of the critical exponent α, the background specific heat C_0 and J^2A_1 due to the ν_7 (56 cm^{-1}) Raman mode (Table 3.1) below and above T_C,according to Eq. (2.7) in NH_4Br (P=0, T_C=233.8 K) ……...… 22

3.4 Values of the Raman frequency of ν_7(56 cm^{-1}) mode, ν_λ(at T_λ), its mode Grüneisen parameter γ_p [65], the order-disorder contribution to the frequency, Δ_p [66] and the volume V_λ (at T_λ) (Eq. 3.8). Values of the slope $(dP/dT)_\lambda$ and the intercept (Eq. 2.1) are also given here within the range of reduced temperature ε below and above T_λ in NH_4Br …….. 30

3.5 Values of the Raman frequency of ν_2(1684 cm^{-1}) mode, ν_λ(at T_λ), its mode Grüneisen parameter γ_p [65], the order-disorder contribution to the frequency, Δ_p [66] and the volume V_λ (at T_λ) (Eq. 3.8). Values of the slope $(dP/dT)_\lambda$ and the intercept (Eq. 2.1) are also given here within the range of reduced temperature ε below and above T_λ in NH_4Br …….. 31

3.6 Values of the parameters h_0, γ_1, γ_2 and γ_3 using the experimental data from the T-P phase diagrams of NH_4Cl and ND_4Cl [69] according to Eq. (3.26) 35

3.7 Values of the coefficients which we obtained, when the equations indicated were fitted to the experimental data [19] for the liquid-solid I (L-I), liquid-solid

II (L-II) and solid I-solid II (I-II) transitions in $(NH_4)_2SO_4/H_2O$. *w* denotes % weight of ammonium sulphate 39

3.8 Values of the coefficients *a*, b, and c according to Eq. (3.70) at the temperature T_t and concentration X_t (Rb) for the transitions indicated on the basis of the experimental (cooling and heating) T-X phase diagram of $LiK_{1-x}Rb_xSO_4$ [25] ……..…… 44

3.9 Values of the coefficients for the transitions according to equations indicated in $LiK_{1-x}Rb_xSO_4$ …….. 45

3.10 Values of the measured temperature T_t and concentration X_t (Rb) on cooling and heating for the transitions indicated, as given in the experimental T-X phase diagram of $LiK_{1-x}Rb_xSO_4$ [25] ……..… 45

3.11 Values of the fitted parameters α_1 and α_2 for the transitions indicated here for the $K_2S_2O_7$-$KHSO_4$ solvent system according to Eq. (3.103) …… 51

3.12 Values of the parameters a, b and c according to Eq. (3.175) for the phase transitions indicated of a binary mixture of cholestanyl myristate (CnM) – cholesteryl myristate (CrM) ……..... 64

3.13 Values of the parameters a, b and c according to Eq. (3.175) for the phase transitions indicated for a binary mixture of cholestanyl myristate (CnM)-cholesteryl oleate (CO) ……... 65

3.14 Values of the parameters a, b and c according to Eq. (3.175) for the phase transitions indicated of a binary mixture for cholestanyl myristate (CnM)-cholesteryl oleate (CO) ……... 66

3.15 Values of the coefficients *a*, b and c determined from fitting Eq.(3.221) to the experimental data [48] and, the values of α_1 and α_2 obtained from Eq. (3.220) with the coordinates of the triple point (T_t, P_t) for the phase transitions indicated of benzene ……... 75

3.16 The functions f_i (T,P), *g* (T,P) and g_{Li} (T,P) with the temperature and pressure ranges, which are defined in the equations indicated (third column) for i=1 to 7

for the liquid-solid phases (first column) of ice. Values of the parameters obtained from the equations (fifth column) fitted to the experimental data [77], are also given here …….. 79

3.17 The function g (T,P) and the values of the parameters obtained from the equations fitted (third column) to the experimental data [77] for the solid-solid transitions (first column) of ice ……... 80

3.18 The functions f_i (T,P) defined in equations indicated (second column), F_i for i=1 to 8 with the temperature and pressure ranges, g (T,P) and the phase line equations for the solid-solid transitions (first column) of ice ……. 81

3.19 Values of the parameters calculated according to Eq.(3.302) within the temperature interval given for the frequencies indicated in the ferroelectric phase ($T<T_c$) of $(NH_4)SO_4$. The figure numbers are also given here to indicate the parameters used for each frequency …….. 99

3.20 Values of the parameters calculated according to Eq.(3.301) within the temperature interval given for the frequencies indicated in the paraelectric phase ($T>T_c$) of $(NH_4)SO_4$. The figure numbers are also given here to indicate the parameters used for each frequency ……... 100

LIST OF FIGURES

2.1 Spontaneous polarization versus temperature, for a scond-order phase transition …….. 14

2.2 The hysteresis loop …...…… 16

3.1 $ln(\nu/\nu_C)$ as a function of the reduced temperature $\varepsilon=|T-T_C|/T_C$ in a log-log scale for the ν_7 (56 cm^{-1}) Raman mode of NH_4Br (P=0, T_C=234 K) according to Eq. (3.4). ν_C denotes the critical frequency. The observed frequencies are shown by squares [54] ..…….. 19

3.2 $ln(\nu/\nu_C)$ as a function of the reduced temperature $\varepsilon=|T-T_C|/T_C$ in a log-log scale for the ν_2 (1684 cm^{-1}) Raman mode of NH_4Br (P=0, T_C=234 K) below T_C according to Eq. (3.4). ν_C denotes the critical frequency. The observed frequencies are shown by squares [54] ……...… 20

3.3 $ln(\nu/\nu_C)$ as a function of the reduced temperature $\varepsilon=|T-T_C|/T_C$ in a log-log scale for the ν_2 (1684 cm^{-1}) Raman mode of NH_4Br (P=0, T_C=234 K) above T_C according to Eq. (3.4). ν_C denotes the critical frequency. The observed frequencies are shown by squares [54] ……...… 21

3.4 Specific heat C_{VI} calculated as a function of temperature for the first order phase transition (P=0, T_C=234 K) using the frequencies of the ν_7 (56 cm^{-1}) Raman mode in NH_4Br. Observed C_P data [3] is also shown here …..……... 23

3.5 Specific heat C_{VI} calculated as a function of temperature for the first order phase transition (P=0, T_C=234 K) using the frequencies of the ν_2 (1684 cm^{-1}) Raman mode in NH_4Br. Observed C_P data [3] is also shown here …..…...… 24

3.6 The specific heat C_p as a function of the frequency shift $\frac{1}{\nu}\left(\frac{\partial\nu}{\partial T}\right)_P$ for the lattice mode of ν_7(56 cm^{-1}) Raman mode of NH_4Br close to the λ-phase transition

below T_λ (P=0, T_λ=234 K) according to Eq.(2.1). The specific heat C_p data is taken from Ref. [65] 27

3.7 The specific heat C_p as a function of the frequency shift $\frac{1}{\nu}\left(\frac{\partial \nu}{\partial T}\right)_P$ for the lattice mode of ν_7(56 cm^{-1}) Raman mode of NH_4Br close to the λ-phase transition above T_λ (P=0, T_λ=234 K) according to Eq.(2.1). The specific heat C_p data is taken from Ref. [65] 28

3.8 The specific heat C_p as a function of the frequency shift $\frac{1}{\nu}\left(\frac{\partial \nu}{\partial T}\right)_P$ for the internal mode of ν_2(1684 cm^{-1}) Raman mode of NH_4Br close to the λ-phase transition below T_λ (P=0, T_λ=234 K) according to Eq.(2.1). The specific heat C_p data is taken from Ref. [65] 29

3.9 The specific heat C_p as a function of the frequency shift $\frac{1}{\nu}\left(\frac{\partial \nu}{\partial T}\right)_P$ for the internal mode of ν_2 (1684 cm^{-1}) Raman mode of NH_4Br close to the λ-phase transition above T_λ (P=0, T_λ=234 K) according to Eq.(2.1). The specific heat C_p data is taken from Ref. [65] 30

3.10 Phase diagram of NH_4Cl for solid II-solid III transition to 40 kbar. Solid line represents our calculated phase line. The experimental data [69] is also shown here 36

3.11 Phase diagram of ND_4Cl for solid II-solid III transition to 40 kbar. Solid line represents our calculated phase line. The experimental data [69] is also shown here 36

3.12 Our calculated phase diagram of $(NH_4)_2SO_4/H_2O$. Calculated phase lines are represented by solid lines. Experimental data [19] is also shown here 38

3.13 T-X phase diagram calculated from our mean field model for the phases indicated for $LiK_{1-x}Rb_xSO_4$. Solid lines represent our calculated phase lines. Experimental data on heating and cooling is also shown here [25] 44

3.14 Phase diagram of the $K_2S_2O_7$-$KHSO_4$ system obtained from Conductance(■), DEA (♦), TA (▲) and NIR (●) measurements [35]. Our calculated phase lines using the mean field theory, are shown as solid lines 51

3.15 T-X(CrM) phase diagram of a binary mixture of cholestanyl myristate (CnM) – cholesteryl myristate (CrM). The experimental data points are taken from Ref. [74] …….. 62

3.16 T-X(CnM) phase diagram of a binary mixture of cholestanyl myristate (CnM)-cholesteryl oleate (CO). The experimental data points are taken from Ref. [74] …….. 63

3.17 T-X(CnM) phase diagram of a binary mixture of cholestanyl myristate (CnM)-cholesteryl oleate (CO). The experimental data points are taken from Ref. [74] …….. 63

3.18 T-P phase diagram calculated from the mean field theory for benzene. Solid lines represent our calculated phase lines. The experimental data points are also shown here for the observed T-P phase diagram of benzene [48]. T_1, T_2 and T_3 are the triple points, A denotes the decomposition point and the chemical transformation line is defined by the points A, B, C and D [48] …. 74

3.19 Our calculated phase diagram of ice. Both experimental [77] and theoretical phase lines are represented in the figure by solid and broken lines. Broken lines represent presumed phase boundaries which have not yet been fully investigated experimentally [77] ……. 78

3.20 Calculated specific heat C_p as a function of temperature for the liquid-solid I transition in ice according to Eq. (3.261). Solid curve represents the best fit to values given here ……. 86

3.21 Calculated order parameter ψ as a function of temperature for the liquid-solid I transition in ice according to Eq. (3.262). Solid curve represents the best fit to values given here ……. 87

3.22 Calculated inverse susceptibility χ_I^{-1} as a function of temperature for the liquid-solid I transition in ice according to Eq. (3.266). Straight line represents the best fit to the values given here ……..… 89

3.23 Calculated specific heat C_p as a function of temperature for the solid I-solid III transition in ice at 1.8 kbar according to Eq. (3.284). Solid curve represents the best fit to values given here …… 92

3.24 Calculated order parameter ψ as a function of temperature for the solid I-solid III transition in ice at 1.8 kbar according to Eq. (3.288). Solid curve represents the best fit to values given here ……... 94

3.25 Calculated inverse susceptibility χ_I^{-1} as a function of temperature for the solid I-solid III transition in ice at 1.8 kbar according to Eq. (3.266). Straight line represents the best fit to the values given here ……... 95

3.26 Inverse susceptibility $\chi^{-1}=1/(\epsilon\text{-}1)$, ϵ is the dielectric constant, calculated from Eq. (3.302) as a function of $T_c\text{-}T$ in the ferroelectric phase ($T<T_c$) of $(NH_4)_2SO_4$ at the frequency of 100 Hz. (■) represents the observed data [78] …….. 99

3.27 Inverse susceptibility $\chi^{-1}=1/(\epsilon\text{-}1)$, ϵ is the dielectric constant, calculated from Eq.(3.301) as a function of $T\text{-}T_c$ in the paraelectric phase ($T>T_c$) of $(NH_4)_2SO_4$ at the frequency of 100 Hz. (■) represents the observed data [78] ……..…….. 100

3.28 Inverse susceptibility $\chi^{-1}=1/(\epsilon\text{-}1)$, ϵ is the dielectric constant, calculated from Eq.(3.302) as a function of $T_c\text{-}T$ in the ferroelectric phase ($T<T_c$) of $(NH_4)_2SO_4$ at the frequency of 500 Hz. (■) represents the observed data [78] ..…….. 101

3.29 Inverse susceptibility $\chi^{-1}=1/(\epsilon\text{-}1)$, ϵ is the dielectric constant, calculated from Eq.(3.301) as a function of $T\text{-}T_c$ in the paraelectric phase ($T>T_c$) within the temperature interval indicated for $(NH_4)_2SO_4$ at the frequency of 500 Hz. (■) represents the observed data [78] ……..… 102

3.30 Inverse susceptibility $\chi^{-1}=1/(\epsilon\text{-}1)$, ϵ is the dielectric constant, calculated from Eq.(3.301) as a function of $T\text{-}T_c$ in the paraelectric phase ($T>T_c$) within the temperature interval indicated for $(NH_4)_2SO_4$ at the frequency of 500 Hz. (■) represents the observed data [78] ……..… 102

3.31 Inverse susceptibility $\chi^{-1}=1/(\epsilon-1)$, ϵ is the dielectric constant, calculated from Eq. (3.302) as a function of T_c-T in the ferroelectric phase ($T<T_c$) within the temperature interval indicated for $(NH_4)_2SO_4$ at the frequency of 2000 Hz. (■) represents the observed data [78] …….. 103

3.32 Inverse susceptibility $\chi^{-1}=1/(\epsilon-1)$, ϵ is the dielectric constant, calculated from Eq. (3.301) as a function of T-T_c in the paraelectric phase ($T>T_c$) within the temperature interval indicated for $(NH_4)_2SO_4$ at the frequency of 2000 Hz. (■) represents the observed data [78] …….. 103

3.33 Polarization calculated from Eq. (3.303) as a function of T_c-T for $(NH_4)_2SO_4$ at the frequency of 100 Hz. (■) represents our calculated values of the polarization at various temperatures and the solid line is the best fit (Eq. 3.303) …… 104

3.34 Polarization calculated from Eq. (3.303) as a function of T_c-T for $(NH_4)_2SO_4$ at the frequency of 500 Hz. (■) represents our calculated values of the polarization at various temperatures and the solid line is the best fit (Eq. 3.303) …… 105

3.35 Polarization calculated from Eq. (3.303) as a function of T_c-T for $(NH_4)_2SO_4$ at the frequency of 2000 Hz. (■) represents our calculated values of the polarization at various temperatures and the solid line is the best fit (Eq. 3.303) …… 105

CHAPTER 1

INTRODUCTION

1.1 Phase Transitions

There are four states of material which are gas, solid, liquid and plasma. A distinct and homogeneous state of a system is known as a phase.

Basically, phase transition is the change from one state to another because of small changes in temperature and pressure. Due to a phase transition, there is no change in the chemical composition of the material. The only change occurs in physical properties, for example the heat capacity.

There are two classifications of phase transitions, Ehrenfest classification and modern classification. Ehrenfest classification labelled the phase transitions by the lowest derivative of the free energy. The free energy is discontinuous at the transition. First-order phase transition exhibit a discontinuity in the first derivative of the free energy with respect to the thermodynamic variable such as volume and entropy whereas second-order phase transitions have a discontinuity in a second derivative of the free energy such as specific heat, thermal expansivity. Under the Ehrenfest classification scheme, there could in principle be third, fourth, and higher-order phase transitions. The Ehrenfest scheme is an inaccurate method of classifying phase transitions, for it does not take into account the case where a derivative of the free energy diverges.

In the modern classification scheme, phase transitions are divided into two broad categories, named similarly to the Ehrenfest classes: The first-order phase transitions are those that involve a latent heat. During such a transition, a system either absorbs or releases a fixed amount of energy. During this process, the

temperature of the system remains constant as the heat is added. The second class of phase transitions is the continuous phase transitions, also called second-order phase transitions. These have no associated latent heat [1].

1.2 Properties of Ammonium Halides

1.2.1 Ammonium Bromide

Ammonium bromide, NH_4Br, is a substance used in manufacturing photographic chemicals and emulsion. It is also used as a flame retardant. Ammonium bromide can be prepared by the direct action of hydrogen bromide on ammonia. The chemical crystallizes in colourless prisms, possessing a saline taste; it sublimes on heating and is easily soluble in water. On exposure to air it gradually assumes a yellow colour and becomes acid in its reaction [2].

NH_4Br undergoes a λ-type phase transition at T= 234 K (P= 0). Its λ-phase transition occurs from the disordered β phase to the antiferro-ordered γ phase, as the temperature decreases. β phase has the CsCl type structure with the O_h^1 symmetry, whereas the γ phase has a tetragonal structure with the D_{4h} symmetry. If the temperature is lowered down to about 78 K, the antiferro-ordered γ phase is transformed into the ferro-ordered δ phase in NH_4Br [3].

In the disordered β phase the NH_4^+ ions have two orientations like up and down orientations of a spin system, which are energetically equal in an Ising system. In this phase the NH_4^+ ions are randomly orientated [4], whereas in the antiferro-ordered γ phase they are orientated in the opposite direction in $a-b$ plane, but they are all parallel along the c axis. The NH_4^+ ions become all parallel to each other in the ferro-ordered δ phase at low temperatures in NH_4Br.

1.2.2 Ammonium and Deutero-Ammonium Chloride

Ammonium chloride (NH_4Cl) is, in its pure form, a clear white water-soluble crystalline salt of ammonia. The aqueous ammonium chloride solution is mildly acidic [5].

NH_4Cl undergoes λ-phase transition at 242.5 K at zero pressure. As the pressure increases up to ~1.6 kbar, the transition temperature between phases II (β phase) and III (γ phase) shifts to 256 K at which the tricritical phase transition occurs, as observed experimentally [6]. As the pressure increases further up to ~2.8 kbar, there occurs a second order phase transition at 268 K, as also observed experimentally [6]. However, the λ-phase transition in ND_4Cl takes place at ~250 K at atmospheric pressure, which is a multicritical point [7], as observed in NH_4Cl at ~1.6 kbar [6]. As the pressure increases up to ~1.5 kbar, a second order phase change becomes dominant in ND_4Cl [8], which occurs at ~2.8 kbar in NH_4Cl [6]. Compared to the second order phase transition in ND_4Cl at ~1.5 kbar, the first order phase transition at zero pressure in this crystal has minimal thermal hysteris [9, 10] which diminishes at 0.1 MPa to about 30 to 80 mK [7, 8, 11, 12].

Phase II (β phase) has the CsCl structure with the O_h^1-Pm3m symmetry. In this phase NH_4^+ ions are distributed randomly between two energetically equivalent orientations [4]. Phase III (δ phase) has the CsCl structure with the T_d^1-$P\bar{4}3m$ symmetry. In this phase all the NH_4^+ ions are parallel to each other.

1.2.3 Ammonium Sulphate

Ammonium sulfate, ($(NH_4)_2SO_4$), is an inorganic chemical compound commonly used as a fertilizer. It contains 21% nitrogen as ammonium ions and 24% sulfur as sulfate ions. Ammonium sulfate occurs naturally as the rare mineral mascagnite in volcanic fumaroles and due to coal fires on some dumps [13].

$(NH_4)_2SO_4$ exhibits a phase transition from the paraelectric orthorhombic phase with the space group D_{2h}^{16} to the ferroelectric orthorhombic phase with the space group C_{2v}^{9} [14, 15]. This ferroelectric phase involves ordering of two inequivalent $(NH_4)_I$ and $(NH_4)_{II}$ groups which are orientated antiparallel to one another. With these orientations of the tetrahedra, SO_4^{-2} is assigned as a pseudospin $\sigma = \pm 1$, which can then be considered in an Ising model [16].

The mechanism of an order-disorder type of phase transition in $(NH_4)_2SO_4$ has been explained theoretically by means of the reorientation of the dipoles of the

distorted NH_4^+ ions [17]. A soft mode model has also been suggested to explain the mechanism of the phase transition in $(NH_4)_2SO_4$ [18].

As a binary mixture, the $(NH_4)_2SO_4/H_2O$ system's equilibrium and metastability phase diagrams from 40 ^{0}C to -50 ^{0}C have been obtained [19]. $(NH_4)_2SO_4.4H_2O$ melts at -19.35 ^{0}C. Below -19.35 ±0.05 ^{0}C, it undergoes a solid-solid (solid I-solid II) phase transition to form a tetrahydrate phase [19], as also pointed out in our recent study [20].

1.3 Properties of Lithium Potassium Rubidium Sulfate

$LiK_{1-x}Rb_xSO_4$ is one of the ferrielectric materials. At low temperatures, it is a ferroelastic crystal. Mixed $LiK_{1-x}Rb_xSO_4$ crystals exhibit successive phase transitions starting from phase II to phase V through phases III and IV, as the temperature is lowered. At very high temperatures, it undergoes the most symmetrical phase I, which has a hexagonal structure with the space group $P6_3/mmc$ (D_{6h}^4), and the $SO_4^=$ ions are randomly oriented (complete disorder) here [21]. Phase II occurs at temperatures down to about 700 K on heating and cooling, which has an orthorhombic structure with the space group Pnma (D_{2h}^{16}) [22, 23]. It has been argued that phase II can have an incommensurate structure in the temperature interval 940 to 743 K and a modulated superstructure in the temperature interval 743 to 711 K [21, 24], as also indicated previously [25]. Below 700 K, phase II undergoes a pyroelectric phase III [26], which extends down to room temperature. This phase has a hexagonal structure with the space group $P6_3$(C_6^6), as determined in earlier studies [27, 28]. As the temperature decreases further down to about 200 K, phase III transforms into phase IV, which occurs in a large temperature shift between the two phases (III and IV) on heating and cooling [25]. This is due to the fact that a first-order phase transition from phase III to phase IV is more pronounced here in comparison with the first-order transitions between II and III, and also between IV and V. Phase IV has a trigonal crystal structure with the space group P3/c (C_{3v}^4) [26, 29]. Below 190 K, phase IV disappears and phase V as a ferroelastic phase takes place, which has a monoclinic

structure with the space group $C_c(C_s^4)$ [30, 31]. As the temperature is lowered down to 20 K, it has been reported that a low-temperature phase VI occurs, on the basis of experimental measurements [32].

1.4 Properties of Potassium Pyrosulfate-Potassium Hydrogensulfate (Potassium bisulfate)

Potassium pyrosulfate (potassium disulfate) is a chemical compound, with the molecular formula $K_2S_2O_7$. From powder diffraction data, $K_2S_2O_7$ has a monoclinic structure with the space group *C*2/*c***.** In $K_2S_2O_7$, the neighbouring chains are antiparallel. It contains the pyrosulfate anion $S_2O_7^{2-}$ which has a dichromate like structure and can be visualised as two corner sharing SO_4 tetrahedra, with a bridging oxygen atom [33]. Potassium pyrosulfate is most commonly found as a preservative in consumer foods. As a food additive or preservative $K_2S_2O_7$ is also known as potassium metabisulphite. Potassium pyrosulfate is used in analytical chemistry; samples are fused with potassium pyrosulfate (or a mixture of potassium pyrosulfate and potassium fluoride, KF), to ensure complete dissolution prior to a quantitative analysis [34].

Potassium bisulfate is the potassium salt of bisulfate anion, with the molecular formula $KHSO_4$. This compound is commonly used in the conversion of tartrates to bitartrates in wine. Potassium bisulfate is also used as a disintegrating agent in analytical chemistry. A solution of potassium bisulfate behaves as if the two related compounds (K_2SO_4 and H_2SO_4) were side by side uncombined [34].

The phase diagram of the catalytically important $K_2S_2O_7$-$KHSO_4$ solvent system exhibits an eutectic at X_{KHSO_4} = 0.94 with a temperature of fusion of 205 $^{\circ}$C. No compound is formed in the system, but the strong α→β solid-solid transition of $K_2S_2O_7$, found at 318 ^{0}C with ΔH_{tr} = 21.8 kJ/mol, gives rise to a marked change in the slope of the liquidus curve at this temperature. ^{39}K, ^{1}H, ^{17}O, and ^{33}S NMR measurements on the molten $K_2S_2O_7$-$KHSO_4$ mixtures up to 540 $^{\circ}$C show that a fast ionic exchange takes place in the melt at all compositions. The conductivities

of the solid and molten $K_2S_2O_7$-$KHSO_4$ systems were measured at 13 different compositions in the whole composition range, X_{KHSO_4} = 0-1 [35].

1.5 Properties of Cholesteryl Myristate-Cholestanyl Myristate and Cholestanyl Myristate-Cholesteryl Oleate Binary Systems

Cholestany myristate (cholestanyl tetradecanoate) is bilayer and has the chemical formula of $C_{41}H_{74}O_2$, cholesteryl myristate is monoclinic, space group *A*2 and has the formula of $C_{41}H_{72}O_2$.

Cholesteryl Myristate-Cholestanyl Myristate Binary System: Cholesteryl myristate possesses stable smectic and cholesteric mesophases; that is, the mesophases are formed on heating the crystal as well as cooling the isotropic liquid. The crystal to smectic transition occurs at 72 ^{0}C, the smectic to cholesteric transition at 80 ^{0}C, and the cholesteric to isotropic transition at 85.5 ^{0}C. Cholestanyl myristate, on the other hand, melts directly to an isotropic liquid at 91 ^{0}C. The mesophases are metastable; the cholesteric mesophase is only formed when the isotropic liquid is undercooled, and crystallization takes place so rapidly that the smectic phase has an extremely short lifetime [36].

Cholestanyl Myristate-Cholesteryl Oleate ($C_{45}H_{78}O_2$) Binary System: Like cholestanyl myristate, cholesteryl oleate forms metastable mesophases, i.e., the mesophases are only formed by undercooling the isotropic liquid. The crystal to isotropic transition occurs at 51 ^{0}C, and the smectic to cholesteric and cholesteric to isotropic transitions occur at 42 and 47 ^{0}C, respectively [37, 38]. Unlike the mesophases of cholestanyl myristate, the mesophases of cholesteryl oleate can exist for several minutes below the crystal to isotropic transition temperature before crystallization occurs [36].

1.5 Properties of Benzene

Benzene is one of the most investigated molecular organic compounds with the formula C_6H_6. It is sometimes abbreviated Ph–H. Benzene is a colorless and highly flammable liquid with a sweet smell and a relatively high melting point. It is

carcinogenic and its use as an additive in gasoline is now limited, but it is an important industrial solvent and precursor in the production of drugs, plastics, synthetic rubber, and dyes. Benzene is a natural constituent of crude oil, but it is usually synthesized from other compounds present in petroleum. Benzene is an aromatic hydrocarbon and the second [*n*]-annulene ([6]-annulene), a cyclic hydrocarbon with a continuous pi bond [39].

Its crystalline forms have been studied extensively. It crystallizes into the solid phase I below the melting temperature (278.5 K) at atmospheric pressure [40]. It is orthorhombic Pbca (D_{24}^{15}) in this phase with four molecules per unit cell, as determined by X-ray [41, 42], neutron [43] techniques. When the solid I phase is heated up to 373 K at 1.2 GPa, solid II [44] phase occurs. This phase has the monoclinic structure. As the pressure increases up to 4 GPa at room temperature, solid phase II is transformed into the solid III [44, 45] phase, which has also the monoclinic structure. This phase is then transformed into another solid phase III' above 11 GPa [40]. This transition between the solid phases III and III' is of a second order, whereas the solid I-II and II-III transitions are of a first order. At higher pressures of about 24 GPa, it has been indicated by the X-ray diffraction pattern that there exists a new phase called IV [39]. It has been reported that III'-IV transition is an irreversible chemical transformation which has a first order in character, as also observed at 30 GPa by Pruzan et al. [46].

The melting curves for the solid phases I and II intersect the I-II equilibrium line at the triple point L-I-II (T_1) with the coordinates 12±0.5 kbar and 204±5 ^{0}C [45, 47]. Also, there exists a second triple point L-II-III (T_2) with the coordinates 22.5±0.5 kbar and 335±5 ^{0}C, as given in the phase diagram of benzene [45] (see also Fig. 1). At higher pressure and temperature, the existence of a third triple point (T_3) with the coordinates 5 GPa and 400^{0}C has been obtained experimentally [48]. Above 40 kbar and 580 ^{0}C, benzene disassociates, a phase called decomposed compounds, as indicated in the experimentally determined T-P phase diagram [48]. So, decomposition which is due to pressurization of hydrocarbons, contains amorphous carbon [49]. Also, this static pressurization is associated with an

opening of the benzene rings, which leads to a formation of polymer by highly cross-linked carbon chains [46].

1.7 Properties of Ice

Ice is a solid phase, usually crystalline, of a non-metallic substance that is liquid or gas at room temperature, such as ammonia ice or methane ice. However, the word "ice" normally means *water ice,* technically restricted to one of the 15 known crystalline phases of water. In non-scientific contexts, it usually describes ice I_h, which is known to be the most abundant of these phases. It can appear transparent or an opaque bluish-white color, depending on the presence of impurities such as air. The addition of other materials such as soil may further alter the appearance. The most common phase transition to ice I_h occurs when liquid water is cooled below 0 °C (273.15 K, 32 °F) at standard atmospheric pressure.

Ice appears in nature in forms as varied as snowflakes and hail, icicles, glaciers, pack ice, and entire polar ice caps. It is an important component of the global climate, particularly in regard to the water cycle. Furthermore, ice has numerous cultural applications, from the ice cooling one's drink to winter sports and ice sculpture.

As a naturally occurring crystalline solid, ice is considered a mineral consisting of hydrogen oxide. An unusual property of ice frozen at a pressure of one atmosphere is that the solid is some 8% less dense than liquid water. Ice is the only known non-metallic substance to expand when it freezes. Ice has a density of 0.9167 g/cm³ at 0 °C, where as water has a density of 0.9998 g/cm³ at the same temperature. Liquid water is densest, essentially 1.00 g/cm³, at 4 °C and becomes less dense as the water molecules begin to form the hexagonal crystals of ice as the temperature drops to 0 °C. This is due to hydrogen bonds forming between the water molecules, which line up molecules less efficiently (in terms of volume) when water is frozen. The result of this is that ice floats on liquid water, which is an important factor in Earth's climate. Density of ice increases slightly with decreasing temperature (density of ice at −180 °C (93 K) is 0.9340 g/cm³) [50].

CHAPTER 2

THEORY

2.1 Classification of Phase Transition

There are three distinct types of thermal behaviour occuring along lines separating different phases or modifications of a substance, the normal transition with latent heat, the λ-transition without latent heat but a very high (perhaps infinite) peak of specific heat, and the so-called second-order transition in which there is no latent heat and a finite discontinuity in specific heat. The first and last members of a classification introduced by Ehrenfest, in which the "order" of a transition is determined by the lowest order of differential coefficients of the Gibbs function which shows a discontinuity on the transition line. Thus in a phase transition which involves latent heat, g is continuous across the line, but its derivatives $(\partial g/\partial T)_P$ and $(\partial g/\partial P)_T$ are discontinuous; such a transition is said to be of the first order. In the transition of a superconductor in zero magnetic field there is no latent heat and no volume change, so that the first derivatives of g are continuous, but the second derivatives, representing specific heat, expansion coefficient and compressibility are discontinuous, so that this is a transition of the second order [51].

First-order transitions are solid-liquid-vapour transitions. Many allotropic transitions in solids are the examples of the first-order phase transition. Second-order transitions are superconducting transition in zero field. λ-transitions are order-disorder transformation in β-brass, ammonium salts, crystalline quartz, solid hydrogen and many other solids [51].

2.2 Pippard Relations

Pippard [51] has established his relations which relate the specific heat C_P to the thermal expansivity α_P and α_P to the isothermal compressibility κ_T linearly. The Pippard relations are important thermodynamically to correlate the thermodynamic quantities C_p, α_p and κ_T in the vicinitiy of the λ-transition line. This modified version of the Pippard relations which we have obtained, can also be important spectroscopically to correlate the spectroscopic parameters, in particular, the frequency shifts with those thermodynamic quantities considered in the vicinity of the λ-phase line. Thus, by measuring the frequency shifts $(1/\nu)\ (\partial\nu/\partial T)_p$ and $(1/\nu)\ (\partial\nu/\partial P)_T$ experimentally, the thermodynamic quantities, namely, C_p, α_p and κ_T can be predicted close to the λ-transition line by means of our modified Pippard relations. Since our relations contain the isobaric (γ_P)and isothermal (γ_T) mode Grüneisen parameters, the thermodynamic quantities C_p, α_p and κ_T can be predicted using the frequencies of the appropriate modes of a crystalline system close to the λ-phase transitions. Considering several modes of a crystalline system, when appropriate for its λ-phase transition, those thermodynamic quantities can then be predicted for each mode separately and all these predictions can be compared with the experimentally measured quantities. Thus, by means of the modified Pippard relations, calculated C_p, α_p and κ_T can be re-examined when compared with those measured experimentally close to the λ-transition line [52].

The spectroscopically modified Pippard relations [52] are as follows:

$$C_P = -\frac{TV}{\gamma_P}\left(\frac{dP}{dT}\right)_\lambda \frac{1}{\nu}\left(\frac{\partial \nu}{\partial T}\right)_P + T\left(\frac{dS}{dT}\right)_\lambda \tag{2.1}$$

and

$$\alpha_P = \frac{1}{\gamma_T}\left(\frac{dP}{dT}\right)_\lambda \frac{1}{\nu}\left(\frac{\partial \nu}{\partial P}\right)_T + \frac{1}{V}\left(\frac{dV}{dT}\right)_\lambda \tag{2.2}$$

In Eqs. (2.1) and (2.2) isobaric and isothermal mode Grüneisen parameters are defined as:

$$\gamma_P \equiv -\frac{1}{\alpha_P}\frac{1}{v}\left(\frac{\partial v}{\partial T}\right)_P \tag{2.3}$$

and

$$\gamma_T \equiv \frac{1}{\kappa_T}\frac{1}{v}\left(\frac{\partial v}{\partial P}\right)_T \tag{2.4}$$

respectively. α_P (Eq. 2.3) is the thermal expansivity and κ_T (Eq. 2.4) is the isothermal compressibility [52].

2.3 Ising Model

Ising model is the drosophila of the theory of phase transitions. It is remarkably simple to express:

Consider a lattice in *d* dimensions. At each lattice point, labelled by *i*, resides a classical spin σ_i which can take two values +1 or -1. The total energy of the system is given by the Ising Hamiltonian

$$H = -J\sum_{<i,j>}\sigma_i\sigma_j \tag{2.5}$$

where *J* is the interaction parameter

This model was introduced by Ising in 1925, while working with Lenz on his PhD thesis to understand ferromagnetism in metals such as iron. Since the energy of the system is decreased by *J* if any two neighbouring spins point in the same direction while it is increased when they point in the opposite direction, energetically the system would prefer to be in a state where all spins point in the same direction. This is the ferromagnetic state that Ising and Lenz were after and it has thermal fluctuations that destroy this ordered phase and cause the magnet to lose its (ferro-) magnetic property. Though this model and many variants have served for generations of physicists as an invaluable tool to understand phase transitions and critical phenomena [53].

The critical behaviour of the specific heat can be described near the λ-phase transition on the basis of an Ising model. The two orientations of the ions can be

identified with the spin-up and the spin-down orientations in an Ising model. The Ising part of the free energy is

$$F_1 = A_0 + A_1\varepsilon^{2-\alpha} \tag{2.6}$$

where α is the critical exponent, A_0 and A_1 are constatnts. ε=|T-T_C|/T_C denotes the reduced temperature with the critical temperature T_C. Using Eq. (2.6), the second derivative of the free energy with respect to the temperature gives a power-law formula for the specific heat C_{VI} expressed as

$$C_{VI} = C_0 - J^2\frac{A_1 T}{T_C^2}(1-\alpha)(2-\alpha)|\varepsilon|^{-\alpha} \tag{2.7}$$

where α is now the critical exponent for the specific heat C_{VI} and J is the interaction energy between the nearest-neigbour ions in the crystal. In Eq. (2.7) C_0 denotes the background specific heat, as we have used for the analysis of NH_4Br [54].

2.4 Mean Field Model

A many-body system with interactions is generally very difficult to solve exactly, except for exteremely simple cases (Gaussian field theory, 1D Ising model). The great difficulty (e.g. when computing the partition function of the system) is the treatment of combinatorics generated by the interaction terms in the Hamitonian when summing over all states. The goal of the mean field theory is to resolve these combinatorial problems.

The main idea of the mean field theory is to replace all interactions to any one body with an average or effective interaction. This reduces any multi-body problem into an effective one-body problem. The ease of solving the problems in mean field theory means that some insight into the behaviour of the system can be obtained at a relatively low cost.

In the mean field theory, the Hamiltonian may be expanded in terms of the magnitude of fluctuations around the mean of the field. In general, dimensionality plays a strong role in determining whether a mean-field approach will work for any particular problem. In mean field theory, many interations are replaced by one

effective interaction. Then, it naturally follows that if the field or particle exhibits many interactions in the original system, mean field theory will be more accurate for such a system.

While mean field theory arose primarily in the field of statistical mechanics, it has more recently been applied elsewhere, for example in inference in graphical models theory in artificial intelligence [55].

The mean field theory is a means by which to approximate the specific interactions between a given molecule and all the other molecules in the system. A common feature of mean field theories is the identification of an order parameter [56].

For our calculations, we first define the free energies of liquid and solid with the order parameter by means of the mean field theory. The free energy of the liquid is

$$F_L = 0 \tag{2.8}$$

and the free energy of the solid phase is

$$F_{solid} = a_2\psi^2 + a_4\psi^4 + a_6\psi^6 \tag{2.9}$$

where ψ is the order parameter and a_2, a_4 and a_6 are the coefficients which depend on temperature and pressure or concentration according to their usage. In order to express the order parameter in terms of the coefficients, we minimize the free energy with respect to its order parameter. We then obtain

$$\psi^2 = \frac{1}{3a_6}\left[-a_4 + (a_4^2 - 3a_2a_6)^{1/2}\right] \tag{2.10}$$

Thus, using the temperature and pressure or concentration dependences of the coefficients a_2, a_4 and a_6, the order parameter can be obtained as the functions of temperature and pressure or concentration.

2.5 Ferroelectricity

In classical electromagnetism, the polarization density (or electric polarization, or simply polarization) is the vector field that expresses the density of

permanent or induced electric dipole moments in a dielectric material. The polarization vector P is defined as the dipole moment per unit volume. In the SI unit system its unit is coulombs per square metre [57]. Fig. 2.1 shows the polarization as a function of temperature for a second order phase transition [58].

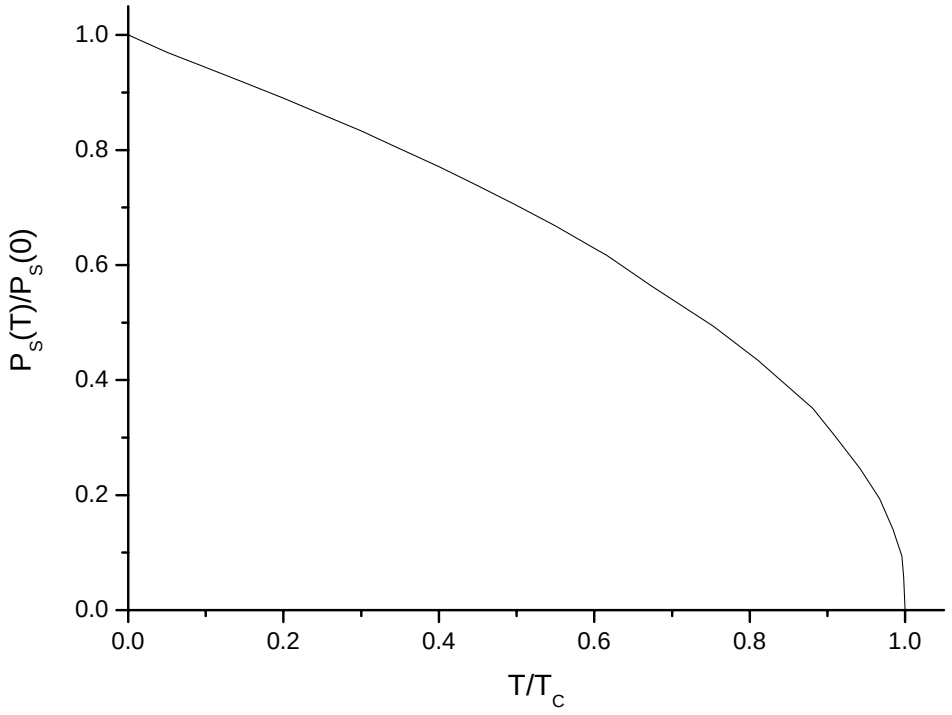

Figure 2.1 Spontaneous polarization versus temperature, for a scond-order phase transition

In a homogeneous linear and isotropic dielectric medium, the polarization is aligned with and proportional to the electric field E. In an anisotropic material, the polarization and the field are not necessarily in the same direction. Then, the i th component of the polarization is related to the j th component of the electric field according to:

$$P_i = \sum_j \varepsilon_0 \chi_{ij} E_j \tag{2.11}$$

where ε_0 is the permittivity of free space, and χ is the electric susceptibility tensor of the medium [57].

The dielectric constant ε of an isotropic or cubic medium relative to vacuum is defined in terms of the macroscopic field E:

$$\varepsilon = \frac{\varepsilon_0 E + P}{\varepsilon_0 E} = 1 + \chi \tag{2.12}$$

where P is polarization and χ is susceptibility [58].

The ferroelectric effect is an electrical phenomenon whereby certain ionic crystals may exhibit a spontaneous dipole moment. The term ferroelectricity refers to the similarity with ferromagnetism, in which a material exhibits a permanent magnetic moment [59]. A ferroelectric crystal exhibits an electric dipole moment even in the absence of an external electric field. In the ferroelectric state the center of the positive charge of the crystal does not coincide with the center of negative charge [60].

The plot of polarization versus electric field for the ferroelectric state shows a hysteresis loop (Fig. 2.2). A crystal in a normal dielectric state usually does not show significant hysteresis when the electric field is increased and then reversed, both slowly [58]. The phenomenon of hysteresis can conceptually be explained as follows: a system can be divided into subsystems or domains, much larger than an atomic volume, but still microscopic. Such domains occur in ferroelectric and ferromagnetic systems, since individual dipoles tend to group with each other, forming a small isotropic region. Each of the system's domains can be shown to have a metastable state. The metastable domains can in turn have two or more substates. Such a metastable state fluctuates widely from domain to domain, but the average represents the configuration of lowest energy. The hysteresis is simply the sum of all domains, or the sum of all metastable states [60].

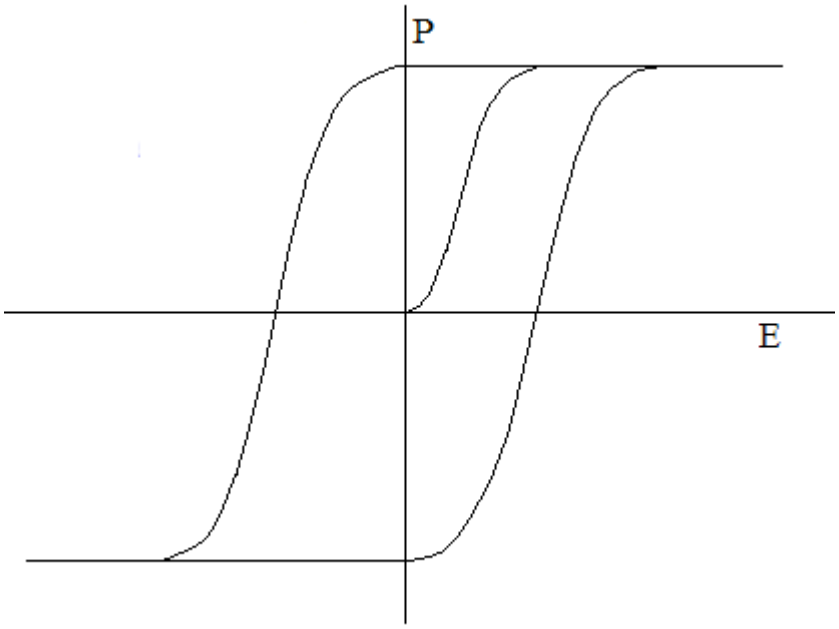

Figure 2.2 The hysteresis loop.

Ferroelectric materials often have very large dielectric constants, and thus are often found in capacitors. They also often have unusually large nonlinear optical coefficients [59].

Ferroelectricity usually disappears above a certain temperature called the transition temperature. Above the transition the crystal is said to be in a paraelectric state [58]. Paraelectricity is a phenomenon, or rather "crystal phase", where electric dipoles are unaligned (i.e. unordered domains that are electrically charge) and thus have the potential to align in an external electric field and strength it [61]. Paraelectric materials have a characteristic of a rapid drop in the dielectric constant as the temperature increases [58]. In comparison to ferroelectricity phase, the domains are unordered and the internal field is weak [61].

CHAPTER 3

CALCULATIONS AND RESULTS

3.1 Lambda-Phase Transition in Ammonium Bromide

λ-transitions ocur in various systems such as the order-disorder transformation in β-brass, ammonium salts (ammonium halides), crystalline quartz and many other solids [51], as stated in section 2.1. Also, this λ-shape in the specific heat C_P appears in liquid helium and the antiferromagnetic transition in $MnBr_2$ is a symmetrical λ-transition. Two dimensional Ising model of the order-disorder transformation exhibits also a symmetrical λ-transition [51]. Here we consider the λ-type of phase transition that occurs in the specific heat C_P of ammonium bromide. The λ-transition takes place at 234 K (T_λ) in NH_4Br as an order-disorder transition.

3.1.1 Critical Behaviour of the Specific Heat Calculated Using the Raman Frequencies of the Lattice and Internal Modes Near the Lambda-Phase Transition in Ammonium Bromide

The critical behaviour of the specific heat can be interpreted quantitatively from the Raman frequency shifts in NH_4Br. By means of correlations between the specific heat C_{VI} (or C_P) and the Raman frequency shifts $\frac{1}{\nu}\left(\frac{\partial \nu}{\partial T}\right)_P$ or $\frac{1}{\nu}\left(\frac{\partial \nu}{\partial P}\right)_T$ close to the λ-phase transition of NH_4Br, the specific heat can be calculated from the Raman data. This is done by assuming that the specific heat and the Raman frequency shifts exhibit similar critical behaviour with the same critical exponent α near the λ-phase transition of NH_4Br. Thus, expressing the critical behaviour of the frequency shifts $\frac{1}{\nu}\left(\frac{\partial \nu}{\partial T}\right)_P$ by a power-law formula

$$\frac{1}{\nu}\left(\frac{\partial \nu}{\partial T}\right)_P = A\varepsilon^{-\alpha} \tag{3.1}$$

with the critical exponent α and the amplitude *A*, we can evaluate the specific heat C_{VI} as a function of temperature in NH_4Br near its λ-phase transition according to Eq. (2.7). In order to find the critical exponent α, first of all we integrate Eq. (3.1)

$$\int \frac{\partial \nu}{\nu} = \int A\varepsilon^{-\alpha}\partial T \tag{3.2}$$

After integration, we find

$$ln\left(\frac{\nu}{\nu_C}\right) = \left(\frac{AT_C}{1-\alpha}\right)|\varepsilon|^{1-\alpha} \tag{3.3}$$

with the critical frequency ν_C of the Raman mode and taking the logarithm of both sides, we obtain the relation

$$ln\left[ln\left(\frac{\nu}{\nu_C}\right)\right] = ln\left(\frac{AT_C}{1-\alpha}\right) + (1-\alpha)ln|\varepsilon| \tag{3.4}$$

for the λ-phase transition in NH_4Br. A plot $ln(\nu/\nu_C)$ as a function of the reduced temperature ε in a log-log scale gives the critical exponent α for the frequency shift $\frac{1}{\nu}\left(\frac{\partial \nu}{\partial T}\right)_P$ of those Raman modes considered in NH_4Br. Once, we determined the critical exponent α from the Raman frequency data, this will then describe the critical behaviour of the specific heat C_{VI} according to Eq. (2.7). So, using the Raman frequencies of those modes studied at various temperatures close to the λ-phase transition in NH_4Br, the specific heat C_{VI} can be calculated by means of Eq. (2.7) for an Ising model and it can be compared with the thermodynamically measured C_P values for its crystalline system.

In this section, we calculate the specific heat C_{VI} as a function of temperature using the Raman frequencies for the ν_7 (56 cm^{-1}) and the ν_2 (1684 cm^{-1}) modes in NH_4Br near the λ-phase transition [54]. In order to calculate the specific heat C_{VI}, we first calculate the critical exponent α and the amplitude *A* by using the log-log graph of $ln(\nu/\nu_C)$ against the reduced temperature ε. Fig. 3.1 shows the log-log graph of $ln(\nu/\nu_C)$ versus the reduced temperature ε for the ν_7 (56 cm^{-1}) mode of NH_4Br (P=0, T_C=234 K). By using Fig. 3.1, we obtain

$$-ln[|\ln(\nu/\nu_C)|] = 1.89 - 0.81|ln\varepsilon| \quad (3.5)$$

By equating Eqs. (3.4) and (3.5), we obtain the critical exponent α and the amplitude *A* whose values are given in Table 3.1.

Table 3.1 Values of the critical exponent α and the amplitude *A* for the Raman frequency shifts $\frac{1}{\nu}\left(\frac{\partial \nu}{\partial T}\right)_P$ of the frequency ν_7 (56 cm^{-1}) mode in NH_4Br (P=0) within the interval of the reduced temperature ε according to Eq. (3.4). ν_C indicates the critical frequency of this mode (T_C=234 K)

Raman Mode	α	$A\times10^{-4}$ (K^{-1})	ν_C (cm^{-1})	$\varepsilon=\lvert T-T_C\rvert/T_C$
ν_7 (56 cm^{-1})	0.19	5.23	57.05	$3\times10^{-3}<\varepsilon<7\times10^{-2}$

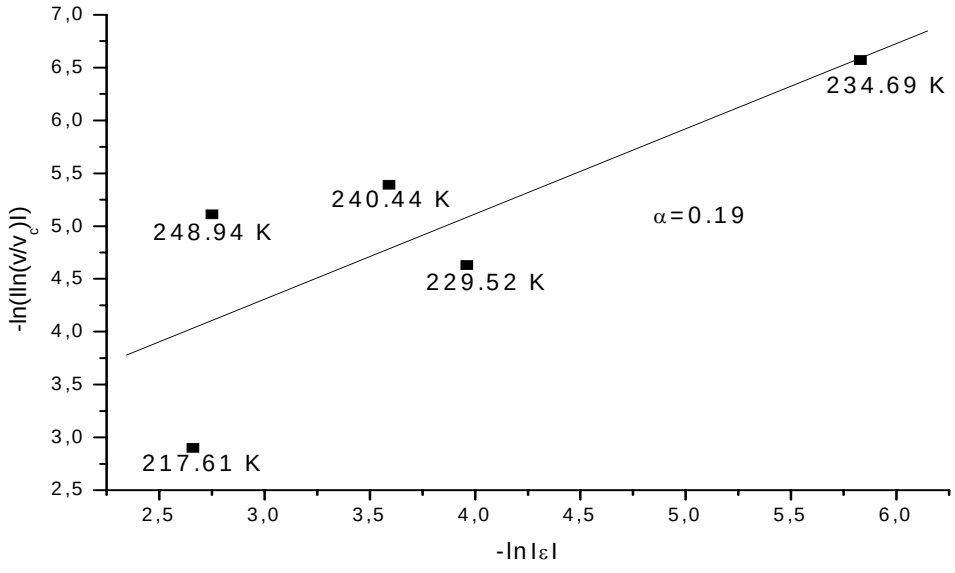

Figure 3.1 $ln(\nu/\nu_C)$ as a function of the reduced temperature $\varepsilon=|T-T_C|/T_C$ in a log-log scale for the ν_7 (56 cm^{-1}) Raman mode of NH_4Br (P=0, T_C=234 K) according to Eq. (3.4). ν_C denotes the critical frequency. The observed frequencies are shown by squares [54].

Similarly, we also analyzed the temperature dependence of the Raman frequency shifts for the internal mode of ν_2 (1684 cm^{-1}) below and above T_C according to Eq. (3.4). In a log-log scale a plot of $ln(\nu/\nu_C)$ against the reduced temperature ε, gives the equation for below T_C as

$$-ln[ln(\nu/\nu_C)] = 5.28 - 0.55ln\varepsilon \quad (3.6)$$

Equating Eqs (3.4) and (3.6), we find the critical exponent α=0.45 ($T<T_C$) and

$$-ln[ln(\nu/\nu_C)] = 5.74 - 0.43ln\varepsilon \quad (3.7)$$

By using Eqs (3.4) and (3.7), we obtain α=0.57 ($T>T_C$), as tabulated in Table 3.2. Our plots are given in Figs. 3.2 and 3.3, respectively, for $T<T_C$ and $T>T_C$ in NH_4Br (P=0, T_C=234 K).

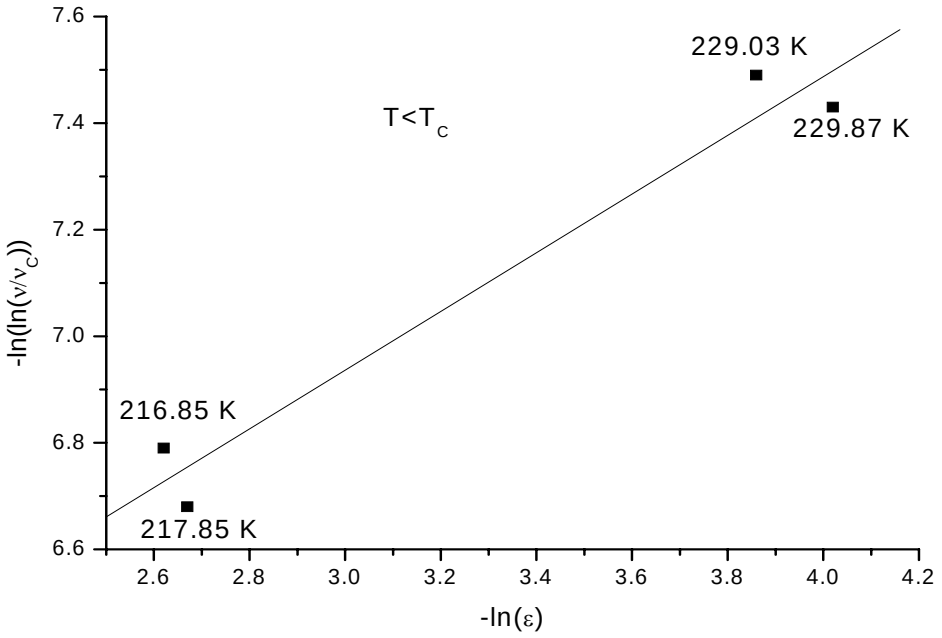

Figure 3.2 $ln(\nu/\nu_C)$ as a function of the reduced temperature $\varepsilon=|T - T_C|/T_C$ in a log-log scale for the ν_2 (1684 cm^{-1}) Raman mode of NH_4Br (P=0, T_C=234 K) below T_C according to Eq. (3.4). ν_C denotes the critical frequency. The observed frequencies are shown by squares [54].

Table 3.2 Values of the critical exponent α and the amplitude A for the Raman frequency shifts $\frac{1}{\nu}\left(\frac{\partial \nu}{\partial T}\right)_P$ of the frequency ν_2 (1684 cm^{-1}) mode within the interval of the reduced temperature ε in NH_4Br (P=0, T_C=234 K) according to Eq. (3.4). Our values of C_0 and J^2A_1 below and above T_C are also given.

ν_2 (1684 cm^{-1})	α	$A\times10^{-4}$ (K^{-1})	$\varepsilon=\lvert T-T_C\rvert/T_C$	C_0(J/ mol K)	$-J^2A_1$(J/mol)
$T<T_C$	0.45	0.12	$1.5\times10^{-2}<\varepsilon<7.4\times10^{-2}$	60	2831.71
$T>T_C$	0.57	0.059	$0.3\times10^{-2}<\varepsilon<7\times10^{-2}$	70	1225.37

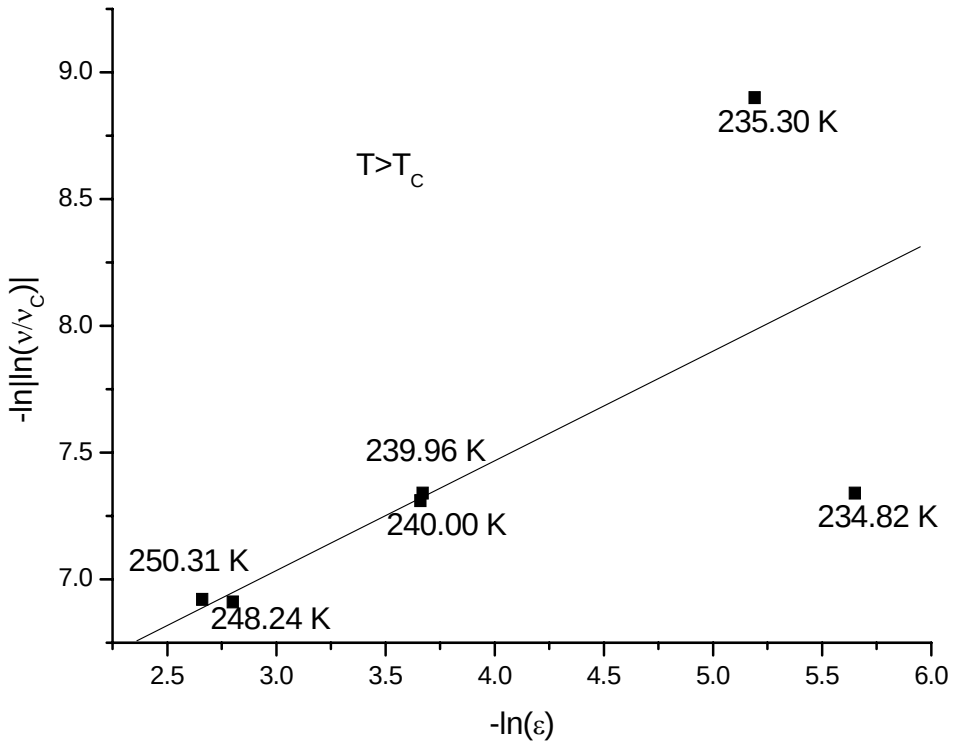

Figure 3.3 $ln(\nu/\nu_C)$ as a function of the reduced temperature $\varepsilon=\lvert T-T_C\rvert/T_C$ in a log-log scale for the ν_2 (1684 cm^{-1}) Raman mode of NH_4Br (P=0, T_C=234 K) above T_C according to Eq. (3.4). ν_C denotes the critical frequency. The observed frequencies are shown by squares [54].

From our analysis of the Raman frequency data for both modes ν_7 (56 cm^{-1}) and ν_2 (1684 cm^{-1}), we were then able to calculate the specific heat C_{VI} according to Eq. (2.7). To calculate the specific heat C_{VI}, we also needed the value of J^2A_1. We used the observed C_P data [3] at various temperatures as C_{VI} in Eq. (2.7) with C_0=0. Thus, the J^2A_1 values were calculated, as given in Table 3.2 and Table 3.3.

Table 3.3 Values of the critical exponent α, the background specific heat C_0 and J^2A_1 due to the ν_7 (56 cm^{-1}) Raman mode (Table 3.1) below and above T_C, according to Eq. (2.7) in NH_4Br (P=0, T_C=233.8 K)

ν_7 (56 cm^{-1})	A	C_0 (J/mol K)	- J^2A_1 (J/mol)
$T<T_C$	0.19	32	6435.10
$T>T_C$	0.19	-25	6248.87

After calculating J^2A_1 values, we calculated the specific heat C_{VI} as a function of temperature according to Eq. (2.7). The observed C_P [2] and the calculated C_{VI} values against temperature are shown in Fig. 3.4 for the ν_7 (56 cm^{-1}) Raman mode.

Similarly, we calculated the J^2A_1 values for the ν_2 (1684 cm^{-1}) mode in NH_4Br, as given in Table 3.2. Finally, we plot the specific heat (observed C_P [3] and calculated C_{VI}) against the temperature graph for the ν_2 (1684 cm^{-1}) mode in Fig. 3.5.

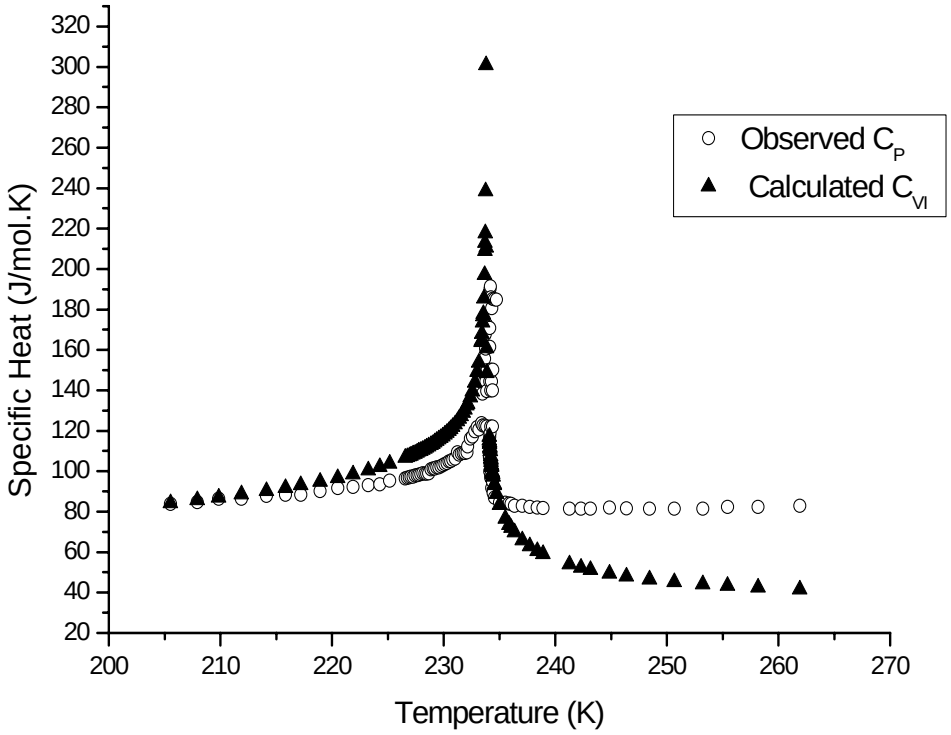

Figure 3.4 Specific heat C_{VI} calculated as a function of temperature for the first order phase transition (P=0, T_C=234 K) using the frequencies of the ν_7 (56 cm^{-1}) Raman mode in NH_4Br. Observed C_P data [3] is also shown here.

Our calculated C_{VI} using the frequencies of the Raman modes of ν_7 (56 cm^{-1}) and ν_2 (1684 cm^{-1}), as given by Figs. 3.4 and 3.5, respectively, exhibit a λ-type of phase transition with the observed C_P [3] for NH_4Br. Agreement is better below T_λ for the C_{VI} values calculated here for both phonons, whereas above T_λ the calculated C_{VI} values are much lower than those observed C_P due to the ν_7 (56 cm^{-1}) Raman mode of NH_4Br (Fig. 3.4). For the ν_2 (1684 cm^{-1}) Raman mode above T_λ, agreement between the calculated C_{VI} and the observed C_P data [3], is reasonably good (Fig. 3.5).

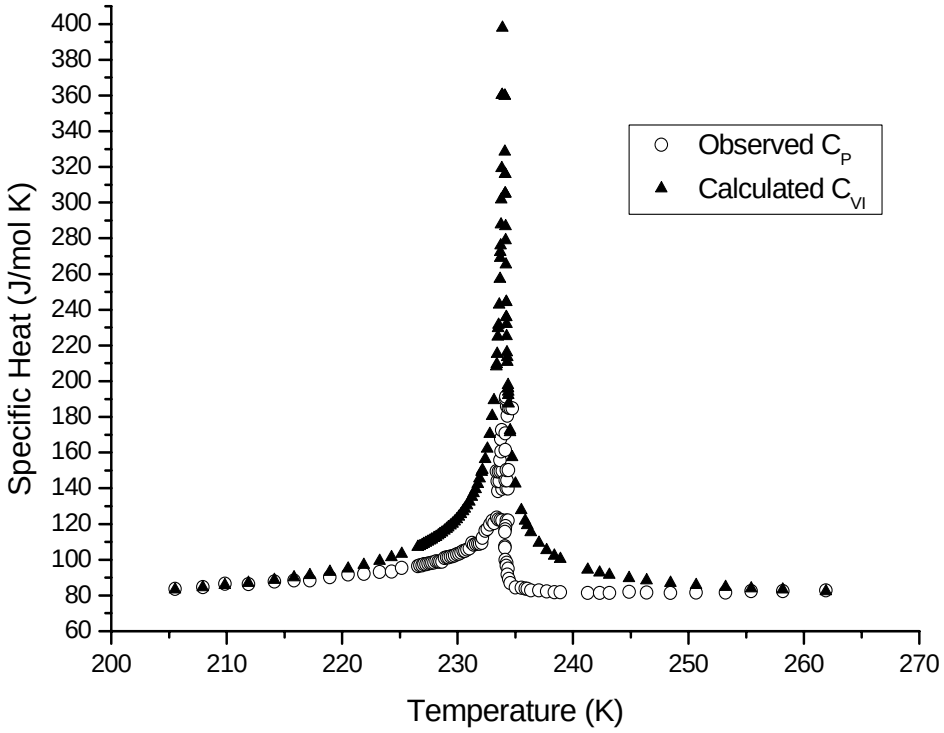

Figure 3.5 Specific heat C_{VI} calculated as a function of temperature for the first order phase transition (P=0, T_C=234 K) using the frequencies of the ν_2 (1684 cm^{-1}) Raman mode in NH_4Br. Observed C_P data [3] is also shown here.

Discrepancies which occur close to the transition temperature just below and above T_λ (Figs. 3.4 and 3.5), may be due to the fact that we compare our calculated C_{VI} with the observed C_P instead of C_V which is not accessible experimentally. Although there are discrepancies, in particular close to T_λ, our calculated values of the specific heat C_{VI} are reasonably in good agreement with the observed C_P for NH_4Br, as we see from Figs. 3.4 and 3.5.

Above T_λ, there occurs some discrepancy in the specific heat C_{VI} calculated using the frequency of the ν_7 (56 cm^{-1}) Raman mode of NH_4Br, as shown in Fig. 3.4 in comparison with the observed C_P data. This can be explained on the basis of the pseudospin-phonon coupling in an Ising model due to Yamada et al. [62] for

NH_4Br. The ν_7 (56 cm^{-1}) mode is the disorder-allowed Raman mode at the zone boundary (M point) in the Brillouin zone of the disordered β phase in NH_4Br, which is relocated at the zone center (Γ point) in the Brillouin zone of the antiferro-ordered γ phase in this crystal. In this intermediate phase (γ phase), two orientations of the NH_4^+ ions in analogy with the up and down orientations of spins, are accompanied by the antiparallel displacements of Br^- ions from the corner site in the $a-b$ plane. As pointed out by Yamada et al. [50], displacements of Br^- ions correspond to the polarization of a normal mode (TA_1 branch) at (110) zone boundary in the disordered β phase of NH_4Br. Thus, due to this interaction with the NH_4^+ ions of the ν_7 (56 cm^{-1}) phonon in an Ising pseudospin-phonon coupled model [62], which becomes much more important above T_λ than below T_λ, contributions to the specific heat C_{VI} are lowered above T_λ, as shown in Fig. 3.4.

Also, in our analysis of the frequency shifts $\frac{1}{\nu}\left(\frac{\partial \nu}{\partial T}\right)_P$ for the ν_7 (56 cm^{-1}) Raman mode of NH_4Br, we obtained the same value of α=0.19 below and above T_λ (Fig. 3.1), which was then used to calculate the specific heat C_{VI} for the transition between the disordered β and the antiferro-ordered γ phases in crystal. If the critical behaviour of the frequency shifts for the ν_7 (56 cm^{-1}) Raman mode is not the same in the β and γ phases of NH_4Br, in other words, the temperature dependence of $\frac{1}{\nu}\left(\frac{\partial \nu}{\partial T}\right)_P$ is accompanied with a different value of the critical exponent α above T_λ, this may effect our calculated values of C_{VI} in the β phase. As a result of this, our calculated C_{VI} values can agree better with the observed C_P [3] above T_λ in NH_4Br, as we obtained for the ν_2 (1684 cm^{-1}) mode (Fig. 3.5) using two different values of the critical exponent α below and above T_λ (Table 3.2).

For the β-γ transition we studied here as a second order phase transition in NH_4Br, the values of the critical exponent α deduced for the ν_7 (56 cm^{-1}) mode (Table 3.1) and the ν_2 (1684 cm^{-1}) mode (Table 3.2), can be compared with the predictions of an Ising model. Our value of α=0.19 (below and above T_λ) due to the ν_7 (56 cm^{-1}) mode is close to the critical exponent value of 0.125 (=1/8) for the specific heat C_P predicted from a three-dimensional Ising model.However, our values of α=0.45 ($T<T_\lambda$) and α=0.57 ($T>T_\lambda$) due to the ν_2 (1684 cm^{-1}) mode in NH_4Br, are very large compared to the Ising value. Our values can be reasonably

compared with the value of $\alpha' \approx 0.67$ obtained from the experimental measurements of C_P data for NH_4Cl [63].

3.1.2 Pippard Relations Applied To The Lambda-Phase Transition In NH_4Br

Eq.(2.1) assumes that the specific heat C_P varies linearly with the frequency shifts $(1/\nu)(\partial\nu/\partial T)_P$. Similarly, Eq.(2.2) assumes that the thermal expansivity α_P varies linearly with the frequency shifts $(1/\nu)(\partial\nu/\partial P)_T$ close to the λ-point. We also assume here that the mode Grüneisen parameters γ_P and γ_T remain constant across the λ-phase transitions.

In this study we applied Eqs.(2.1) and (2.2) to NH_4Br close to its λ-phase transition (T_λ=234 K, P=0). For this application we used the observed frequencies for the lattice mode of ν_7 (56 cm^{-1}) and for the internal mode of ν_2 (1684 cm^{-1}) in NH_4Br [49]. By analyzing the temperature dependence of the frequency shifts $\frac{1}{\nu}\left(\frac{\partial\nu}{\partial T}\right)_P$ for those modes according to a power-law formula (Eq. 3.1), we established the first Pippard relation (Eq. 2.1) [46], as also given in our recent study [64].

According to the calculation in section 3.1.1, we established a linear variation of C_P with the $\frac{1}{\nu}\left(\frac{\partial\nu}{\partial T}\right)_P$ for this lattice mode of ν_7 (56 cm^{-1}) in NH_4Br (P=0) with the critical exponent value of α=0.19 and the amplitude value of $A=5.23\times10^{-4}$. In order to draw a graph of C_P versus $\frac{1}{\nu}\left(\frac{\partial\nu}{\partial T}\right)_P$, we should calculate the $\frac{1}{\nu}\left(\frac{\partial\nu}{\partial T}\right)_P$ values by using the power law formula (Eq. 3.1). We calculated the reduced temperature $\varepsilon^{-\alpha}$ and multiplied with the amplitude A to obtain the values of $\frac{1}{\nu}\left(\frac{\partial\nu}{\partial T}\right)_P$. Figs. 3.6 and 3.7 represent the specific heat C_P [65] as a function of the frequency shifts $\frac{1}{\nu}\left(\frac{\partial\nu}{\partial T}\right)_P$ for the ν_7 (56 cm^{-1}) lattice mode of NH_4Br below and above T_λ, respectively (T_λ=234 K, P=0) [64].

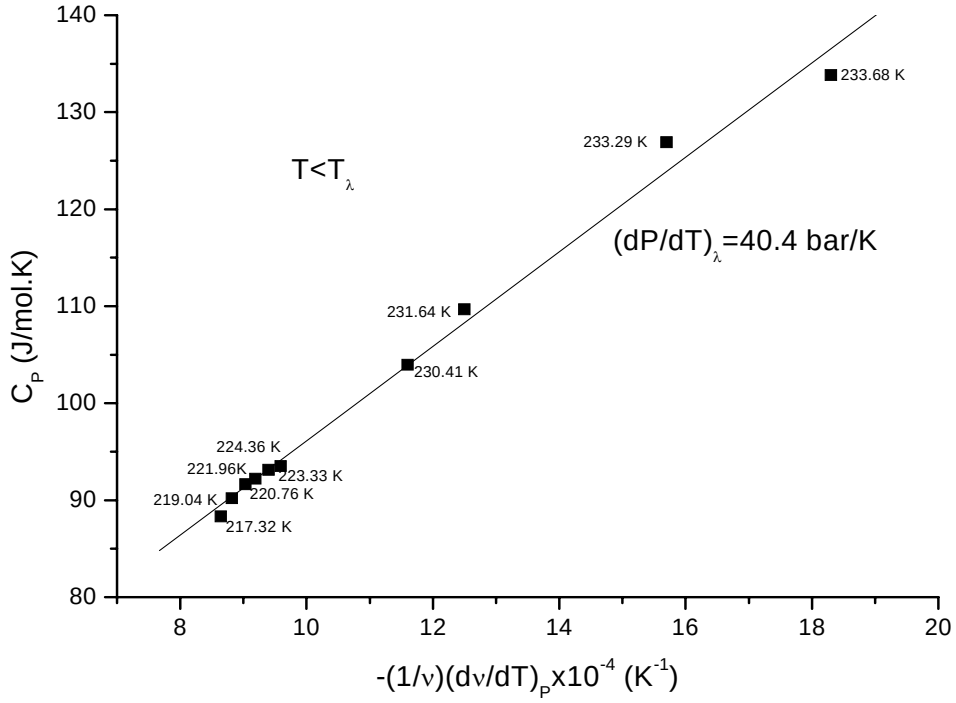

Figure 3.6 The specific heat C_p as a function of the frequency shift $\frac{1}{\nu}\left(\frac{\partial \nu}{\partial T}\right)_P$ for the lattice mode of ν_7 (56 cm^{-1}) Raman mode of NH_4Br close to the λ-phase transition below T_λ (P=0, T_λ=234 K) according to Eq.(2.1). The specific heat C_p data is taken from Ref. [65].

Similarly, we obtained the values of $\frac{1}{\nu}\left(\frac{\partial \nu}{\partial T}\right)_P$ for the internal mode of ν_2 (1684 cm^{-1}) using the calculation in section 3.1.1. Figs. 3.8 and 3.9 give our linear plots of C_P [64] against $\frac{1}{\nu}\left(\frac{\partial \nu}{\partial T}\right)_P$ for the ν_2 (1684 cm^{-1}) Raman mode of NH_4Br below and above T_λ, respectively.

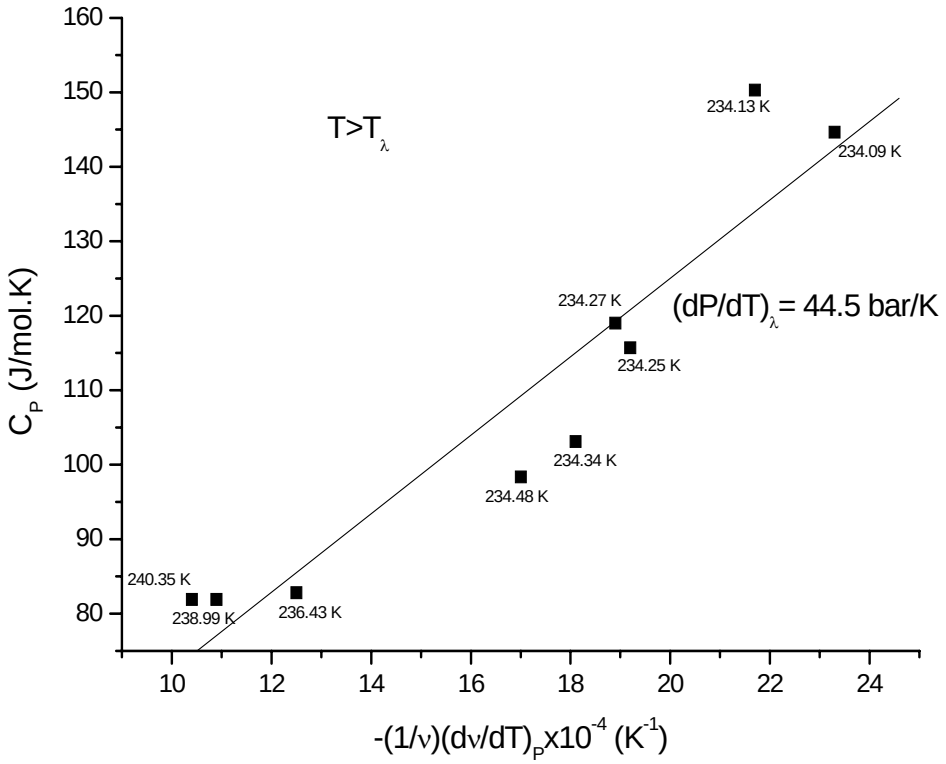

Figure 3.7 The specific heat C_p as a function of the frequency shift $\frac{1}{\nu}\left(\frac{\partial \nu}{\partial T}\right)_P$ for the lattice mode of ν_7 (56 cm^{-1}) Raman mode of NH_4Br close to the λ-phase transition above T_λ (P=0, T_λ=234 K) according to Eq.(2.1). The specific heat C_p data is taken from Ref. [65].

From our plots (Figs. 3.6-3.9), we deduced the values of the slope $(dP/dT)_\lambda$ and the intercept $T(dS/dT)_\lambda$ according to Eq. (2.1) for the Raman modes of ν_7 (56cm^{-1}) and ν_2(1684cm^{-1}), as tabulated in Tables 3.4 and 3.5, respectively. In order to deduce the values of the slope $(dP/dT)_\lambda$, we used the values of $V=V_\lambda$ at $T=T_\lambda$ and the mode Grüneisen parameter γ_P, as given in Tables 3.4 and 3.5, for the ν_7 (56 cm^{-1}) and ν_2 (1684cm^{-1}) modes, respectively. The V_λ values were calculated here by means of the relation

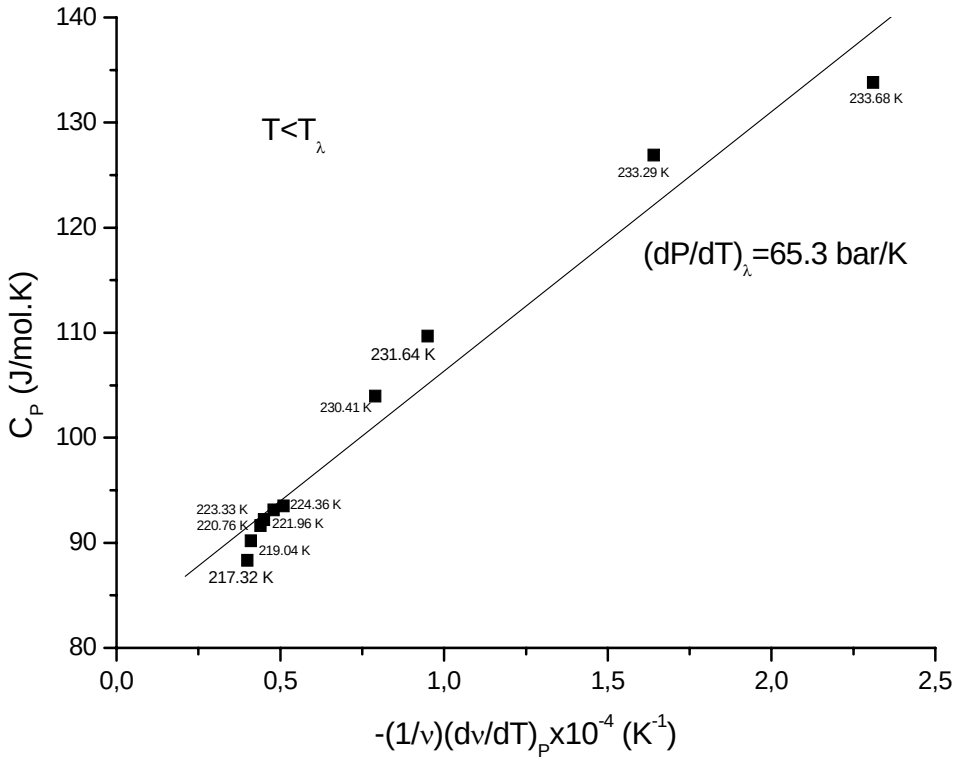

Figure 3.8 The specific heat C_p as a function of the frequency shift $\frac{1}{\nu}\left(\frac{\partial \nu}{\partial T}\right)_P$ for the internal mode of ν_2 (1684 cm^{-1}) Raman mode of NH_4Br close to the λ-phase transition below T_λ (P=0, T_λ=234 K) according to Eq.(2.1). The specific heat C_p data is taken from Ref. [65].

$$\nu_P(T) = \Delta_P + \nu_1 exp[-\gamma_P ln(V_P(T)/V_1)] \quad (3.8)$$

where ν_1 and V_1 are the values of the frequency and volume at room temperature (T=296 K), and Δ_P is defined as the order-disorder contribution to the frequency ($\Delta_P \neq 0$, $T \leq T_\lambda$ and $\Delta_P=0$, $T > T_\lambda$), as given in an earlier study [66]. Using the values of γ_P and Δ_P [66], the V_λ values were calculated for the ν_7 (56 cm^{-1}) and ν_2(1684cm^{-1}) modes (Eq. 3.8), and then the values of the slope $(dP/dT)_\lambda$ were obtained according to Eq. (2.1) below and above T_λ in NH_4Br (Tables 3.4 and 3.5).

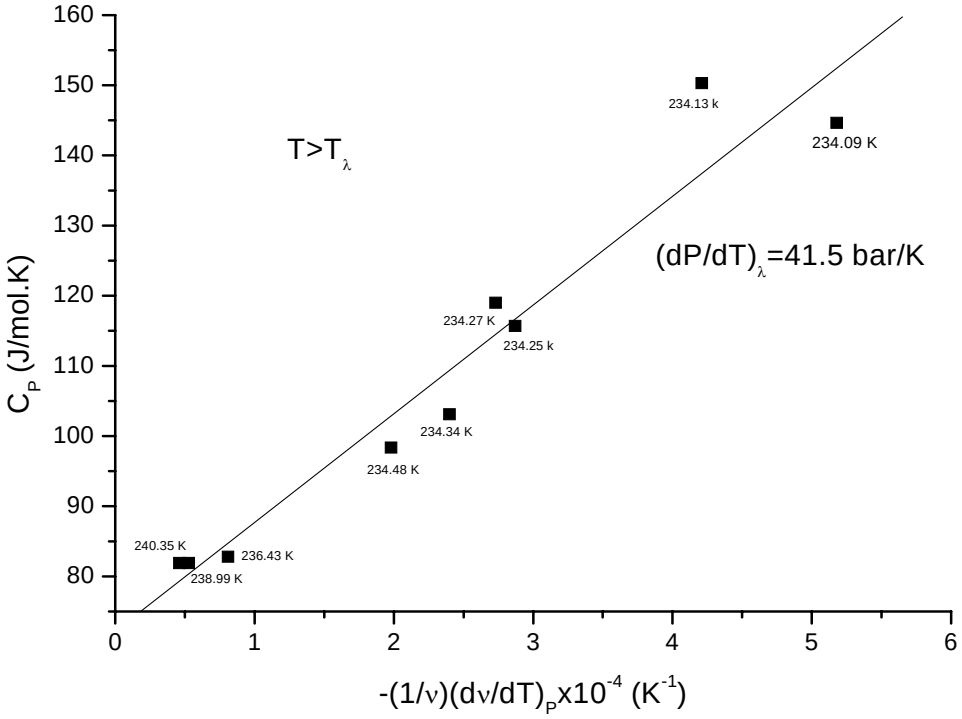

Figure 3.9 The specific heat C_p as a function of the frequency shift $\frac{1}{\nu}\left(\frac{\partial \nu}{\partial T}\right)_P$ for the internal mode of ν_2 (1684 cm^{-1}) Raman mode of NH_4Br close to the λ-phase transition above T_λ (P=0, T_λ=234 K) according to Eq.(2.1). The specific heat C_p data is taken from Ref. [65].

Table 3.4 Values of the Raman frequency of ν_7(56 cm^{-1}) mode, ν_λ(at T_λ), its mode Grüneisen parameter γ_p [65], the order-disorder contribution to the frequency, Δ_p [66] and the volume V_λ (at T_λ) (Eq. 3.8). Values of the slope $(dP/dT)_\lambda$ and the intercept (Eq. 2.1) are also given here within the range of reduced temperature ε below and above T_λ in NH_4Br.

T_λ=234 K	ν_λ(cm^{-1})	γ_p	Δ_p (cm^{-1})	V_λ(cm^3 /mol)	$(dP/dT)_\lambda$ (bar/K)	$T(dS/dT)_\lambda$ (J/mol.K)	$\varepsilon = \lvert T-T_\lambda \rvert / T_\lambda$
$T< T_\lambda$	57.05	7.9	7.50	40.742	40.4	47.42	$1.37\times10^{-3}<\varepsilon<7.13\times10^{-2}$
$T> T_\lambda$	57.05	7.9	0	40.022	44.5	19.66	$3.85\times10^{-4}<\varepsilon<2.71\times10^{-2}$

Table 3.5 Values of the Raman frequency of ν_2(1684 cm^{-1}) mode, ν_λ(at T_λ), its mode Grüneisen parameter γ_p [65], the order-disorder contribution to the frequency, Δ_p [66] and the volume V_λ (at T_λ) (Eq. 3.8). Values of the slope $(dP/dT)_\lambda$ and the intercept (Eq. 2.1) are also given here within the range of reduced temperature ε below and above T_λ in NH_4Br.

T_λ=234 K	$\nu_\lambda(cm^{-1})$	γ_p	Δ_p (cm^{-1})	$V_\lambda(cm^3$ /mol)	$(dP/dT)_\lambda$ (bar/K)	$T(dS/dT)_\lambda$ (J/mol.K)	$\varepsilon = \lvert T-T_\lambda \rvert / T_\lambda$
$T< T_\lambda$	1686.6	0.25	4.64	40.391	65.3	81.64	$1.37\times10^{-3}<\varepsilon<7.13\times10^{-2}$
$T> T_\lambda$	1687.7	0.25	0	39.84	41.5	72.19	$3.85\times10^{-4}<\varepsilon<2.71\times10^{-2}$

3.2 Calculation of the Phase Diagram Using the Mean Field Theory

A phase diagram is common way to represent the various phases of a substance and the conditions under which each phase exists.

A phase diagram is a plot of pressure (P or lnP) vs temperature (T). Lines on the diagram represent conditions (T,P) under which a phase change is at equilibrium. That is, at a point on a line, it is possible for two (or three) phases to coexist at equilibrium. In other regions of the plot, only one phase exists at equilibrium [67].

Phase diagrams provide a graphical means of presenting the results of experimental studies of complex natural processes, such that at a given temperature and pressure for a specific system at equilibrium the phase or phases present can be determined [68].

Phase diagrams (temperature vs pressure or temperature vs concentration) can be calculated for various physical systems using the mean field theory. By expanding the free energy in terms of the order parameters according to the Landau–phenomenological theory, the phase line equations can be derived. Assuming the temperature and pressure (or concentration) dependence of the coefficients in the free energy expansion, the temperature versus pressure (T-P) or the temperature versus concentration (T-X) phase diagrams of the systems can be calculated.

In order to interpret the experimentally measured phase diagrams, the phase line equations derived from the Landau–phenomenological theory can be fitted to the experimental data. Below, we derive the phase line equations from the mean field theory and they are fitted to the experimental data for various physical systems.

3.2.1 Ammonium and Deutero-Ammonium Chloride

We have two solid phases of NH_4Cl and ND_4Cl, solid II and solid III. According to Eq. (2.9), we can write the free energy of these two solid phases as

$$F_{\mathrm{II}} = a_2\psi^2 + a_4\psi^4 + a_6\psi^6 \tag{3.9}$$

and

$$F_{\mathrm{III}} = b_2\eta^2 + b_4\eta^4 + b_6\eta^6 \tag{3.10}$$

where ψ and η are the order parameters of solid II and solid III, respectively. Solid II and III phases are both considered as ordered phases in NH_4Cl and ND_4Cl as the pressure increases to 40 kbar, according to the experimental T-P phase diagrams in those crystalline systems [69]. Here, the coefficients a_2, a_4 and a_6 (Eq.3.9), and b_2, b_4 and b_6 (Eq.3.10) depend on both temperature and pressure. We also consider that $a_2>0$, $a_4<0$ and $a_6>0$ (Eq. 3.9), and $b_2>0$, $b_4<0$ and $b_6>0$ (Eq. 3.10) as the condition for a first-order phase transition. This is in accordance with the experimental results for both NH_4Cl and ND_4Cl that at higher pressures the transition is likely of a first order [69]. We note that in Eqs. (3.9) and (3.10) the odd powers of Ψ and η are not included for symmetry reasons.

From minimization of the free energies with respect to the order parameters, as given in the section 2.4, we have

$$\psi^2 = \frac{1}{3a_6}\left[-a_4 + (a_4^2 - 3a_2a_6)^{1/2}\right] \tag{3.11}$$

and

$$\eta^2 = \frac{1}{3b_6}\left[-b_4 + (b_4^2 - 3b_2b_6)^{1/2}\right] \tag{3.12}$$

By substituting Eq. (3.11) into Eq. (3.9), the free energy of solid II phase in NH_4Cl and ND_4Cl can be expressed as

$$F_{II} = -\frac{a_2 a_4}{3a_6} + \frac{2a_4^3}{27a_6^2} - \frac{2}{27a_6^2}(a_4^2 - 3a_2 a_6)^{3/2} \tag{3.13}$$

Similarly, by substituting Eq. (3.12) into Eq. (3.10), the free energy of solid III phase in NH_4Cl and ND_4Cl can be written as

$$F_{III} = -\frac{b_2 b_4}{3b_6} + \frac{2b_4^3}{27b_6^2} - \frac{2}{27b_6^2}(b_4^2 - 3b_2 b_6)^{3/2} \tag{3.14}$$

On the transition line between phase II and phase III in NH_4Cl and ND_4Cl, we have $F_{II}=F_{III}$ or

$$-\frac{a_2 a_4}{3a_6} + \frac{2a_4^3}{27a_6^2} - \frac{2}{27a_6^2}(a_4^2 - 3a_2 a_6)^{3/2} - \frac{b_2 b_4}{3b_6} + \frac{2b_4^3}{27b_6^2} + \frac{2}{27b_6^2}(b_4^2 - 3b_2 b_6)^{3/2} = h = 0 \tag{3.15}$$

This is the phase line equation for the transition between solid II and solid III phases in NH_4Cl and ND_4Cl at high pressures.

We calculated here T-P phase diagrams of NH_4Cl and ND_4Cl between the solid II and solid III transition. For this calculation, the phase line equation (Eq. 3.15) was expressed in terms of the temperature and pressure dependence of the coefficients a_2, a_4, a_6 and b_2, b_4 and b_6 in the polynomial form. We assume here that the coefficients a_2 and a_4 are temperature dependent only and that their dependences are given by

$$a_2 = a_{20}(T - T_t)^{2/3} \tag{3.16}$$

$$a_4 = a_{40}(T - T_t)^{1/3} \tag{3.17}$$

which corresponds to $a_2 \sim a_4^2$. We choose a_6=1, T_t is the transition temperature. We also assume that the coefficients b_2, b_4 and b_6 depend on the pressure only, and that their dependences are as follows:

$$b_2 = b_{20}(P - P_t)^2 \tag{3.18}$$

$$b_4 = b_{40}(P - P_t) \tag{3.19}$$

$$b_6 = b_{60}(P - P_t) \tag{3.20}$$

which corresponds to $b_2 \sim b_4^2 \sim b_6^2$. P_t represents the transition pressure. In Eqs. (3.16-3.20) a_{20}, a_{40}, b_{20}, b_{40} and b_{60} are all constants.

By substituting these temperature and pressure dependences (Eqs. 3.16-3.20) into the phase line relation (Eq. 3.15), we then obtain

$$-\frac{a_{20}(T-T_t)^{\frac{2}{3}}a_{40}(T-T_t)^{\frac{1}{3}}}{3} + \frac{2a_{40}^3(T-T_t)}{27} - \frac{2}{27}\left(a_{40}^2(T-T_t)^{\frac{2}{3}} - 3a_{20}(T-T_t)^{\frac{2}{3}}\right)^{\frac{3}{2}}$$

$$+\frac{b_{20}b_{40}(P-P_t)^3}{3b_{60}(P-P_t)} - \frac{2b_{40}^3(P-P_t)^3}{27b_{6o}^2(P-P_t)^2} +$$

$$\frac{2}{27b_{60}^2(P-P_t)^2}(b_{40}^2(P-P_t)^2 - 3b_{20}b_{60}(P-P_t)^3)^{3/2} = h = 0 \tag{3.21}$$

after some algebra, we get

$$h = A(T-T_t) - \frac{2b_{40}^3}{27b_{60}^2}(P-P_t) + \frac{b_{20}b_{40}}{3b_{60}}(P-P_t)^2$$

$$-\frac{2b_{40}^3}{27b_{60}^2}(P-P_t)\left[1 - \frac{3b_{20}b_{60}}{b_{40}^2}(P-P_t)\right]^{3/2} \tag{3.22}$$

where

$$A = \frac{2a_{40}^3}{27} - \frac{a_{20}}{3} + \frac{2}{27}(a_{40}^2 - 3a_{20})^{3/2} \tag{3.23}$$

The bracket in the last term of Eq. (3.22) can be expanded to a power series up to the quadratic term and we can neglect the higher order terms. This then gives

$$h = A(T-T_t) + B(P-P_t) + C(P-P_t)^2 + D(P-P_t)^3 \tag{3.24}$$

where

$$B = -\frac{4b_{40}^3}{27b_{60}^2} \quad , \quad C = \frac{2b_{20}b_{40}}{3b_{60}} \quad , \quad D = -\frac{b_{20}^2}{4b_{40}} \tag{3.25}$$

Eq. (3.24) can be rewritten as

$$h = h_0\{(T-T_t) - [\gamma_1(P-P_t) + \gamma_2(P-P_t)^2 + \gamma_3(P-P_t)^3]\} \tag{3.26}$$

with the parameters A=h_0, B= - $h_0\gamma_1$, C= - $h_0\gamma_2$ and D= - $h_0\gamma_3$. In this expression h_0, γ_1, γ_2 and γ_3 are constants. As given in Eqs. (3.23) and (3.25), the coefficients A, B, C and D which are defined as the functional forms of a_{20}, a_{40}, b_{20}, b_{40} and b_{60}, are related to the coefficients h_0, γ_1, γ_2 and γ_3 of the polynomial (Eq. 3.26). So, by means of the phase line relation (Eq. 3.15), which we derived from the mean field theory, the coefficients a_2, a_4 and a_6 of the free energy F_{II} (Eq.3.13), and the coefficients b_2, b_4 and b_6 of the free energy F_{III} (Eq. 3.14) can be calculated as functional forms since they are coupled to each other. The physical meaning of these coefficients a_2, a_4, a_6 (Eq. 3.13) and b_2, b_4 and b_6 (Eq. 3.14) is the same as in the Landau mean field theory. In Eq. (3.26) (T_t, P_t) represents coordinates of the transition point on the T-P phase line between solid II and solid III phases in NH_4Cl and ND_4Cl. Here we took T_t= -30.24^{0}C at P_t= 0 kbar [55]. Eq. (3.26) which we derived from the mean field theory, was then fitted to the experimental T-P data for NH_4Cl and ND_4Cl [66]. From this fitting, we obtained the values of the best-fitted equations as:

$$T = -28.48 + 8.16P - 0.17P^2 + 0.0015P^3 \quad (3.27)$$

$$T = -25.02 + 7.22P - 0.16P^2 + 0.0017P^3 \quad (3.28)$$

for both NH_4Cl (Eq. 3.27) and ND_4Cl (Eq. 3.28). Figs 3.10 and 3.11 give our plots for T-P phase diagrams of NH_4Cl and ND_4Cl, respectively, according to Eq. (3.26). The observed data [69] is also shown in our plots [70]. Equating Eq. (3.26) to the Eqs. (3.27) and (3.28), we can calculate the parameters h_0, γ_1, γ_2, γ_3 which are given in Table 3.6.

Table 3.6 Values of the parameters h_0, γ_1, γ_2 and γ_3 using the experimental data from the T-P phase diagrams of NH_4Cl and ND_4Cl [69] according to Eq. (3.26)

Crystal	h_0	γ_1 (^{0}C/kbar)	γ_2 (^{0}C/kbar^2)	γ_3 (^{0}C/kbar^3)
NH_4Cl	0.942	8.66	-0.18	0.0016
ND_4Cl	1.07	6.75	-0.15	0.0016

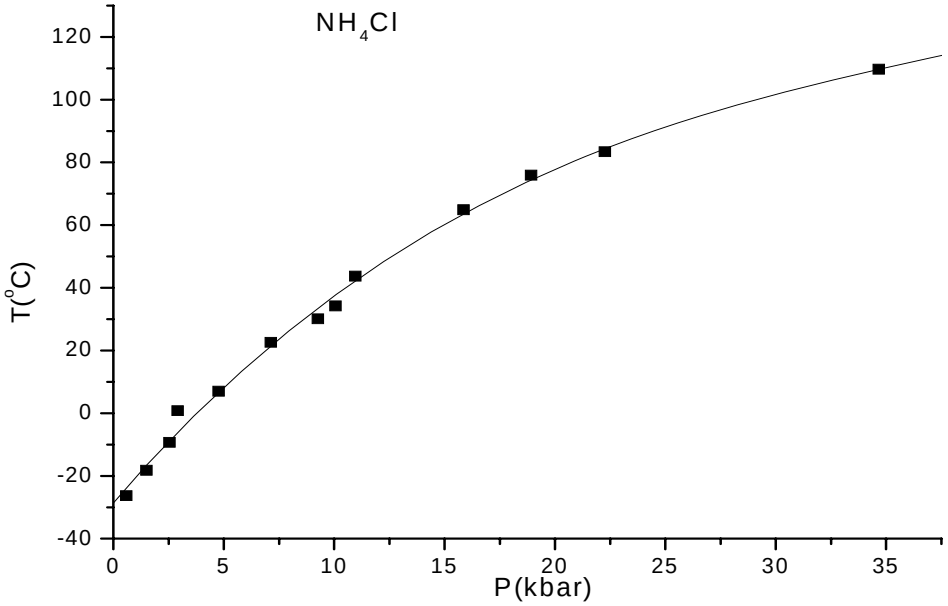

Figure 3.10 Phase diagram of NH_4Cl for solid II-solid III transition to 40 kbar. Solid line represents our calculated phase line. The experimental data [69] is also shown here.

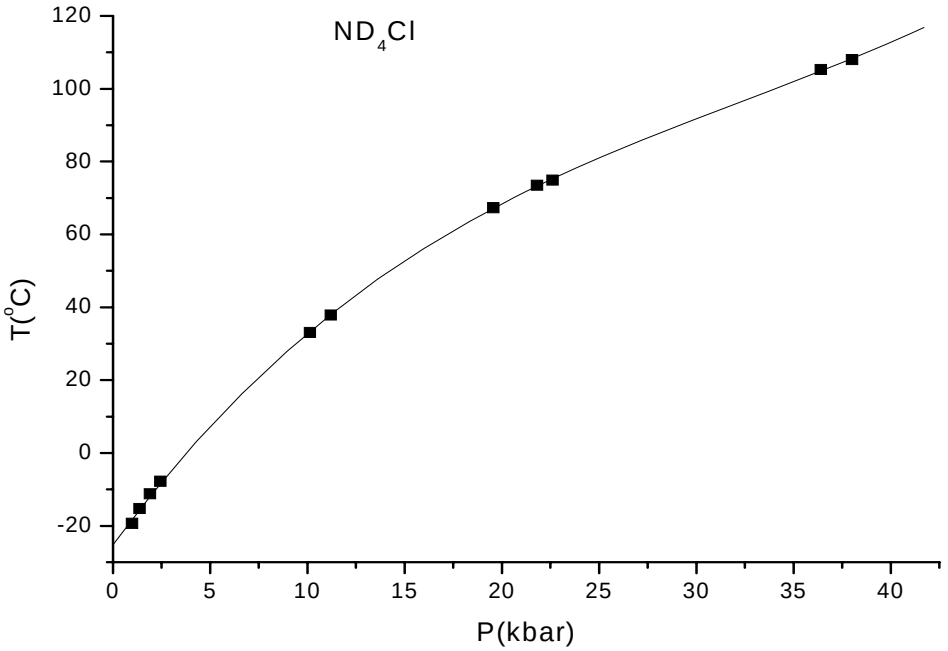

Figure 3.11 Phase diagram of ND_4Cl for solid II-solid III transition to 40 kbar. Solid line represents our calculated phase line. The experimental data [69] is also shown here.

3.2.2 Ammonium Sulfate

There are two solid phases, solid I and solid II, and liquid phase of $(NH_4)_2SO_4$ and according to section 2.4, their free energies can be written as:

$$F_I = \alpha_2\mu^2 + \alpha_4\mu^4 + \alpha_6\mu^6 \quad (3.29)$$

$$F_{II} = \beta_2\nu^2 + \beta_4\nu^4 + \beta_6\nu^6 \quad (3.30)$$

and

$$F_L = 0 \quad (2.8)$$

where μ and ν are the order parameters of the solid I and II phases, respectively. Since we study here a T-X phase diagram of the $(NH_4)_2SO_4/H_2O$ system, we assume that in Eqs. (3.29) and (3.30) the parameters α_2, α_4 and α_6; β_2, β_4 and β_6 are all dependent upon the temperature and concentration. Due to the fact that the phase lines in the T-X phase diagram of this system represent a first order phase transition, we take $\alpha_2>0$, $\alpha_4<0$ and $\alpha_6>0$; $\beta_2>0$, $\beta_4<0$ and $\beta_6>0$.

In order to apply the condition for the first order transition between liquid and solid I phases, we minimize the free energy F_I with respect to the order parameter μ, which gives

$$\mu^2 = \frac{1}{3\alpha_6}\left[-\alpha_4 + (\alpha_4^2 - 3\alpha_2\alpha_6)^{1/2}\right] \quad (3.31)$$

Inserting Eq. (3.31) into Eq. (3.29), we get

$$F_I = -\frac{\alpha_2\alpha_4}{3\alpha_6} + \frac{2\alpha_4^3}{27\alpha_6^2} - \frac{2}{27\alpha_6^2}(\alpha_4^2 - 3\alpha_2\alpha_6)^{3/2} \quad (3.32)$$

To write the phase line equation of liquid-solid I, we must equate the free energies of these two phases

$$F_L = F_I \quad (3.33)$$

Then, we can write

$$-\frac{\alpha_2\alpha_4}{3\alpha_6} + \frac{2\alpha_4^3}{27\alpha_6^2} - \frac{2}{27\alpha_6^2}(\alpha_4^2 - 3\alpha_2\alpha_6)^{3/2} = 0 \quad (3.34)$$

After some calculations, we obtain

$$(2\alpha_4^3 - 9\alpha_2\alpha_4\alpha_6)^2 = 4((\alpha_4^2 - 3\alpha_2\alpha_6)^{3/2})^2 \quad (3.35)$$

Finally, we can find the phase line equation for the liquid-solid I transition as

$$\alpha_4^2 = 4\alpha_2\alpha_6 \quad (3.36)$$

or

$$a = \alpha_4^2 - 4\alpha_2\alpha_6 = 0 \quad (3.37)$$

This is the phase line equation for the liquid-solid I transition, which represents the melting curve in the phase diagram of $(NH_4)_2SO_4/H_2O$.

In order to obtain T-X phase diagram of $(NH_4)_2SO_4/H_2O$, as we have given in our recent study [20], we used here our phase line equation, namely, Eq. (3.37) for the liquid-solid I. This was expressed as a functional form of both temperature and concentration in the following:

$$a = 0 = (T - T_m) - [\alpha_1(X - X_m) + \alpha_2(X - X_m)^2 + \alpha_3(X - X_m)^3] \qquad (3.38)$$

where (T_m, X_m) denote the coordinates of the melting point. From the experimental T-X phase diagram of $(NH_4)_2SO_4/H_2O$, the melting point is located at $T_m = -19.515\ ^0C$ and $X_m = 39.950$ as the weight percent of the ammonium sulphate [19]. In Fig. 3.12 we plot the melting curves of liquid-solid I (Eq. 3.38). The observed T-X data is also given in Fig. 3.12.

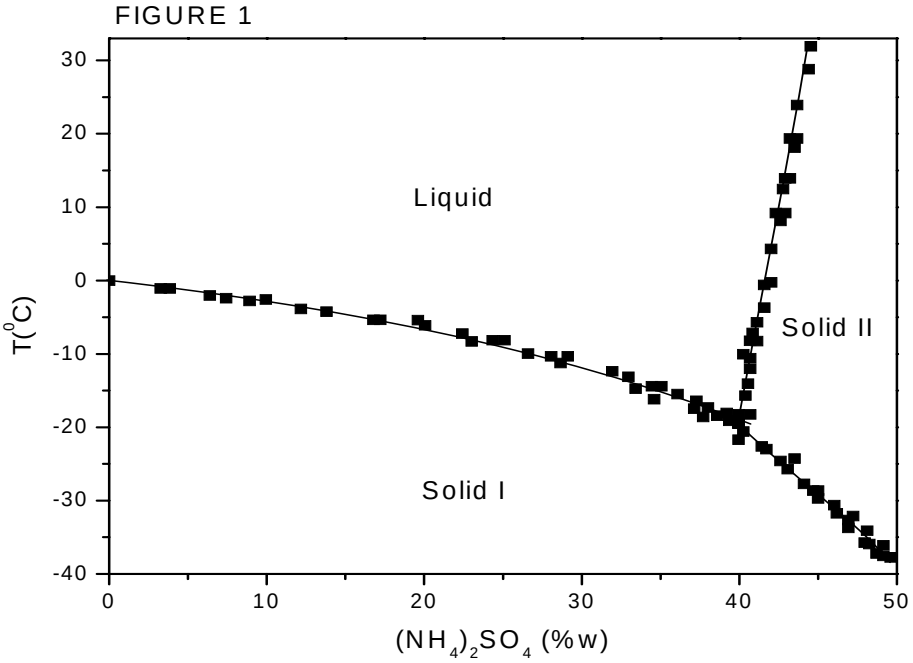

Figure 3.12 Our calculated phase diagram of $(NH_4)_2SO_4/H_2O$. Calculated phase lines are represented by solid lines. Experimental data [19] is also shown here.

In order to calculate the phase line equation by using Fig. 3.12, we fitted the experimental data for liquid-solid I transition and we obtained the equation as:

$$T = -0.121 - 0.295W + 0.00305W^2 - 0.000196W^3 \quad (3.39)$$

Then equating Eqs. (3.38) and (3.39), we can get the coefficients α_1, α_2, α_3 which are given in Table 3.7.

Table 3.7 Values of the coefficients which we obtained, when the equations indicated were fitted to the experimental data [19] for the liquid-solid I (L-I), liquid-solid II (L-II) and solid I-solid II (I-II) transitions in $(NH_4)_2SO_4/H_2O$. *w* denotes % weight of ammonium sulphate.

L-I	Eq. (3.38)	L-II	Eq. (3.46)	I-II	Eq. (3.56)
α_1 (^{0}C/w)	-0.986	β_1 (^{0}C/w)	10.043	γ_1 (^{0}C/w)	-2.024
α_2 (^{0}C/w^2)	-0.0204	β_2 (^{0}C/w^2)	-0.136	γ_2 (^{0}C/w^2)	0.0364
α_3 (^{0}C/w^3)	-1.96x10^{-4}	β_3 (^{0}C/w^3)	0.040	γ_3 (^{0}C/w^3)	-2.7x10^{-3}

Similarly, the phase line equation for the melting curve between liquid and solid II phases, can be obtained from the free energy F_{II} (Eq. 3.30). By minimizing F_{II} with respect to the order parameter ν, we obtain the expression for ν in terms of the coefficients β_2, β_4 and β_6 as follows:

$$\nu^2 = \frac{1}{3\beta_6}\left[-\beta_4 + (\beta_4^2 - 3\beta_2\beta_6)^{1/2}\right] \quad (3.40)$$

Also, by substituting Eq. (3.40) into Eq. (3.30), we get

$$F_{II} = -\frac{\beta_2\beta_4}{3\beta_6} + \frac{2\beta_4^3}{27\beta_6^2} - \frac{2}{27\beta_6^2}(\beta_4^2 - 3\beta_2\beta_6)^{3/2} \quad (3.41)$$

Next, equate the free energies of liquid (Eq. 2.8) and solid II (Eq. 3.41)

$$F_L = F_{II} \quad (3.42)$$

Then, we can write

$$-\frac{\beta_2\beta_4}{3\beta_6} + \frac{2\beta_4^3}{27\beta_6^2} - \frac{2}{27\beta_6^2}(\beta_4^2 - 3\beta_2\beta_6)^{3/2} = 0 \quad (3.43)$$

After some calculations, we can finally find the phase line equation for the liquid-solid II transition as

$$\beta_4^2 = 4\beta_2\beta_6 \tag{3.44}$$

or

$$b = \beta_4^2 - 4\beta_2\beta_6 = 0 \tag{3.45}$$

This is the phase line equation for the liquid-solid II transition, which represents the melting curve in the phase diagram of $(NH_4)_2SO_4/H_2O$.

Similarly, the functional form of both temperature and concentration for the liquid-solid II is given as:

$$b = 0 = (T - T_m) - [\beta_1(X - X_m) + \beta_2(X - X_m)^2 + \beta_3(X - X_m)^3] \tag{3.46}$$

Fig. 3.12 also shows the liquid-solid II phase transition. Our fitted phase line equation of liquid-solid II transition is:

$$T = -3193.60 + 212.43W - 4.93W^2 + 0.040W^3 \tag{3.47}$$

By equating Eqs. (3.46) and (3.47), we can calculate the coefficients β_1, β_2 and β_3 whose values are written in Table 3.7.

In order to derive the phase line equation for the transition between two solid phases, namely, solid I and solid II, we use the condition that

$$c = F_I - F_{II} = 0 \tag{3.48}$$

for the first order transition, as indicated above. In order to calculate this difference between two free energies of the solid phases, we first define the free energies of the solid phases (Eqs. 3.32 and 3.41) as

$$F_I = \frac{d}{\alpha_6^2} \tag{3.49}$$

and

$$F_{II} = \frac{e}{\beta_6^2} \tag{3.50}$$

where

$$d = \frac{1}{108}\left[\alpha_4(9\alpha - \alpha_4^2) - (\alpha_4^2 + 3\alpha)^{3/2}\right] \tag{3.51}$$

$$\alpha = \alpha_2\alpha_6 \tag{3.52}$$

$$e = \frac{1}{108}\left[\beta_4(9\beta - \beta_4^2) - (\beta_4^2 + 3\beta)^{3/2}\right] \tag{3.53}$$

and

$$\beta = \beta_2\beta_6 \tag{3.54}$$

By obtaining the difference between F_I and F_{II} according to Eq. (3.48), we get

$$c = \frac{d}{\alpha_6^2} - \frac{e}{\beta_6^2} = 0 \tag{3.55}$$

This represents the phase line equation for the transition between solid I and solid II in $(NH_4)_2SO_4/H_2O$.

Similarly, the functional form of both temperature and concentration for the solid I-solid II is given as:

$$c = 0 = (T - T_m) - [\gamma_1(X - X_m) + \gamma_2(X - X_m)^2 + \gamma_3(X - X_m)^3] \tag{3.56}$$

Fig. 3.12 also shows the solid I-solid II phase transition. Our fitted phase line equation of liquid-solid II transition is:

$$T = 292.10 - 17.86W + 0.36W^2 - 0.0027W^3 \tag{3.57}$$

By equating Eqs. (3.56) and (3.57), we can calculate the coefficients γ_1, γ_2 and γ_3 whose values are written in Table 3.7.

3.2.3 Lithium Potassium Rubidium Sulfate

There are four solid phases in a mixed crystal of $LiK_{1-x}Rb_xSO_4$. We expand the free energies of phases II, III, IV, and V in terms of their order parameters ψ, η, ξ, and ϕ, respectively. This gives

$$F_{II} = a_2\psi^2 + a_4\psi^4 + a_6\psi^6 \tag{3.58}$$

$$F_{III} = b_2\eta^2 + b_4\eta^4 + b_6\eta^6 \tag{3.59}$$

$$F_{IV} = c_2\xi^2 + c_4\xi^4 + c_6\xi^6 \tag{3.60}$$

$$F_V = d_2\phi^2 + d_4\phi^4 + d_6\phi^6 \tag{3.61}$$

In the above relations, the coefficients a_2, a_4, and a_6 (eq. 3.58), b_2, b_4, and b_6 (eq. 3.59), c_2, c_4, and c_6 (eq. 3.60), and d_2, d_4, and d_6 (eq. 3.61) are assumed to depend upon the temperature T and concentration X. In those relations (eqs. 3.58-3.61), we take $a_2 > 0$, $a_4 < 0$, and $a_6 > 0$ (eq. 3.58), $b_2>0$, $b_4<0$, and $b_6>0$ (eq. 3.59), $c_2>0$,

$c_4<0$, and $c_6>0$ (eq. 3.60), and $d_2>0$, $d_4<0$, and $d_6>0$ (eq. 3.61) as for a first-order transition exhibited by a mixed crystal of $LiK_{1-x}Rb_xSO_4$.

In order to express the order parameters in terms of the coefficients, we minimize the free energies (eqs. 3.58-3.61) with respect to their order parameters (ψ, η, ξ, and ϕ). We then obtain

$$\psi^2 = \frac{1}{3a_6}\left[-a_4 + (a_4^2 - 3a_2a_6)^{1/2}\right] \tag{3.62}$$

$$\eta^2 = \frac{1}{3b_6}\left[-b_4 + (b_4^2 - 3b_2b_6)^{1/2}\right] \tag{3.63}$$

$$\xi^2 = \frac{1}{3c_6}\left[-c_4 + (c_4^2 - 3c_2c_6)^{1/2}\right] \tag{3.64}$$

$$\phi^2 = \frac{1}{3d_6}\left[-d_4 + (d_4^2 - 3d_2d_6)^{1/2}\right] \tag{3.65}$$

Thus, using the temperature and concentration dependences of the coefficients a_2, a_4, and a_6 (eq. 3.62), b_2, b_4, and b_6 (eq. 3.63), c_2, c_4, and c_6 (eq. 3.64) and d_2, d_4, and d_6 (eq. 3.65), the order parameters (ψ, η, ξ, and ϕ) can be obtained as functions of temperature and concentration.

In order to obtain a T –X phase diagram of $LiK_{1-x}Rb_xSO_4$ from our mean field model, we use the condition for a first-order phase transition according to which we equate the free energies of two phases along the transition line. We apply this condition for all the phase transitions occuring in this mixed crystal.

First of all, we calculate the solid II-solid III phase transition. By equating F_{II} to F_{III}, we then get the phase line equation as

$$a_2\psi^2 + a_4\psi^4 + a_6\psi^6 = b_2\eta^2 + b_4\eta^4 + b_6\eta^6 \tag{3.66}$$

This can be written as an f function given by

$$a_2\psi^2 + a_4\psi^4 + a_6\psi^6 - (b_2\eta^2 + b_4\eta^4 + b_6\eta^6) = f = 0 \tag{3.67}$$

By employing the temperature and concentration dependences of the f function, which is due to the temperature and concentration dependences of the coefficients a_2, a_4, and a_6 and b_2, b_4, and b_6, (Eq. 3.67) can be written in a function form as

$$f = 0 = f_0\{(T - T_t) - [\alpha_1(X - X_t) + \alpha_2(X - X_t)^2]\} \quad (3.68)$$

where f_0, α_1, and α_2 are constants. In Eq. (3.68), X_t denotes an equal concentration of Rb and K (X_t=0.5) according to the experimental phase diagram of $LiK_{1-x}Rb_xSO_4$ [25]. T_t corresponds to a constant temperature at $X=X_t$ for the II-III phase transition in this mixed crystal [25]. From Eq. (3.68), we can obtain the T-X phase line equation as

$$T = \frac{1}{f_0}[f_0(T_t - \alpha_1 X_t + \alpha_2 X_t^2) + f_0 X(\alpha_1 - 2\alpha_2 X_t) + f_0 \alpha_2 X^2] \quad (3.69)$$

for the II-III phase transition on cooling in $LiK_{1-x}Rb_xSO_4$ [70].

By fitting the experimental data [25], we calculated here the T-X phase diagram of $LiK_{1-x}Rb_xSO_4$ for the II-III phase transition. When we fitted Eq. (3.69) to the experimental data [25], these relations were reduced to a quadratic equation given by

$$T = a + bX + cX^2 \quad (3.70)$$

where a, b, and c are constants. Using the experimental measurements that have been taken for the II-III, III-IV, and IV-V transitions on cooling and heating [25], we calculated our phase line equations between cooling and heating curves. This is because of the condition for a first-order transition according to which the free energies are equal for the II-III, III-IV, and IV-V transitions in $LiK_{1-x}Rb_xSO_4$ [71].

Using the values of T_t and X_t, as given in Table 3.8 for the II-III transition in Eq. (3.69), the quadratic relation (Eq. 3.70) was employed and the coeffiicents a, b, and c were obtained. We tabulate the values of a, b, and c in Table 3.8 for the II-III transition of $LiK_{1-x}Rb_xSO_4$. Table 3.9 gives the values of α_1, α_2, and f_0 from the fitting of Eq. (3.69) to the experimental data [25] for the II-III transition of this crystal. We present the experimental values for T_t and X_t on cooling and heating [25] for the II-III, III-IV and IV-V transitions in $LiK_{1-x}Rb_xSO_4$ in Table 3.10.

Table 3.8 Values of the coefficients a, b, and c according to Eq. (3.70) at the temperature T_t and concentration X_t (Rb) for the transitions indicated on the basis of the experimental (cooling and heating) T-X phase diagram of $LiK_{1-x}Rb_xSO_4$ [25].

Phase transition	T_t (K)	X_t (c. a)	a (K)	b (K/ c. a)	c[K/(c. a)^2]
II-III	600.43	0.50	708.77	-116.21	-200.46
III-IV	409.42	0.50	224.82	295.54	144.67
IV-V	119.37	0.20	178.82	-85.64	-1045.40

Figure 3.13 shows our calculated T-X phase diagram obtained using the phase line equations for the II-III, III-IV and IV-V transitions of $LiK_{1-x}Rb_xSO_4$, respectively, together with the experimental data points [25].

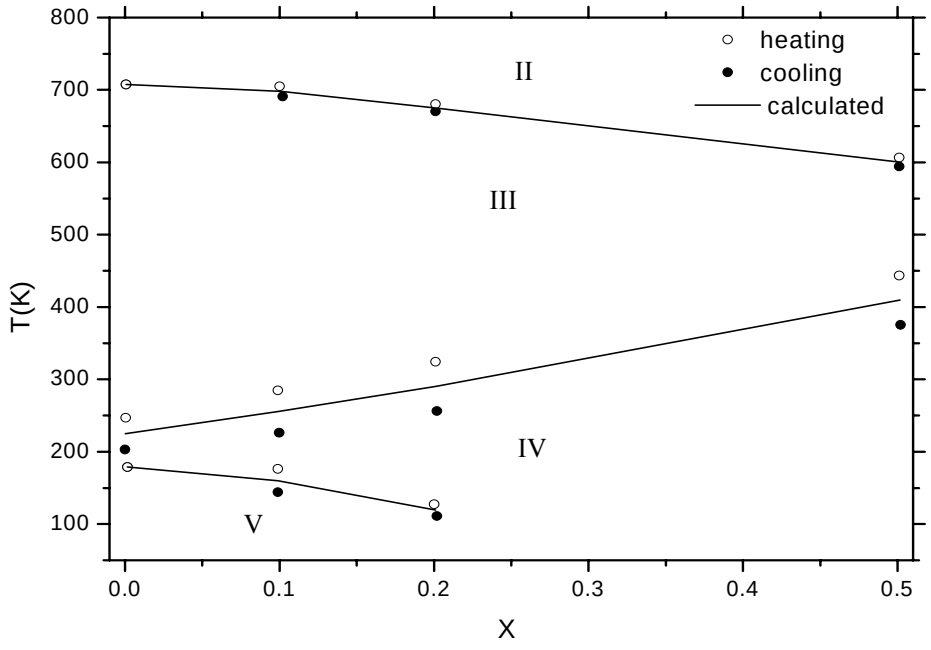

Figure 3.13 T-X phase diagram calculated from our mean field model for the phases indicated for $LiK_{1-x}Rb_xSO_4$. Solid lines represent our calculated phase lines. Experimental data on heating and cooling is also shown here [25].

Table 3.9 Values of the coefficients for the transitions according to equations indicated in $LiK_{1-x}Rb_xSO_4$.

Phase transitions	K/ c. a	K/(c. a)^2	Parameters	Equations
II-III	α_1=-200.46	α_2=-316.67	f_0=1.000	3.69
III-IV	β_1=441.09	β_2=144.96	h_0=0.998	3.75
IV-V	γ_1=-501.79	γ_2=-1041.24	k_0=1.004	3.80

Table 3.10 Values of the measured temperature T_t and concentration X_t (Rb) on cooling and heating for the transitions indicated, as given in the experimental T-X phase diagram of $LiK_{1-x}Rb_xSO_4$ [25].

Phase transitions	Cooling		Heating	
	T_t (K)	X_t (c. a)	T_t (K)	X_t (c. a)2
II-III	594.40	0.50	606.46	0.50
III-IV	375.23	0.50	446.60	0.50
IV-V	112.32	0.20	127.42	0.20

Similarly for the solid III-solid IV phase transition, we have

$$F_{III} = F_{IV} \tag{3.71}$$

Using Eqs. (3.59) and (3.60), Eq. (3.71) becomes

$$b_2\eta^2 + b_4\eta^4 + b_6\eta^6 = c_2\xi^2 + c_4\xi^4 + c_6\xi^6 \tag{3.72}$$

Using the h function here, Eq. (3.72) can be expressed as

$$b_2\eta^2 + b_4\eta^4 + b_6\eta^6 - (c_2\xi^2 + c_4\xi^4 + c_6\xi^6) = h = 0 \tag{3.73}$$

By regarding the temperature and concentration dependences of the coefficients b_2, b_4, and b_6 and c_2, c_4, and c_6, the h function can be written as

$$h = 0 = h_0\{(T - T_t) - [\beta_1(X - X_t) + \beta_2(X - X_t)^2]\} \quad (3.74)$$

where h_0, β_1, and β_2 are constants. Hence, the T-X phase line equation can be obtained from Eq. (3.74) as

$$T = \frac{1}{h_0}[h_0(T_t - \beta_1 X_t + \beta_2 X_t^2) + h_0 X(\beta_1 - 2\beta_2 X_t) + h_0\beta_2 X^2] \quad (3.75)$$

for the III-IV phase transition, where X_t denotes the equal concentrations of Rb and K (X_t=0.5), as before according to the experimental T-X phase diagram of $LiK_{1-x}Rb_xSO_4$ [25].

For the III-IV transition of $LiK_{1-x}Rb_xSO_4$, Eq. (3.75) was fitted to the experimental data [25]. From our fitting, the coefficients β_1, β_2, and h_0 (Eq. 3.75) was obtained, as given in Table 3.9 for the III-IV transition. By using the T_t and X_t values (Table 3.8) in Eq. (3.75), the values of the coefficients a, b, and c were deduced according to Eq. (3.70) for the III-IV transition of $LiK_{1-x}Rb_xSO_4$, as given in Table 3.8 [70].

Finally, we calculate the solid IV-solid V phase transition as

$$F_{IV} = F_V \quad (3.76)$$

Using Eqs. (3.60) and (3.61), we have

$$c_2\xi^2 + c_4\xi^4 + c_6\xi^6 = d_2\phi^2 + d_4\phi^4 + d_6\phi^6 \quad (3.77)$$

By defining a functional k, Eq. (3.77) can be written as

$$c_2\xi^2 + c_4\xi^4 + c_6\xi^6 - (d_2\phi^2 + d_4\phi^4 + d_6\phi^6) = k = 0 \quad (3.78)$$

By employing the temperature and concentration dependences of the coefficients c_2, c_4, and c_6, and d_2, d_4, and d_6, the functional k can be expressed in a quadratic form as functions of temperature and concentration, given by

$$k = 0 = k_0\{(T - T_t) - [\gamma_1(X - X_t) + \gamma_2(X - X_t)^2]\} \quad (3.79)$$

where k_0, γ_1, and γ_2 are constants. Thus, the phase line equation for the IV-V transition can be obtained as

$$T = \frac{1}{k_0}[k_0(T_t - \gamma_1 X_t + \gamma_2 X_t^2) + k_0 X(\gamma_1 - 2\gamma_2 X_t) + k_0 \gamma_2 X^2] \quad (3.80)$$

where X_t=0.20 (concentration of Rb %20) according to the experimental data in the T-X phase diagram of $LiK_{1-x}Rb_xSO_4$ [25]. T_t corresponds to a constant temperature on the phase line between phases IV and V in this mixed crystal. For the IV-V transition of $LiK_{1-x}Rb_xSO_4$, Eq. (3.80) was fitted to the experimental data [25] and, the coefficients γ_1, γ_2, and k_0 were extracted, which we tabulate in Table 3.9 for the IV-V phase transition of this mixed crystal. Again, using the values of T_t and X_t (Table 3.8), values of a, b, and c according to Eq. (3.70) were obtained, as given in Table 3.8 for the IV-V phase transition in $LiK_{1-x}Rb_xSO_4$.

3.2.4 Potassium Pyrosulfate-Potassium Hydrogensulfate (Potassium bisulfate)

For this system, we have four phases, which are labelled as liquid, solid I, solid II and solid III. We obtain the phase line equations for the liquid-solid I, liquid-solid II, solid I-solid II, solid II-solid III and liquid-solid III transitions for the $K_2S_2O_7$-$KHSO_4$ system by using the mean field theory [72]. In order to calculate the phase line equations, first, we define the free energies of these four phases. The free energies of the solid phases are expanded in terms of the order parameters. Using the conditions for the first order or second order transitions, the phase line equations are derived in terms of the coefficients given in the free energy expansion [72].

$$F_L = 0 \quad (2.8)$$

$$F_I = a_2\psi^2 + a_4\psi^4 + a_6\psi^6 \quad (3.81)$$

$$F_{II} = b_2\eta^2 + b_4\eta^4 + b_6\eta^6 \quad (3.82)$$

$$F_{III} = c_2\mu^2 + c_4\mu^4 + c_6\mu^6 \quad (3.83)$$

where ψ, η and μ are the order parameters of solid I, solid II and solid III, respectively. Minimizing the free energies with respect to the their order parameters gives

$$\psi^2 = \frac{1}{3a_6}\left[-a_4 + (a_4^2 - 3a_2a_6)^{1/2}\right] \quad (3.84)$$

$$\eta^2 = \frac{1}{3b_6}\left[-b_4 + (b_4^2 - 3b_2b_6)^{1/2}\right] \quad (3.85)$$

$$\mu^2 = \frac{1}{3c_6}\left[-c_4 + (c_4^2 - 3c_2c_6)^{1/2}\right] \quad (3.86)$$

Inserting these order parameters (Eqs. 3.84-3.86) into the free energy equations (Eqs. 3.81-3.83), we get

$$F_I = -\frac{a_2a_4}{3a_6} + \frac{2a_4^3}{27a_6^2} - \frac{2}{27a_6^2}(a_4^2 - 3a_2a_6)^{3/2} \quad (3.87)$$

$$F_{II} = -\frac{b_2b_4}{3b_6} + \frac{2b_4^3}{27b_6^2} - \frac{2}{27b_6^2}(b_4^2 - 3b_2b_6)^{3/2} \quad (3.88)$$

$$F_{III} = -\frac{c_2c_4}{3c_6} + \frac{2c_4^3}{27c_6^2} - \frac{2}{27c_6^2}(c_4^2 - 3c_2c_6)^{3/2} \quad (3.89)$$

After writing the free energies of the solid states, the phase line equations are obtained by using the first order condition in $K_2S_2O_7$-$KHSO_4$. First of all, we calculate the liquid-solid I phase transition by using the equation of

$$F_I = F_L \quad (3.90)$$

or

$$0 = -\frac{a_2a_4}{3a_6} + \frac{2a_4^3}{27a_6^2} - \frac{2}{27a_6^2}(a_4^2 - 3a_2a_6)^{3/2} \quad (3.91)$$

Then, we get

$$-\frac{9a_2a_4a_6}{27a_6^2} + \frac{2a_4^3}{27a_6^2} = \frac{2}{27a_6^2}(a_4^2 - 3a_2a_6)^{3/2} \quad (3.92)$$

Next, we eliminate the denominators and take the square of both sides. Finally we get the phase line equation as

$$a_4^2 = 4a_2a_6 \quad (3.93)$$

This is the phase line equation for liquid-solid I in $K_2S_2O_7$-$KHSO_4$.

Next, to calculate the phase line equation for liquid-solid II, we equate the free energies of these two phases.

$$F_L = F_{II} \quad (3.94)$$

We get

$$0 = -\frac{b_2 b_4}{3b_6} + \frac{2b_4^3}{27b_6^2} - \frac{2}{27b_6^2}(b_4^2 - 3b_2 b_6)^{3/2} \quad (3.95)$$

We calculate the liquid-solid II phase line equation as phase line equation for liquid-solid I.

$$b_4^2 = 4b_2 b_6 \quad (3.96)$$

This is liquid-solid II phase line equation in $K_2S_2O_7$-$KHSO_4$.

The third phase transition is liquid-solid III transition. To get the phase line equation for this transition, we, similarly, equate the free energies of both phases.

$$F_L = F_{III} \quad (3.97)$$

This gives us

$$0 = -\frac{c_2 c_4}{3c_6} + \frac{2c_4^3}{27c_6^2} - \frac{2}{27c_6^2}(c_4^2 - 3c_2 c_6)^{3/2} \quad (3.98)$$

Doing the same calculations with the liquid-solid I part, we obtain

$$c_4^2 = 4c_2 c_6 \quad (3.99)$$

This is liquid-solid III phase line equation in $K_2S_2O_7$-$KHSO_4$.

The fourth phase transition in $K_2S_2O_7$-$KHSO_4$ is solid I-solid II phase transition. Equating the free energies of solid I and solid II, we get

$$-\frac{a_2 a_4}{3a_6} + \frac{2a_4^3}{27a_6^2} - \frac{2}{27a_6^2}(a_4^2 - 3a_2 a_6)^{3/2} = -\frac{b_2 b_4}{3b_6} + \frac{2b_4^3}{27b_6^2} - \frac{2}{27b_6^2}(b_4^2 - 3b_2 b_6)^{3/2} \quad (3.100)$$

Eq. (3.100) is the phase line equation for the solid I-solid II transition.

Finally, we calculate the fifth phase transition in $K_2S_2O_7$-$KHSO_4$, which is solid II-solid III phase transition.

$$F_{II} = F_{III} \quad (3.101)$$

Inserting Eqs. (3.88) and (3.89) into Eq. (3.101), the phase line equation for the solid II-solid III transition is obtained as

$$-\frac{b_2 b_4}{3b_6}+\frac{2b_4^3}{27b_6^2}-\frac{2}{27b_6^2}(b_4^2-3b_2 b_6)^{3/2}=-\frac{c_2 c_4}{3c_6}+\frac{2c_4^3}{27c_6^2}-\frac{2}{27c_6^2}(c_4^2-3c_2 c_6)^{3/2} \qquad (3.102)$$

After obtaining the five phase line equations for the transitions of liquid-solid I (L-I)(Eq. 3.93), liquid-solid II (L-II) (Eq. 3.96), liquid-solid III (L-III) (3.99), solid I-solid II (I-II) (3.100) and solid II-solid III (II-III) (Eq. 3.102), we fit the experimental data [35] in a quadratic form as given below:

$$f(\tau-\xi)=\tau-\alpha_1\xi-\alpha_2\xi^2=0 \qquad (3.103)$$

where τ =T-T_t and ξ = X-X_t represent the temperature and concentration variables with the triple point (T_t, X_t). For the $K_2S_2O_7$-$KHSO_4$ system we consider the triple point as the melting point.

By writing the temperature and concentration dependencies of the coefficients in the free energies of solid I, solid II and solid III, we get the phase line equations of five phase transitions as given above (Eq. 3.103). By fitting the experimental data [35], we obtain the T-X phase diagram of $K_2S_2O_7$-$KHSO_4$ system. After obtaining this T-X phase diagram, we calculate the values of the coefficients α_1 and α_2 for the transitions L-I, L-II, L-III, I-II and II-III which are given in Table 3. 11. In Eq. (3.103), for the transitions among the liquid-solid I (α-$K_2S_2O_7$+liquid) and liquid-solid II (β- $K_2S_2O_7$+liquid), the melting point has the coordinates of T_t=318 ^{0}C and X_t=0.45, as measured experimentally [35]. This is also the triple point among the phase lines of L-I, L-II and I-II in $K_2S_2O_7$-$KHSO_4$. With those values of the fitted parameters α_1 and α_2, we calculated phase lines for the transitions considered here and we obtained T- X_{KHSO_4} phase diagram, as given in Fig. 3.14. Experimental data points are also plotted here. For the phase lines related to the transitions of L-I, L-II and I-II we used the values of the triple point, as given above. For the transitions of L-III and II-III, we used the values of the melting point or the coordinates of the triple point, namely, T_t=205 ^{0}C and X_t=0.92 [35] for this system. The melting curve between liquid and solid II also terminates at this triple point [72].

Table 3.11 Values of the fitted parameters α_1 and α_2 for the transitions indicated here for the $K_2S_2O_7$-$KHSO_4$ solvent system according to Eq. (3.103).

Eq. 3.1	α_1 (^{0}C/mole)	α_2 (^{0}C/mole^2)
L-I	267.002	64.451
L-II	37.378	422.292
I-II	43.534	89.964
L-III	-106.25	312.5
II-III	5.989	15.211

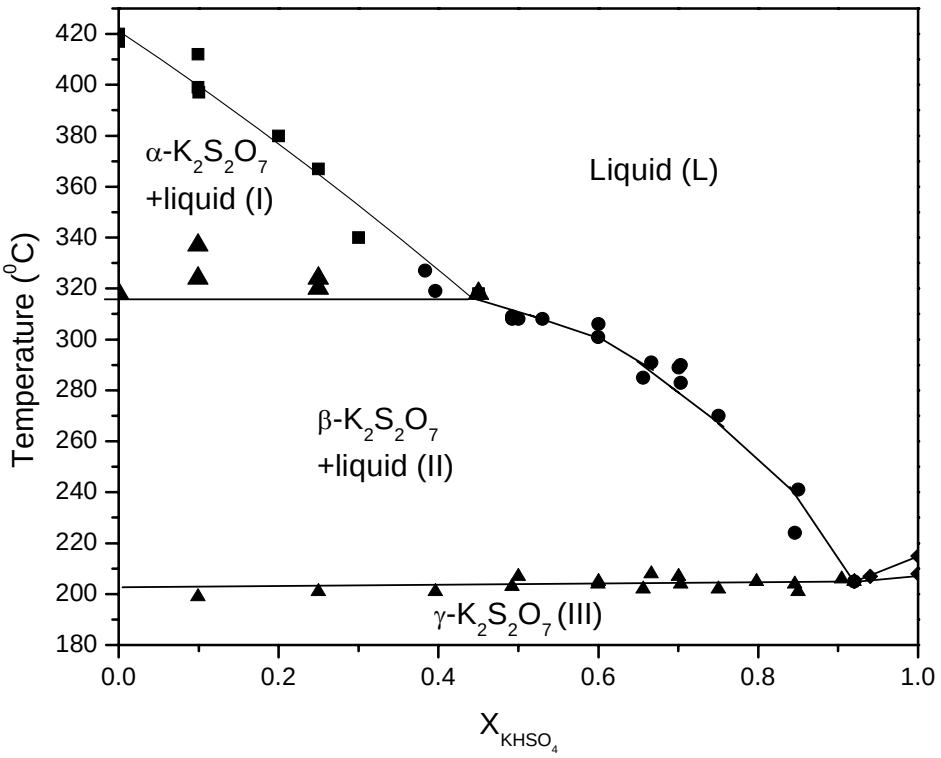

Figure 3.14 Phase diagram of the $K_2S_2O_7$-$KHSO_4$ system obtained from Conductance(■), DEA (♦), TA (▲) and NIR (●) measurements [35]. Our calculated phase lines using the mean field theory, are shown as solid lines.

3.2.5 Cholestanyl Myristate (CnM)-Cholesteryl Myristate (CrM) and Cholestanyl Myristate (CnM)-Cholesteryl Oleate (CO)

We have three different temperature versus concentration diagrams for binary mixtures of cholestanyl myristate-cholesteryl myristate and cholestanyl myristate-cholesteryl oleate. We calculate four phases transition of the first binary mixture, cholestanyl myristate-cholesteryl myristate and six phase transition for the binary mixture of cholestanyl myristate-cholesteryl oleate.

We start with the phase transitions of cholestanyl myristate-cholesteryl myristate. First, we have isotropic liquid- cholesteric phase transition. As mentioned in the section 2.4, we write the free energy of the isotropic liquid as

$$F_L = 0 \tag{2.8}$$

The free energy of the cholesteric phase is:

$$F_{CL} = a_2\eta^2 + a_4\eta^4 + a_6\eta^6 \tag{3.104}$$

where η is the orientational order parameter, a_2, a_4 and a_6 are dependent on the temperature and concentration and F_{CL} denotes the free energy of the cholesteric (C) phase which undergoes the isotropic liquid (L) [73]. After defining the free energies of these two states, we minimize the free energy F_{CL} with respect to the orientational order parameter η and we get

$$\eta^2 = \frac{1}{3a_6}\left[-a_4 + (a_4^2 - 3a_2a_6)^{1/2}\right] \tag{3.105}$$

Using the ansazt $\frac{a_2a_6}{a_4^2} \ll 1$, we write

$$(a_4^2 - 3a_2a_6)^{1/2} \cong a_4\left(1 - \frac{3}{2}\frac{a_2a_6}{a_4^2}\right) = a_4 - \frac{3}{2}\frac{a_2a_6}{a_4} \tag{3.106}$$

Insert Eq. (3.106) into Eq. (3.105),

$$\eta^2 = \frac{1}{3a_6}\left[-a_4 + a_4 - \frac{3}{2}\frac{a_2a_6}{a_4}\right] = -\frac{a_2}{2a_4} \tag{3.107}$$

Using Eq. (3.107) into Eq. (3.104), we get

$$F_{CL} = -\frac{a_2^2}{4a_4} - \frac{a_2^3a_6}{8a_4^3} \tag{3.108}$$

To get the phase line equation, we equate the free energies of the isotropic liquid (Eq. 2.8) and the cholesteric (Eq. 3.108) phases:

$$a_2 a_6 = -2a_4^2 \tag{3.109}$$

After writing the phase line equation, we calculate the temperature and concentration dependence of the phase line by assuming the temperature and the concentration dependencies of the coefficients which are given below:

$$a_2 = a_{20}(T - T_C)^{1/2} \tag{3.110}$$

$$a_4 = a_{40} + a_{41}(X - X_C) \tag{3.111}$$

$$a_6 = a_{60}(T - T_C)^{1/2} \tag{3.112}$$

Using the Eqs. (3.109)-(3.112), we obtain

$$T = T_C - \frac{2a_{40}^2}{a_{20}a_{60}} - \frac{4a_{40}a_{41}}{a_{20}a_{60}}(X - X_C) - \frac{2a_{41}^2}{a_{20}a_{60}}(X - X_C)^2 \tag{3.113}$$

This is the phase line equation for the isotropic liquid-cholesteric transition.

The second phase transition is the cholesteric-smectic phase transition. Since the orientational order parameter η exists in both cholesteric and smectic phases, for the transition between the two phases, we expand the free energy in terms of the positional order parameter ψ of the smectic phase. The free energy of the smectic phase for the cholesteric – smectic transition is then expressed as [73]

$$F_{CS} = b_2\psi^2 + b_4\psi^4 + b_6\psi^6 \tag{3.114}$$

In this free energy expansion the coefficients b_2, b_4 and b_6 are taken as temperature and concentration dependent. We minimize the free energy F_{CS} with respect to the positional order parameter ψ and using the ansatz $\frac{b_2 b_6}{b_4^2} \ll 1$, similarly as the above phase transition calculations, we get

$$\psi^2 = -\frac{b_2}{2b_4} \tag{3.115}$$

By inserting Eq. (3.115) into Eq. (3.114) and equating this obtained equation to Eq. (3.108) , we get

$$a_2^2 b_4(2a_4^2 + a_2 a_6) = a_4 b_2^2\left(2 + \frac{b_2 b_6}{b_4^2}\right) \tag{3.116}$$

The temperature and concentration dependencies of the coefficients are given below:

$$b_2 = b_{20}(T - T_C)(X - X_C)^{1/2} \tag{3.117}$$

$$b_4 = b_{40}(T - T_C)(X - X_C) \tag{3.118}$$

$$b_6 = b_{60}(T - T_C)(X - X_C)^{3/2} \tag{3.119}$$

By using Eqs. (3.110)-(3.112), (3.116) and (3.117)-(3.119), we end up with the phase line equation of cholesteric – smectic transition:

$$T = \left\{ T_C + \frac{\left[a_{40}^3 b_{20}\left(2+\frac{b_{20}b_{60}}{b_{40}^2}\right) - 2a_{20}^2 b_{40} a_{40}^2 \right]}{a_{20}^3 a_{60} b_{40}} \right\} + \frac{\left[3a_{40}^2 a_{41} b_{20}\left(2+\frac{b_{20}b_{60}}{b_{40}^2}\right) - 4a_{20}^2 a_{40} a_{41} b_{40} \right]}{a_{20}^3 a_{60} b_{40}} (X - X_C) + \frac{\left[3a_{40} a_{41}^2 b_{20}\left(2+\frac{b_{20}b_{60}}{b_{40}^2}\right) - 2a_{20}^2 a_{41}^2 b_{40} \right]}{a_{20}^3 a_{60} b_{40}} (X - X_C)^2 \tag{3.120}$$

where we assume that $a_{41}^3 b_{20}\left(2 + \frac{b_{20}b_{60}}{b_{40}^2}\right) \approx 0$.

The third phase transition is smectic-isotropic liquid phase transition. We expand the free energy in terms of the two order parameters, orientational order parameter η and the positional order parameter ψ of the smectic phase. Since the free energy of the isotropic liquid phase is zero (Eq. 2.8), we then write [59]

$$F_{SL} = a_2\eta^2 + a_4\eta^4 + a_6\eta^6 + b_2\psi^2 + b_4\psi^4 + b_6\psi^6 + c\eta^2\psi^2 \tag{3.121}$$

In this expansion *c* is the coupling constant between the two order parameters η and ψ. The coupling constant *c* can also depend on temperature and concentration.

By inserting Eqs. (3.107) and (3.115) into Eq. (3.121), we finally end up with the below equation

$$F_{SL} = -\frac{a_2^2}{4a_4} - \frac{a_2^3 a_6}{8a_4^3} - \frac{b_2^2}{4b_4} - \frac{b_2^3 b_6}{8b_4^3} + \frac{c a_2 b_2}{4a_4 b_4} \tag{3.122}$$

To obtain the phase line equation, we use the equality of the free energies of the isotropic liquid (Eq 2.8) and the smectic (Eq. 3.122) phases

$$2c a_2 b_2 a_4^2 = a_2^2 b_4 (2a_4^2 + a_2 a_6) + a_4^3 b_2^2 \left(2 + \frac{b_2 b_6}{b_4^2}\right) \tag{3.123}$$

and finally insert Eqs. (3.110)-(3.112) and (3.117)-(3.119) into Eq. (3.123) with $c = c_0(T - T_C)^{-3/2}(X - X_C)^{-1/2}(a_{40} + a_{41}(X - X_C))^{-2}$.

$$T = -\left\{T_C + 2c_0a_{20}b_{20} + \frac{\left[a_{40}^3 b_{20}\left(2+\frac{b_{20}b_{60}}{b_{40}^2}\right)+2a_{20}^2 b_{40}a_{40}^2\right]}{a_{20}^3 a_{60}b_{40}}\right\} -$$

$$\frac{\left[3a_{40}^2 a_{41}b_{20}\left(2+\frac{b_{20}b_{60}}{b_{40}^2}\right)+4a_{20}^2 a_{40}a_{41}b_{40}\right]}{a_{20}^3 a_{60}b_{40}}(X - X_C) -$$

$$\frac{\left[3a_{40}a_{41}^2 b_{20}\left(2+\frac{b_{20}b_{60}}{b_{40}^2}\right)+2a_{20}^2 a_{41}^2 b_{40}\right]}{a_{20}^3 a_{60}b_{40}}(X - X_C)^2 \qquad (3.124)$$

Eq. (3.124) is the phase line equation for the smectic – isotropic liquid transition in a binary mixture of cholesteryl myristate-cholestanyl myristate.

The fourth phase in a binary mixture of cholesteryl myristate-cholestanyl myristate is the isotropic liquid-solid solution phase transition. By defining the long-range order parameter Q for the solid solution phase (free energy is zero in the isotropic liquid phase), the free energy of the solid solution can be expanded simply in terms of the order parameter Q. The free energy of the solid phase for the transition between the isotropic liquid and the solid solution is then written as [73]

$$F_S = c_2Q^2 + c_4Q^4 + c_6Q^6 \qquad (3.125)$$

Here the coefficients c_2, c_4 and c_6 are also assumed to depend upon the temperature and concentration. Minimizing the free energy F_S with respect to the order parameter Q gives

$$Q^2 = \frac{-c_4+(c_4^2-3c_2c_6)^{1/2}}{3c_6} \qquad (3.126)$$

By inserting Eq. (3.126) into Eq. (3.125), we have

$$F_S = -\frac{c_2c_4}{3c_6} + \frac{2c_4^3}{27c_6^2} - \frac{2}{27c_6^2}(c_4^2 - 3c_2c_6)^{3/2} \qquad (3.127)$$

To obtain the phase transition, equate Eq. (3.127) to Eq. (2.8) which gives

$$\frac{2c_4^3}{27c_6^2} - \frac{9c_2c_4c_6}{27c_6^2} = \frac{2}{27c_6^2}(c_4^2 - 3c_2c_6)^{3/2} \qquad (3.128)$$

After some calculations, we obtain

$$c_4^2 = 4c_2c_6 \tag{3.129}$$

This is the phase line equation of the isotropic liquid-solid solution. The temperature and the concentration dependencies of the coefficients are given below:

$$c_2 = c_{20}(X - X_C) \tag{3.130}$$

$$c_4 = c_{40}(T - T_C)^{1/2} \tag{3.131}$$

$$c_6 = c_{60} + c_{61}(X - X_C) \tag{3.132}$$

By inserting Eqs. (3.130)-(3.132) into Eq. (3.129), we obtain

$$T = T_C + \frac{4c_{20}c_{60}}{c_{40}^2}(X - X_C) + \frac{4c_{20}c_{61}}{c_{40}^2}(X - X_C)^2 \tag{3.133}$$

Eq. (3.133) represents the phase line equation for the transition of isotropic liquid - solid solution [73].

The fifth phase transition is the isotropic liquid-(solid CnM+liquid) phase transition in a binary mixture of cholestanyl myristate-cholesteryl oleate. Since the solid phase of cholestanyl myristate (CnM) is the ordered phase with the long-range order parameter ψ below the transition temperature T_C, the free energy of this phase can be expressed as

$$F_{CnM} = a_2\psi^2 + a_4\psi^4 + a_6\psi^6 \tag{3.134}$$

The free energy of the isotropic liquid phase is zero (Eq. 2.8), as before. The coefficients a_2, a_4 and a_6 are taken as functions of temperature and concentration. In order to obtain the phase line equation for the transition of isotropic liquid-(solid CnM+liquid), we minimize the free energy F_{CnM} with respect to the long-range order parameter ψ and use the ansazt $\frac{a_2a_6}{a_4^2} \ll 1$. This gives

$$\psi^2 = \frac{-a_2}{2a_4} \tag{3.135}$$

By inserting Eq. (3.135) into Eq. (3. 134), we get

$$F_{CnM} = -\frac{a_2^2}{4a_4} - \frac{a_2^3a_6}{8a_4^3} \tag{3.136}$$

and then equating Eq.(3.136) to Eq. (2.8), we get

$$a_2 a_6 = -2a_4^2 \tag{3.137}$$

This is the phase line equation of the isotropic liquid-(solid CnM+liquid) transition in a binary mixture of cholestanyl myristate-cholesteryl oleate. The temperature and the concentration dependencies of the coefficients are given below:

$$a_2 = a_{20}(T - T_C)^{1/2} \tag{3.138}$$

$$a_4 = a_{40} + a_{41}(X - X_C) \tag{3.139}$$

$$a_6 = a_{60}(T - T_C)^{1/2} \tag{3.140}$$

when we insert these three equations into Eq. (3.137), we get the temperature and concentration dependent phase line equation of the isotropic liquid-(solid CnM+liquid) in a binary mixture of cholestanyl myristate-cholesteryl oleate:

$$T = T_C - \frac{2a_{40}^2}{a_{20}a_{60}} - \frac{4a_{40}a_{41}}{a_{20}a_{60}}(X - X_C) - \frac{2a_{41}^2}{a_{20}a_{60}}(X - X_C)^2 \tag{3.141}$$

The sixth one is the isotropic liquid-(solid CO+liquid) phase transition. For this transition, we define the free energy of (solid CO+liquid) phase according to the long-range order parameter η.

$$F_{CO} = b_2\eta^2 + b_4\eta^4 + b_6\eta^6 \tag{3.142}$$

where the coefficients b_2, b_4 and b_6 are also temperature and concentration dependent as before. By minimizing the free energy F_{CO} of the (solid CO+ liquid) phase for a binary mixture of cholestanyl myristate (CnM)-cholesteryl oleate (CO) and using the ansazt $\frac{b_2 b_6}{b_4^2} \ll 1$, we then obtain the relation

$$\eta^2 = \frac{-b_2}{2b_4} \tag{3.143}$$

After inserting Eq. (3.140) into Eq. (3.139), we find the free energy of (solid CO +liquid) as:

$$F_{CO} = -\frac{b_2^2}{4b_4} - \frac{b_2^3 b_6}{8b_4^3} \tag{3.144}$$

By equating Eqs. (3.141) to (2.8), we get the phase line equation of the isotropic liquid-(solid CO+liquid) transition.

$$b_2 b_6 = -2b_4^2 \tag{3.145}$$

Let's assume that the temperature and the concentration dependencies of the coefficients as follows:

$$b_2 = b_{20}(T - T_C)^{1/2} \tag{3.146}$$

$$b_4 = b_{40} + b_{41}(X - X_C) \tag{3.147}$$

$$b_6 = b_{60}(T - T_C)^{1/2} \tag{3.148}$$

Finally use Eqs. (3.146)-(3.148) in Eq. (3.145). This gives

$$T = T_C - \frac{2b_{40}^2}{b_{20}b_{60}} - \frac{4b_{40}b_{41}}{b_{20}b_{60}}(X - X_C) - \frac{2b_{41}^2}{b_{20}b_{60}}(X - X_C)^2 \tag{3.149}$$

This is the phase line equation for the isotropic liquid-(solid CO+liquid) transition in CnM-CO mixture.

The seventh transition is the (solid CO+liquid)-(solid CO+solid CnM) transition. Since both solid phases, solid CO and (solid CO+solid CnM) have the order parameters, the mean field theory can be used by expanding the free energies in terms of both order parameters and their coupling (solid CO+solid CnM). Thus, the free energy of the (solid CO+liquid) phase is given by Eq. (3.142). Similarly, the free energy of the (solid CO+solid CnM) phase can be written as

$$F_{Co+CnM} = b_2\eta^2 + b_4\eta^4 + b_6\eta^6 + a_2\psi^2 + a_4\psi^4 + a_6\psi^6 + c\eta^2\psi^2 \tag{3.150}$$

where *c* is the coupling parameter for the (solid CO+liquid) – (solid CO+solid CnM) phase transition, which can depend on the temperature and concentration, as the coefficients a_2, a_4, a_6 ,b_2, b_4 and b_6 in Eq.(3.150). First, we calculate the free energy of (solid CO+solid CnM) in the following form by using the Eqs. (3.135)and (3.143)

$$F_{CO+CnM} = -\frac{a_2^2}{4a_4} - \frac{a_2^3 a_6}{8a_4^3} - \frac{b_2^2}{4b_4} - \frac{b_2^3 b_6}{8b_4^3} + \frac{ca_2b_2}{4a_4b_4} \tag{3.151}$$

To obtain the phase line equation, equate the free energies of (solid CO+liquid) and (solid CO+solid CnM).

$$-\frac{b_2^2}{4b_4} - \frac{b_2^3 b_6}{8b_4^3} = -\frac{a_2^2}{4a_4} - \frac{a_2^3 a_6}{8a_4^3} - \frac{b_2^2}{4b_4} - \frac{b_2^3 b_6}{8b_4^3} + \frac{ca_2b_2}{4a_4b_4} \tag{3.152}$$

And, then we obtain

$$\frac{a_2}{4a_4}\left[a_2+\frac{a_2^2a_6}{2a_4^2}\right]=\frac{a_2}{4a_4}\frac{cb_2}{b_4} \tag{3.153}$$

Finally, we obtain the phase line equation as

$$\frac{cb_2}{b_4}=a_2+\frac{a_2^2a_6}{2a_4^2} \tag{3.154}$$

Insert Eqs. (3.138), (3.139), (3.140), (3.146) and (3.147) into Eq. (3.154) and by using $c=c_1+c_2(X-X_C)$ with $c_1=c_0b_{40}$ and $c_2=c_0b_{41}$, we get

$$T=\left[T_C+\frac{2a_{40}^2(c_0b_{20}-a_{20})}{a_{20}^2a_{60}}\right]+\frac{4a_{40}a_{41}(c_0b_{20}-a_{20})}{a_{20}^2a_{60}}(X-X_C)$$

$$+\frac{2a_{41}^2(c_0b_{20}-a_{20})}{a_{20}^2a_{60}}(X-X_C)^2 \tag{3.155}$$

Thus, the phase line equation is given by Eq. (3.155) for the (solid CO+liquid) and (solid CO+solid CnM) transition.

The eight phase transition is the (solid CnM+liquid)-(solid CO+solidCnM) transition. To calculate the equation of this transition, we equate the free energies of (solid CnM+liquid) phase (Eq. 3.136) and (solid CO+solid CnM) phase (Eq. 3.151).

$$-\frac{a_2^2}{4a_4}-\frac{a_2^3a_6}{8a_4^3}=-\frac{a_2^2}{4a_4}-\frac{a_2^3a_6}{8a_4^3}-\frac{b_2^2}{4b_4}-\frac{b_2^3b_6}{8b_4^3}+\frac{ca_2b_2}{4a_4b_4} \tag{3.156}$$

As before, all the coefficients a_2, a_4, a_6, b_2, b_4 and b_6 and c are assumed to depend upon the temperature and concentration. We calculate the phase equation of this transition similar to the seventh phase transition, we finally get

$$\frac{ca_2}{a_4}=b_2+\frac{b_2^2b_6}{2b_4^2} \tag{3.157}$$

Insert Eqs. (3.138), (3.139), (3.146), (3.147) and (3.148) into Eq. (3.157) and by using $c=c_1+c_2(X-X_C)$ with $c_1=c_0a_{40}$ and $c_2=c_0a_{41}$, we then obtain

$$T=\left[T_C+\frac{2b_{40}^2(c_0a_{20}-b_{20})}{b_{20}^2b_{60}}\right]+\frac{4b_{40}b_{41}(c_0a_{20}-b_{20})}{b_{20}^2b_{60}}(X-X_C)$$

$$+\frac{2b_{41}^2(c_0a_{20}-b_{20})}{b_{20}^2b_{60}}(X-X_C)^2 \tag{3.158}$$

This is the phase line equation for the (solid CnM+liquid) – (solid CO+solid CnM).

We also calculate here in a separate T-X phase diagram for a binary mixture of cholestanyl myristate (CnM)-cholesteryl oleate (CO) for their transitions of the isotropic liquid-cholesteric and cholesteric-smectic using the mean field theory as the ninth and tenth phase transitions in this system. We start with the isotropic liquid-cholesteric phase transition. By defining again the orientational order parameter η for the cholesteric phase, the free energy can be expanded in terms of η for the isotropic liquid-cholesteric transition. Since the free energy of the isotropic liquid is zero Eq. (2.8), the free energy of the cholesteric phase can be written as

$$F_{CL} = a_2\eta^2 + a_4\eta^4 + a_6\eta^6 \tag{3.159}$$

Here, a_2, a_4 and a_6 are taken as the coefficients which depend on temperature and concentration, as before. By minimizing the free energy F_{CL} with respect to the order parameter η and using the ansazt $\frac{a_2 a_6}{a_4^2} << 1$, we obtain that

$$\eta^2 = \frac{-a_2}{2a_4} \tag{3.160}$$

By inserting the order parameter equation (Eq. 3.160) into the free energy equation (Eq. 3.159), we find

$$F_{CL} = -\frac{a_2^2}{4a_4} - \frac{a_2^3 a_6}{8a_4^3} \tag{3.161}$$

and then equating Eq.(3.161) to F_L=0 (Eq. 2.8), we get

$$a_2 a_6 = -2a_4^2 \tag{3.162}$$

Let us assume that the temperature and the concentration dependencies of the coefficients are given below:

$$a_2 = a_{20}(T - T_C)^{1/2} \tag{3.163}$$

$$a_4 = a_{40} + a_{41}(X - X_C) \tag{3.164}$$

$$a_6 = a_{60}(T - T_C)^{1/2} \tag{3.165}$$

Then, we find the phase line equation given by

$$T = T_C - \frac{2a_{40}^2}{a_{20}a_{60}} - \frac{4a_{40}a_{41}}{a_{20}a_{60}}(X - X_C) - \frac{2a_{41}^2}{a_{20}a_{60}}(X - X_C)^2 \quad (3.166)$$

for the isotropic liquid-cholesteric transition in a binary mixture of cholestanyl myristate (CnM) – cholestery oleate (CO).

Finally, we calculate the cholesteric-smectic phase transition. Since both cholesteric and smectic phases have the orientational order parameter, for the transition between cholesteric and smectic phases we can only expand the free energy of the smectic phase in terms of the positional (translational) order parameter ψ due to smectic layering. This gives

$$F_{CS} = b_2\psi^2 + b_4\psi^4 + b_6\psi^6 \quad (3.167)$$

In Eq. (3.167) the coefficients can depend on temperature and concentration, as before. The phase line equation for the cholesteric-smectic transition in this mixture (CnM – CO), can be obtained by minimizing the free energy F_{CS} with respect to ψ with the ansatz of $\frac{b_2 b_6}{b_4^2} << 1$. We then obtain that

$$\psi^2 = \frac{-b_2}{2b_4} \quad (3.168)$$

And inserting Eq. (3.168) into Eq. (3.167), we obtain

$$F_{CS} = -\frac{b_2^2}{4b_4} - \frac{b_2^3 b_6}{8b_4^3} \quad (3.169)$$

Finally, we equate the free energies of smectic (Eq. 3.167) and cholestric (Eq. 3.161) phases, we get

$$a_2^2 b_4(2a_4^2 + a_2 a_6) = a_4 b_2^2\left(2 + \frac{b_2 b_6}{b_4^2}\right) \quad (3.170)$$

The temperature and concentration dependencies of the coefficients are given by Eqs. (3.163)-(3.165) for a_2, a_4 and a_6, and

$$b_2 = b_{20}(T - T_C)(X - X_C)^{1/2} \quad (3.171)$$

$$b_4 = b_{40}(T - T_C)(X - X_C) \quad (3.172)$$

$$b_6 = b_{60}(T - T_C)(X - X_C)^{3/2} \quad (3.173)$$

By using Eqs. (3.163)-(3.165) and (3.171)-(3.173) and in Eq. (3.170), we end up with the phase line equation of the cholesteric – smectic transition as

$$T = \left\{ T_C + \frac{\left[a_{40}^3 b_{20}\left(2+\frac{b_{20}b_{60}}{b_{40}^2}\right) - 2a_{20}^2 a_{40}^2 b_{40} \right]}{a_{20}^3 a_{60} b_{40}} \right\} + \frac{\left[3a_{40}^2 a_{41} b_{20}\left(2+\frac{b_{20}b_{60}}{b_{40}^2}\right) - 4a_{20}^2 a_{40} a_{41} b_{40} \right]}{a_{20}^3 a_{60} b_{40}} (X - X_C) + \frac{\left[3a_{40} a_{41}^2 b_{20}\left(2+\frac{b_{20}b_{60}}{b_{40}^2}\right) - 2a_{20}^2 a_{41}^2 b_{40} \right]}{a_{20}^3 a_{60} b_{40}} (X - X_C)^2 \quad (3.174)$$

We plot our phase lines calculated from the mean field theory for the two binary mixture systems considered here. Fig. 3.15 gives the concentration dependence of the temperature or T-X (CrM) phase diagram of cholestanyl myristate (CnM)-cholesteryl myristate (CrM). The experimental data points [74] are also shown in the figure. We give T-X (CnM) phase diagram for a binary mixture of cholestanyl myristate (CnM)-cholesteryl oleate (CO) with the experimental data points [74] in Fig. 3.16. Finally, Fig. 3.17 gives our calculated phase diagram, T- X (CnM) of the cholestanyl myristate (CnM)-cholesteryl oleate (CO) system. The experimental data [74] are also plotted in this figure.

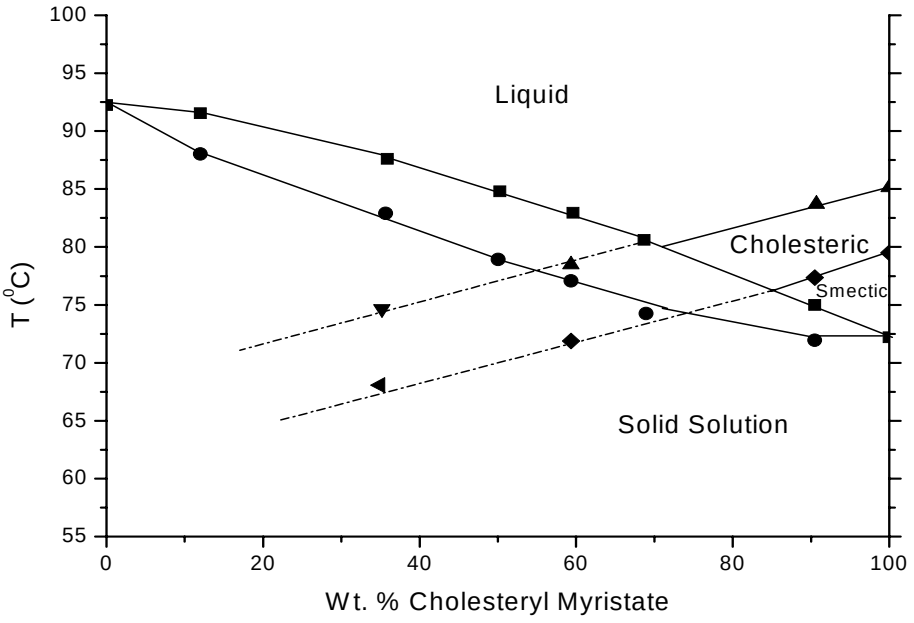

Figure 3.15 T-X(CrM) phase diagram of a binary mixture of cholestanyl myristate (CnM) – cholesteryl myristate (CrM). The experimental data points are taken from Ref. [74].

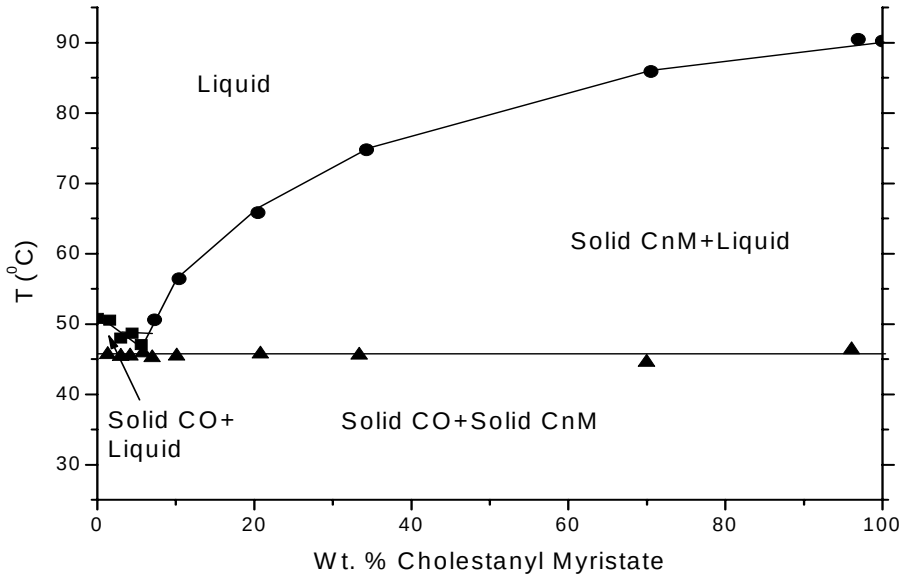

Figure 3.16 T-X(CnM) phase diagram of a binary mixture of cholestanyl myristate (CnM)-cholesteryl oleate (CO). The experimental data points are taken from Ref. [74].

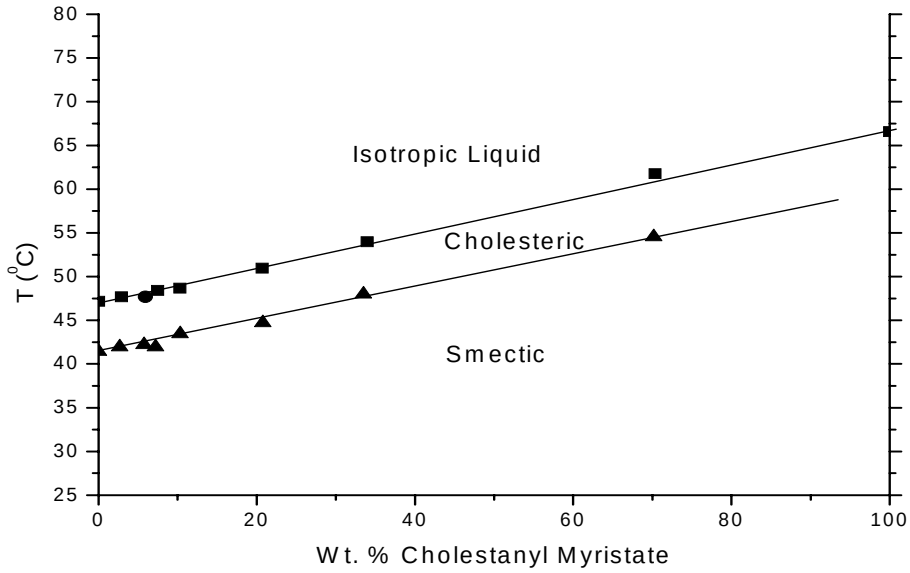

Figure 3.17 T-X(CnM) phase diagram of a binary mixture of cholestanyl myristate (CnM)-cholesteryl oleate (CO). The experimental data points are taken from Ref. [74].

For a binary mixture of cholesteryl myristate (CrM)-cholestanyl myristate (CnM), we obtained the phase line equations, Eqs. (3.113), (3.120), (3.124) and (3.133), for the transitions of the isotropic liquid – cholesteric, cholesteric – smectic, smectic – isotropic liquid and isotropic liquid – solid solution, respectively. Our phase line equations (3.113, 3.120, 3.124 and 3.133) were then fitted to the experimental data for binary phase map of cholestanyl myristate (CnM)-cholesteryl myristate (CrM) system obtained by differential scanning calorimetry (DSC) and microscopy [60]. The experimental binary phase map of CnM-CrM system was obtained as temperature (T) against weight percent (w %) of CrM [73]. Since our phase line equations (3.113, 3.120, 3.124 and 3.133) were obtained as a quadratic equation in terms of the coefficients which depend on temperature and concentration, we were able to deduce the values of the fitting parameters for all the transitions studied here. From our phase line equations, concentration or the weight percent of cholesteryl myristate (CrM) as a function of temperature for a binary mixture of cholestanyl myristate (CnM) – cholesteryl myristate (CrM), can be expressed as

$$T = a + bX + cX^2 \tag{3.175}$$

where a, b and c are constants. Table 3.12 gives the values of the fitting parameters a, b and c for the transitions considered according to the experimental phase diagram [74].

Table 3.12 Values of the parameters a, b and c according to Eq. (3.175) for the phase transitions indicated of a binary mixture of cholestanyl myristate (CnM) – cholesteryl myristate (CrM).

Phase Transition	a(^{0}C)	b(^{0}C/wt%CrM)	c x10^{-4} [^{0}C/(wt% CrM)^2]
Liquid-Cholesteric	80.35	0.17	1.89
Liquid-Smectic	76.99	-0.33	5.62
Liquid-Solid (LowTemperatures)	71.04	0.22	3.54
Liquid-Solid (HighTemperatures)	80.20	0.26	-12.00
Smectic-Cholesteric	76.99	0.14	34.70

For a binary mixture of cholestanyl myristate (CnM)-cholesteryl oleate (CO), we also obtained the phase line equations, Eqs. (3.141), (3.149), (3.155) and (3.158) for the transitions of isotropic liquid-(solid CnM+liquid), isotropic liquid-solid CO, (solid CnM+liquid)-(solid CO+solid CnM) and solid CO-(solid CO+solid CnM), respectively. Our phase line equations (Eqs. 3.141, 3.149, 3.155 and 3.158) were then fitted to the experimental data [74] according to Eq. 3.175, where X represents weight percent (w %) of cholestanyl myristate (CnM) for a binary mixture of CnM-CO. We summarize the values of the fitted parameters a, b and c in Table 3.13 for a binary mixture of cholestanyl myristate-cholesteryl oleate. For this binary mixture, the phase line equations were derived from the mean field theory for its transitions of the isotropic liquid-cholesteric and cholesteric-smectic, as given by Eqs. (3.166) and (3.174), respectively. When fitted to the experimental data [74] according to Eq. (3.175), the values of the parameters a, b and c were deduced, as tabulated in Table 3.14 for a mixture of CnM-CO [73].

Table 3.13 Values of the parameters a, b and c according to Eq. (3.175) for the phase transitions indicated of a binary mixture for cholestanyl myristate (CnM)-cholesteryl oleate (CO).

Phase Transition	a (^{0}C)	b (^{0}C/wt% CnM)	c x10^{-3} [^{0}C/(wt% CnM)^2]
Liquid- (Solid CnM+Liquid)	49.87	1.04	-6.52
Liquid-Solid CO	46.30	1.32	-90.08
(Solid CnM+Liquid) - (Solid CO+Solid CnM)	45.51	0.022	-0.13
Solid CO - (Solid CO+Solid CnM)	45.53	-0.0076	0.048

Table 3.14 Values of the parameters a, b and c according to Eq. (3.175) for the phase transitions indicated for a binary mixture of cholestanyl myristate (CnM)-cholesteryl oleate (CO).

Phase Transition	a (^{0}C)	b(^{0}C/wt% CnM)	c x10^{-3} [^{0}C/(wt% CnM)^2]
Isotropic Liquid -Cholesteric	46.34	0.22	-1.77
Cholesteric-Smectic	41.00	0.19	0.46

3.2.6 Benzene

There are nine phases of benzene, namely, liquid, solid I, solid II, solid III, solid III', solid IV, decomposed compounds, polymer 1 and polymer 2. Among these nine phases, we calculate all together fourteen phase transitions. Thirteen of these phase transitions are the first order phase transitions and one of them is the second order transition. First, we calculate the phase transition between liquid and solid I phases. For this transition, we use the free energies of the liquid (Eq. 2.8) and solid I which is given below.

$$F_I = a_2\psi^2 + a_4\psi^4 + a_6\psi^6 \tag{3.176}$$

where ψ is the order parameter of solid I and it describes the reorientations of the benzene molecules in the orthorhombic structure. By minimizing the free energy of the solid I phase of benzene, the order parameter ψ can be obtained as

$$\psi^2 = \frac{1}{3a_6}\left[-a_4 + (a_4^2 - 3a_2a_6)^{1/2}\right] \tag{3.177}$$

By inserting Eq. (3.177) into Eq. (3.176), we get

$$F_I = -\frac{a_2a_4}{3a_6} + \frac{2a_4^3}{27a_6^2} - \frac{2}{27a_6^2}(a_4^2 - 3a_2a_6)^{3/2} \tag{3.178}$$

The condition for a first order transition ($a_2 > 0, a_4 < 0$ and $a_6 > 0$) between liquid and solid I phases requires the equality of the free energies of these two phases (Eq. 2.8 and 3.178).

$$a_4^2 = 4a_2a_6 \text{ or } a_4^2 - 4a_2a_6 = 0 = f \tag{3.179}$$

which is the phase line equation for the liquid-solid I transition in benzene.

The second phase transition is the liquid-solid II transition. The free energy of solid II has the order parameter η which describes the reorientations in the monoclinic structure, as given below:

$$F_{II} = b_2\eta^2 + b_4\eta^4 + b_6\eta^6 \tag{3.180}$$

By minimizing the free energy of the solid II phase of benzene, we get

$$\eta^2 = \frac{1}{3b_6}\left[-b_4 + (b_4^2 - 3b_2b_6)^{1/2}\right] \tag{3.181}$$

By inserting Eq. (3.181) into Eq. (3.180), we obtain

$$F_{II} = -\frac{b_2b_4}{3b_6} + \frac{2b_4^3}{27b_6^2} - \frac{2}{27b_6^2}(b_4^2 - 3b_2b_6)^{3/2} \tag{3.182}$$

To obtain the phase line equation, we equate the free energies of the liquid and solid II phases (Eq. 2.8 and 3.182), which gives

$$b_4^2 = 4b_2b_6 \text{ or } b_4^2 - 4b_2b_6 = 0 = f \tag{3.183}$$

This is the phase line equation for the liquid-solid II transition in benzene.

The third phase transition is the liquid-decomposed compounds transition. The free energy of the decomposed compounds has the order parameter Q. At higher temperatures, since the hydrocarbons dissociate, this is characterized by Q.

$$F_{DC} = c_2Q^2 + c_4Q^4 + c_6Q^6 \tag{3.184}$$

By minimizing the free energy of the decomposed compounds phase according to order parameter Q, we have

$$Q^2 = \frac{1}{3c_6}\left[-c_4 + (c_4^2 - 3c_2c_6)^{1/2}\right] \tag{3.185}$$

By inserting Eq. (3.185) into Eq. (3.184), we get

$$F_{DC} = -\frac{c_2c_4}{3c_6} + \frac{2c_4^3}{27c_6^2} - \frac{2}{27c_6^2}(c_4^2 - 3c_2c_6)^{3/2} \tag{3.186}$$

We equate the free energies of the liquid phase and the decomposed compounds phase (Eq. 2.8 and 3.186) which gives

$$c_4^2 = 4c_2c_6 \text{ or } c_4^2 - 4c_2c_6 = 0 = f \tag{3.187}$$

This equation is the phase line equation for the liquid-decomposed compounds transition in benzene.

The fourth phase transition is the solid I-solid II phase transition. To calculate this phase line equation, we equate the Eqs. (3.178) (solid I free energy) and (3.182) (solid II free energy) as follows:

$$-\frac{a_2a_4}{3a_6} + \frac{2a_4^3}{27a_6^2} - \frac{2}{27a_6^2}(a_4^2 - 3a_2a_6)^{\frac{3}{2}} + \frac{b_2b_4}{3b_6} - \frac{2b_4^3}{27b_6^2} + \frac{2}{27b_6^2}(b_4^2 - 3b_2b_6)^{3/2} = 0 \tag{3.188}$$

This is the phase line equation of solid I-solid II phase transition.

The fifth one is the solid II-solid III transition. To calculate the phase line equation, first we expand the free energy of solid III phase.

$$F_{III} = d_2\xi^2 + d_4\xi^4 + d_6\xi^6 \tag{3.189}$$

where ξ is the order parameter and it represents the molecular disorder by polymerization. By minimizing the free energy of solid III phase with respect to the order parameter ξ, we have

$$\xi^2 = \frac{1}{3d_6}\left[-d_4 + (d_4^2 - 3d_2d_6)^{1/2}\right] \tag{3.190}$$

By inserting Eq. (3.190) into Eq. (3.189), we get

$$F_{III} = -\frac{d_2d_4}{3d_6} + \frac{2d_4^3}{27d_6^2} - \frac{2}{27d_6^2}(d_4^2 - 3d_2d_6)^{3/2} \tag{3.191}$$

The phase line equation is found by equating the free energies of solid II (Eq. 3.182) and solid III (Eq. 191).

$$-\frac{b_2b_4}{3b_6} + \frac{2b_4^3}{27b_6^2} - \frac{2}{27b_6^2}(b_4^2 - 3b_2b_6)^{3/2} + \frac{d_2d_4}{3d_6} - \frac{2d_4^3}{27d_6^2} + \frac{2}{27d_6^2}(d_4^2 - 3d_2d_6)^{3/2} = 0 \tag{3.192}$$

This is the phase line equation for the solid II-solid III transition in benzene.

Next, we calculate the liquid-solid IV phase transition. At higher temperatures, the molecular disorder that occurs in the solid phase III increases by the chemical transformation in the solid phase IV prior to melting which is denoted by ϕ. The free energy of liquid is given by Eq. (2.8). By expanding the free energy of solid IV and using the order parameter ϕ, we get

$$F_{IV} = e_2\phi^2 + e_4\phi^4 + e_6\phi^6 \tag{3.193}$$

Similarly, by minimizing the free energy with respect to the order parameter, we calculate the free energy as

$$F_{IV} = -\frac{e_2 e_4}{3e_6} + \frac{2e_4^3}{27e_6^2} - \frac{2}{27e_6^2}(e_4^2 - 3e_2e_6)^{3/2} \tag{3.194}$$

Equating the Eqs. (2.8) and (3.194), we obtain

$$e_4^2 = 4e_2e_6 \text{ or } e_4^2 - 4e_2e_6 = 0 = f \tag{3.195}$$

Eq. (3.195) is the phase line equation of liquid-solid IV transition.

Then, we calculate the phase line equation of solid II-solid IV as the seventh phase transition. To find this phase line equation, we equate the free energies of solid II (Eq. 3.182) and solid IV (Eq. 3.194)

$$-\frac{b_2 b_4}{3b_6} + \frac{2b_4^3}{27b_6^2} - \frac{2}{27b_6^2}(b_4^2 - 3b_2b_6)^{3/2} + \frac{e_2e_4}{3e_6} - \frac{2e_4^3}{27e_6^2} + \frac{2}{27e_6^2}(e_4^2 - 3e_2e_6)^{3/2} = 0 \tag{3.196}$$

This is the phase line equation of liquid-solid IV transition.

The nexth phase transition is the solid III-solid IV phase transition. The equality between the free energies of solid III (Eq. 3.191) and solid IV (Eq. 3.194) gives the phase line equation as

$$-\frac{d_2 d_4}{3d_6} + \frac{2d_4^3}{27d_6^2} - \frac{2}{27d_6^2}(d_4^2 - 3d_2d_6)^{3/2} + \frac{e_2e_4}{3e_6} - \frac{2e_4^3}{27e_6^2} + \frac{2}{27e_6^2}(e_4^2 - 3e_2e_6)^{3/2} = 0 \tag{3.197}$$

This is the phase line equation of solid III-solid IV phase transition.

The nineth phase transition is the solid IV-decomposed compounds transition. To calculate the phase line equation for the solid IV-decomposed compounds, we equate Eq. (3.186) and Eq. (3.194)

$$-\frac{c_2c_4}{3c_6}+\frac{2c_4^3}{27c_6^2}-\frac{2}{27c_6^2}(c_4^2-3c_2c_6)^{3/2}+\frac{e_2e_4}{3e_6}-\frac{2e_4^3}{27e_6^2}$$

$$+\frac{2}{27e_6^2}(e_4^2-3e_2e_6)^{3/2}=0 \qquad (3.198)$$

Eq. (3.198) is the phase line equation for the solid IV-decomposed compounds phase transition.

The tenth phase transition is the decomposed compounds-polymer 2 transition. The polymer 2 has no ordering like the liquid phase of benzene, with the free energy

$$F_{P2}=0 \qquad (3.199)$$

The phase line equation is calculated using

$$F_{DC}=F_{P2} \qquad (3.200)$$

and we get

$$c_4^2=4c_2c_6 \text{ or } c_4^2-4c_2c_6=0=f \qquad (3.201)$$

Eq. (3.201) is the phase line equation of the decomposed compounds-polymer 2 transition.

The next phase transition, solid III-polymer 2, is calculated by using Eqs. (3.191) and (3.199)

$$d_4^2=4d_2d_6 \text{ or } d_4^2-4d_2d_6=0=f \qquad (3.202)$$

This is the phase line equation of the solid III-polymer 2 phase transition.

The twelfth one is the polymer 1-polymer 2 phase transition. The free energy of the polymer 1 has the order parameter ν and can be writen as

$$F_{P1} = g_2\nu^2 + g_4\nu^4 + g_6\nu^6 \tag{3.203}$$

By minimizing the free energy with respect to the order parameter and inserting this into the free energy equation, we obtain

$$F_{P1} = -\frac{g_2 g_4}{3g_6} + \frac{2g_4^3}{27g_6^2} - \frac{2}{27g_6^2}(g_4^2 - 3g_2 g_6)^{3/2} \tag{3.204}$$

Equating the Eqs. (3.194) and (3.199), we obtain

$$g_4^2 = 4g_2 g_6 \text{ or } g_4^2 - 4g_2 g_6 = 0 = f \tag{3.205}$$

Eq. (3.205) is the phase line equation of polymer 1-polymer 2 transition.

The thirteenth phase transition is the polymer 1-solid III'. For this phase transition, solid III' has the free energy equation as stated below

$$F_{III'} = h_2\mu^2 + h_4\mu^4 \tag{3.206}$$

By minimizing the free energy, we get

$$\mu^2 = \frac{h_2}{2h_4} \tag{3.207}$$

Inserting this order parameter equation into the free energy equation, we obtain

$$F_{III'} = -\frac{h_2^2}{4h_4} \tag{3.208}$$

Finally, using (3.204) and (3.208), we have

$$-\frac{g_2 g_4}{3g_6} + \frac{2g_4^3}{27g_6^2} - \frac{2}{27g_6^2}(g_4^2 - 3g_2 g_6)^{3/2} + \frac{h_2^2}{4h_4} = 0 \tag{3.209}$$

This is the phase line equation for the solid III'-polymer 1 transition.

The final phase transition is the solid III- solid III'. This transition is of a second order. To calculate the phase line equation, we rewrite the free energy of solid III' as

$$F_{III'} = d_2\xi^2 + d_4\xi^4 + d_6\xi^6 + h_2\mu^2 + h_4\mu^4 + h_6\mu^6 + k\xi^2\mu^2 \tag{3.210}$$

which is not in the same form as given by Eq. (3.206) for the III-III' transition of benzene. This is due to the fact that the solid phases III and III' have the same ξ which is the molecular disorder by polymerization, as stated above. Additionally, in the solid III' phase there exist the reorientations of the benzene molecules by polymerization, denoted by μ which is not defined in the solid III phase. As the solid phase III is transformed into the solid phase III', this order parameter μ describes the solid phase III' by coupling with the molecular disorder ξ by the polymerization of both the solid phases III and III'. This coupling is quadratic and k denotes the coupling constant in Eq. (3.210). As the transition occurs from the solid III to solid III' phase, the molecular disorder by polymerization ξ disappears and the reorientational order parameter μ is the only one that describes the ordering mechanism in the solid III' phase of benzene. From this point of view, the transition between the solid III and III' phases, which is of a second order can be described by deriving the phase line equation.

By minimizing the free energy $F_{III'}$ (Eq. 3.210) with respect to the molecular disorder ξ, we get the $\xi = \xi_0$ expressed in terms of the coefficients c_2, c_4, c_6, k and the reorientational order parameter μ, as given by

$$\xi_0^2 = \frac{1}{3d_6}\left[-d_4 + (d_4^2 - 3d_2d_6 - 3k\mu^2 d_6)^{1/2}\right] \tag{3.211}$$

By assuming that $d_2 d_6 / d_4^2 << 1$ and $k\mu^2 d_6 / d_4^2 << 1$, Eq. (3.211) can be written as

$$\xi_0^2 = -\frac{d_2}{2d_4} - \frac{k\mu^2}{2d_4} \tag{3.212}$$

When we substitute ξ_0^2 (Eq. 3.212) into the free energy $F_{III'}$ (Eq. 3.210), we then obtain $F_{III'}$ in terms of the reorientational order parameter μ only, as given below:

$$F_{III'} = B_0 + B_2\mu^2 + B_4\mu^4 + B_6\mu^6 \tag{3.213}$$

where

$$B_0 = -\frac{d_2^2}{4d_4} - \frac{d_2^3 d_6}{8d_4^3} \tag{3.214}$$

$$B_2 = h_2 - \frac{kd_2}{2d_4} - \frac{3kd_2^2 d_6}{8d_4^3} \tag{3.215}$$

$$B_4 = h_4 - \frac{k^2}{4d_4} - \frac{3k^2 d_2 d_6}{8d_4^3} \tag{3.216}$$

and

$$B_6 = h_6 - \frac{k^3 d_6}{8d_4^3} \tag{3.217}$$

Thus, the phase line equation between the solid III and solid III' phases can be obtained by using a second order transition that B_2=0. This gives

$$8h_2 d_4^3 - 4kc_2 c_4^2 - 3kc_2^2 c_6 = 0 = f \tag{3.218}$$

Since the coefficients given in the free energy expansions depend upon the temperature and pressure, the fourteen phase line equations can be expressed with the temperature and pressure dependence as given below:

$$f = 0 = (T - T_t) - [\alpha_1 (P - P_t) + \alpha_2 (P - P_t)^2] \tag{3.219}$$

or

$$T = [T_t - \alpha_1 P_t + \alpha_2 P_t^2] + [\alpha_1 - 2\alpha_2 P_t]P + \alpha_2 P^2 \tag{3.220}$$

where T_t and P_t represent the coordinates of the triple point for benzene (Fig. 3.16), α_1 and α_2 are constants. By fitting a quadratic expression

$$T = a + bP + cP^2 \tag{3.221}$$

which is equivalent to Eq. (3.220), to the experimental T-P data the coefficients a, b and c are first determined. This then provides to determine the coefficients α_1 and α_2 in Eq. (3.220).

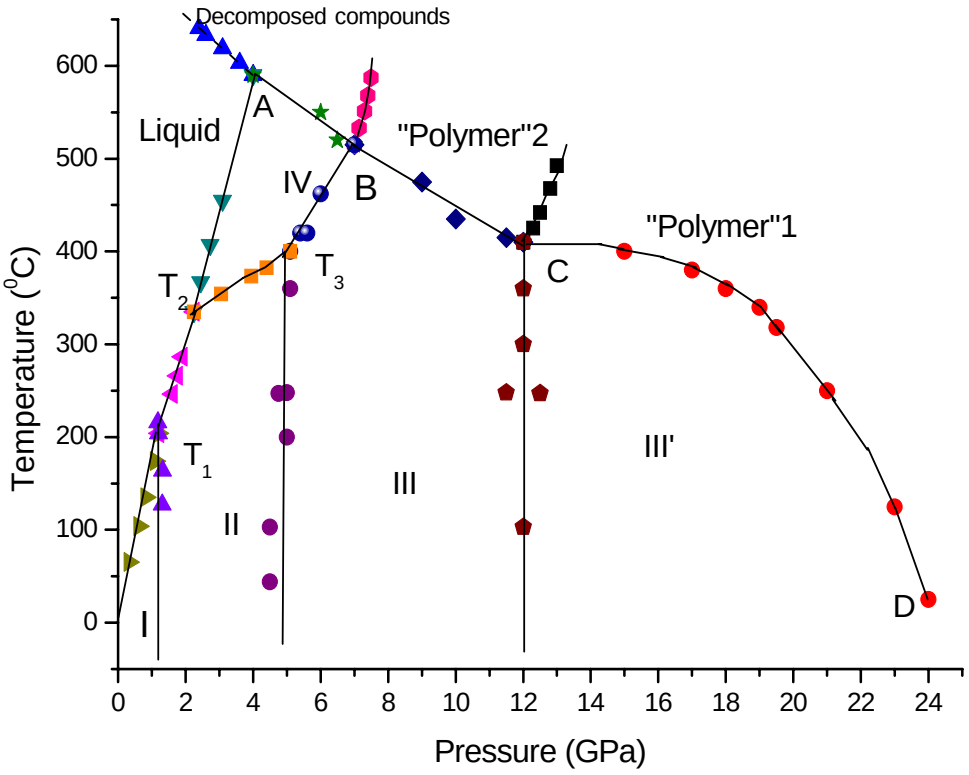

Figure 3.18 T-P phase diagram calculated from the mean field theory for benzene. Solid lines represent our calculated phase lines. The experimental data points are also shown here for the observed T-P phase diagram of benzene [48]. T_1, T_2 and T_3 are the triple points, A denotes the decomposition point and the chemical transformation line is defined by the points A, B, C and D [48].

We determined here the coefficients a, b and c by fitting Eq. (3.221) to the experimental T-P data [48] for benzene for all the transitions studied. By the equivalent expression (Eq. 3.220), we were then able to determine the coefficients α_1 and α_2 for those transitions of benzene. Table 3.15 summarizes the values of a, b, c (Eq. 3.221) and α_1 and α_2 (Eq. 3.220) which we obtained for the transitions indicated in benzene. Fig 3.18 gives our calculated phase lines by also showing the experimental data points [48] in the T-P phase diagram of benzene. In our recent

work, we have given T-P phase diagram except the III-III' transition in benzene [75].

Table 3.15 Values of the coefficients a, b and c determined from fitting Eq.(3.221) to the experimental data [48] and, the values of α_1 and α_2 obtained from Eq. (3.220) with the coordinates of the triple point (T_t, P_t) for the phase transitions indicated of benzene.

Phase Transition	a (^{0}C)	b(^{0}C/ GPa)	c(^{0}C/ (GPa)^2)	T_t(^{0}C)	P_t (GPa)	α_1(^{0}C/ GPa)	α_2(^{0}C/ (GPa)^2)
Liquid-Solid I	34.1	81.4	46.3	204	1.20	192.52	46.3
Liquid-Solid II	115.74	45.23	23.3	335	2.25	150.08	23.3
Liquid-Solid IV	37.8	126.6	2.9	590	4.00	149.8	2.9
Solid I-Solid II	7737.28	-11596.9	4429.01	204	1.20	-967.32	4429.01
Solid II-Solid III	-10500.9	4059.96	-379.8	400	5.1	186.0	-379.8
Solid II-Solid IV	286.9	21.1	0.19	400	5.1	23.04	0.19
Solid III-Solid IV	21.3	82.5	-1.7	400	5.1	65.16	-1.7
Liquid-Decomposed	711.2	-28.7	-0.39	590	4.00	-31.8	-0.39
Decomposed -Solid IV	600.1	11.2	-3.4	590	4.00	-16.0	-3.4
Decomposed -Polymer 2	4586.5	-1256.2	96.4	515	7.00	93.4	96.4
Polymer 2-Solid III	773.5	-45.3	1.2	410	12.0	-16.5	1.2
Polymer 1-Polymer 2	5812.4	-941.6	40.95	410	12.0	41.2	40.95
Polymer 1-Solid III'	-396.0	114.3	-4.0	410	12.0	18.3	-4.0
Solid III-Solid III'	-26046.8	4391	-183	410	12.0	-1	-183

3.2.7 Ice

The free energies of the phases I, II, III, V, VI, VII and VIII of ice can be written as

$$F_i = a_i\psi_i^2 + b_i\psi_i^4 + c_i\psi_i^6 \tag{3.222}$$

where i = 1, 2, 3, 5, 6, 7, 8 and ψ_i is the order parameter of phases I (i=1), II (i=2), III (i=3), V (i=5), VI (i=6), VII (i=7) and VIII (i=8). In Eq. (3.222) we take $a_i > 0$, $b_i < 0$ and $c_i > 0$ since all the phase lines for ice are of first order. In Eq. (3.222) the coeflicients a_i, b_i and c_i depend upon both temperature and pressure. Since the order parameter can be taken as zero for the liquid phase, the free energy of the liquid phase can be equal to zero (Eq. 2.8). Minimizing Eq.(3.222) with respect to ψ_i gives

$$\psi_i^2 = \frac{1}{3c_i}\left[-b_i + (b_i^2 - 3a_ic_i)^{1/2}\right] \tag{3.223}$$

By making the ansatz

$$a_i = a_{i0}f_i^{2n},\ b_i = b_{i0}f_i^n \text{ and } c_i = c_{i0} \tag{3.224}$$

where a_{i0} and c_{i0}, are positive constants, b_{i0} is a negative constant and n is a real number. In Eq. (3.224) f_i depends on both temperature and pressure, and f_i is chosen as positive. Since the order parameter ψ_i as a positive physical quantity depends on, in general, the temperature and pressure (for a given T-P phase diagram of ice), $(b_i^2 - 3a_ic_i)^{1/2}$ in Eq. (3.223) becomes solvable under the assumption (3.224). By a positive function f_i that depends on both the temperature and pressure, the order parameter ψ_i becomes as a function of temperature and pressure. Inserting Eq. (3.224) into Eq. (3.223) gives

$$\psi_i^2 = k_{i0}f_i^n \tag{3.225}$$

where

$$k_{i0} = \frac{1}{3c_{i0}}\left[-b_{i0} + (b_{i0}^2 - 3a_{i0}c_{i0})^{1/2}\right] \tag{3.226}$$

By substituting Eq. (3.225) into Eq. (3.222), we get

$$F_i = F_{i0} f_i^{3n} \tag{3.227}$$

where

$$F_{i0} = a_{i0} k_{i0} + b_{i0} k_{i0}^2 + c_{i0} k_{i0}^3 \tag{3.228}$$

By choosing n=1/3, Eqs. (3.224), (3.225) and (3.227) become

$$F_i = F_{i0} f_i \tag{3.229}$$

$$\psi_i = k_{i0}^{1/2} f_i^{1/6} \tag{3.230}$$

$$a_i = a_{i0} f_i^{2/3} \tag{3.231}$$

$$b_i = b_{i0} f_i^{1/3} \tag{3.232}$$

$$c_i = c_{i0} \tag{3.233}$$

In Eqs. (3.224), (3.225) and (3.227), n=1/3 is chosen because the functional form of the free energy F_i (Eq. 3.229) is the simplest that one can get, which is obtained from Eq. (3.227) with n=1/3. Since f_i(T,P) is determined by the temperature and pressure dependence of the function g(T,P) as given below, the simplest form of F_i (Eq. 3.229) makes it easier for fitting the phase line equations to the experimental data for the T-P phase diagram of ice. Otherwise, the fitting procedure requires too many fitting parameters.

In order to obtain the phase diagram of ice, as we have calculated recently [76] which is given in Fig. 3.19, we choose the temperature and pressure dependent function $f_i \equiv f_i$(T,P) as

$$f_1(T,P) = -d_{L1} g_{L1}(T,P) - d_{13} g_{13}(T,P) + d_{12} g_{12}(T,P) \tag{3.234}$$

$$f_2(T,P) = -d_{12} g_{12}(T,P) - d_{23} g_{23}(T,P) - d_{25} g_{25}(T,P) - d_{26} g_{26}(T,P) \tag{3.235}$$

$$f_3(T,P) = -d_{L3} g_{L3}(T,P) + d_{13} g_{13}(T,P) + d_{23} g_{23}(T,P) - d_{35} g_{35}(T,P) \tag{3.236}$$

$$f_5(T,P) = -d_{L5} g_{L5}(T,P) + d_{35} g_{35}(T,P) + d_{25} g_{25}(T,P) - d_{56} g_{56}(T,P) \tag{3.237}$$

$$f_6(T,P) = -d_{L6}g_{L6}(T,P) + d_{56}g_{56}(T,P) + d_{26}g_{26}(T,P) - d_{67}g_{67}(T,P) + d_{68}g_{68}(T,P) \quad (3.238)$$

$$f_7(T,P) = -d_{L7}g_{L7}(T,P) + d_{67}g_{67}(T,P) + d_{78}g_{78}(T,P) \quad (3.239)$$

$$f_8(T,P) = -d_{68}g_{68}(T,P) - d_{78}g_{78}(T,P) \quad (3.240)$$

In Eqs. (3.234)-(3.240) d_{L1}, d_{L3}, d_{L5}, d_{L6}, d_{L7}, d_{12}, d_{23}, d_{25}, d_{26}, d_{68} and d_{78} are positive constant in the units of J/C; d_{13}, d_{35}, d_{56} and d_{67} are positive constants in the units of J/kbar. The functions g_{L1}(T,P), g_{L3}(T,P), g_{L5}(T,P), g_{L6}(T,P), g_{12}(T,P) and g_{L7}(T,P) are tabulated in Table 3.16. Also, we tabulate the functions g_{13}(T,P), g_{23}(T,P), g_{25}(T,P), g_{26}(T,P), g_{35}(T,P), g_{56}(T,P), g_{67}(T,P), g_{68}(T,P) and g_{78}(T,P) in Table 3.17.

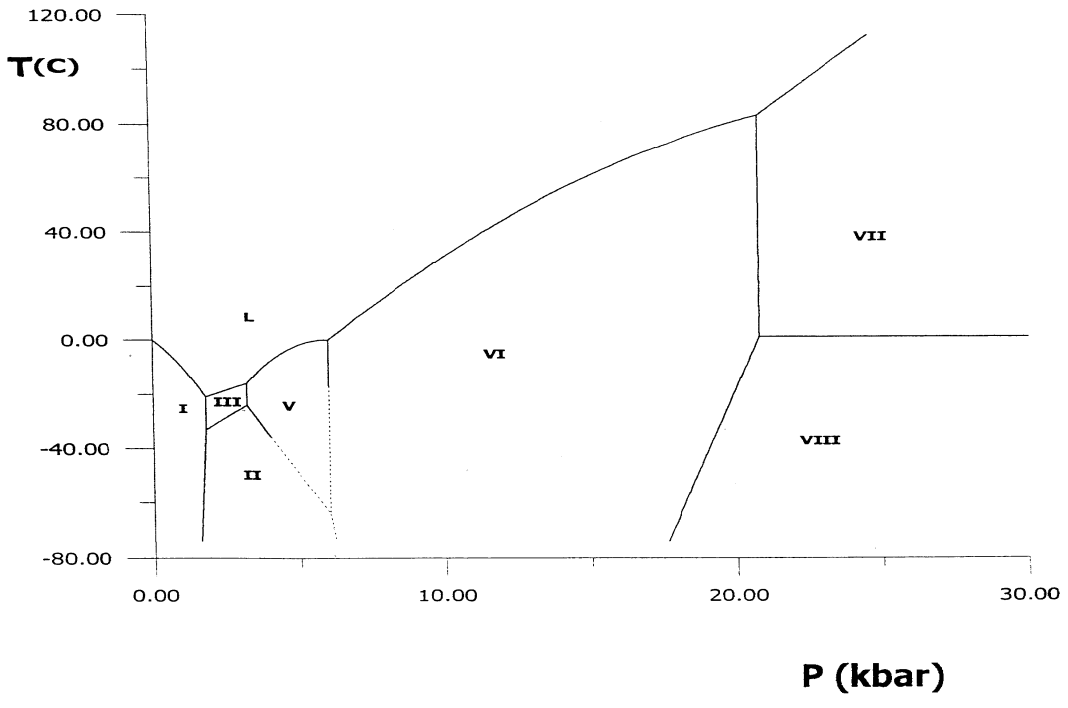

Figure 3.19 Our calculated phase diagram of ice. Both experimental [77] and theoretical phase lines are represented in the figure by solid and broken lines. Broken lines represent presumed phase boundaries which have not yet been fully investigated experimentally [77].

Table 3.16 The functions f_i (T,P), g (T,P) and g_{Li} (T,P) with the temperature and pressure ranges, which are defined in the equations indicated (third column) for i=1 to 7 for the liquid-solid phases (first column) of ice. Values of the parameters obtained from the equations (fifth column) fitted to the experimental data [77], are also given here.

Liquid-Solid Phase	i	f_i (T,P)	g(T,P) T(^{0}C), P(kbar)	g_{Li} (T,P) T(^{0}C), P(kbar)	α_{Li1}	α_{Li2}	α_{Li3}
L-I	1	Eq.(3.234)	g_{12}=0,-74<T<-33 P=1.8 g_{13}=0,-33<T<-21 P=1.8	T+α_{L11}P+α_{L12}P^2 =0 -21<T<0 0≤P<1.8	7.9166 ^{0}C/kbar	2.0833 ^{0}C/ (kbar)^2	--
L-III	3	Eq. (3.236)	g_{13}=0, g_{23}=0,-33<T<-24 1.8<P<3.2 g_{35}=0,-24<T<-16 P=3.2	T+α_{L31}-α_{L32}P=0 -24<T<-16 1.8<P<3.2	27.428 ^{0}C	3.5714 ^{0}C/kbar	--
L-V	5	Eq. (3.237)	g_{35}=0, g_{25}=0,-64<T<-24 3.2<P<6 g_{56}=0,-64<T<0 P=6	T+α_{L51}- α_{L52}P+α_{L53}P^2=0 -16<T<0 3.2<P<6	75.428 5 ^{0}C	25.428 ^{0}C/kbar	2.1428 ^{0}C/ (kbar)^2
L-VI	6	Eq. (3.238)	g_{56}=0, g_{26}=0,-74<T<-64 6<P<6.2 g_{67}=0,1<T<83 P=20.8 g_{68}=0,-74<T<1 18<P<20.8	T+α_{L61}-α_{L62}P=0 When 6<P<6.2, 0<T<1 When 6.2<P<20.8, 1<T<83	57.537 2 ^{0}C	10.738 ^{0}C/kbar	--
L-VII	7	Eq. (3.239)	g_{67}=0 , g_{78}=0 ,T=1 20.8<P<30	T+α_{L71}-α_{L72}P=0 82<T<112 20.8<P<24.6	75.736 8 ^{0}C	7.6315 ^{0}C/kbar	--

Below, the phase line equations are derived using the f_i(T,P) functions (Eqs. 3.234-3.240) for the liquid-solid and solid-solid transitions in ice. Here, we give as examples liquid-solid I transition among all the liquid-solid transitions and also solid I-solid III transition among all the solid-solid transitions. The other liquid-solid transitions are treated similar to the liquid-solid I transition and the results are given in Table 3.16. The other solid-solid transitions are also treated similar to the solid I-solid III transition. Our results of the other solid-solid transitions are also tabulated in Tables 3.17 and 3.18.

Table 3.17 The function g (T,P) and the values of the parameters obtained from the equations fitted (third column) to the experimental data [77] for the solid-solid transitions (first column) of ice.

Solid-Solid Transition	g(T,P)	Equation Fitted	Parameter
I-II	g_{12}(T,P)=0	$T+\alpha_{121}-\alpha_{122}P=0$	α_{121}=402 ^{0}C, α_{122}=205 ^{0}C/kbar
I-III	g_{13}(T,P)=0	$P-\alpha_{131}=0$	α_{131}=1.8 kbar
II-III	g_{23}(T,P)=0	$T+\alpha_{231}-\alpha_{232}P=0$	α_{231}=44.514 ^{0}C, α_{232}=6.4285 ^{0}C/kbar
II-V	g_{25}(T,P)=0	$T-\alpha_{251}+\alpha_{252}P=0$	α_{251}=21.7143 ^{0}C, α_{252}=14.2857 ^{0}C/kbar
II-VI	g_{26}(T,P)=0	$T-\alpha_{261}+\alpha_{262}P=0$	α_{261}=236 ^{0}C, α_{262}=50 ^{0}C/kbar
III-V	g_{35}(T,P)=0	$P-\alpha_{351}=0$	α_{351}=3.2 kbar
V-VI	g_{56}(T,P)=0	$P-\alpha_{561}=0$	α_{561}=6 kbar
VI-VII	g_{67}(T,P)=0	$P-\alpha_{671}=0$	α_{671}=20.8 kbar
VI-VIII	g_{68}(T,P)=0	$T+\alpha_{681}-\alpha_{682}P=0$	α_{681}=486.5 ^{0}C, α_{682}=23.4375 ^{0}C/kbar
VII-VIII	g_{78}(T,P)=0	$T-\alpha_{781}=0$	α_{781}=1 ^{0}C

Table 3.18 The functions f_i (T,P) defined in equations indicated (second column), F_i for i=1 to 8 with the temperature and pressure ranges, g (T,P) and the phase line equations for the solid-solid transitions (first column) of ice.

Solid-Solid Transition	f_i(T,P)	$F_i=F_{i0}f_i$ Eq.(2.8) for F_{i0}	Temperature and Pressure Range T(^{0}C), P(kbar)	g(T,P)	Phase Line Equation
I-II	Eq.(3.234) for I(i=1) Eq.(3.235) for II(i=2)	$F_1=F_2$	-74<T<-33 1.6<P<1.8	$g_{L1}=0$, $g_{13}=0$, $g_{23}=0$, $g_{25}=0$, $g_{26}=0$	$d_{12}(F_{10}+F_{20})g_{12}=0$ g_{12}(T,P)=0
I-III	Eq.(3.234) for I(i=1) Eq.(3.236) for III(i=3)	$F_1=F_3$	-33<T<-21 P=1.8	$g_{L1}=0$, $g_{12}=0$, $g_{L3}=0$, $g_{23}=0$, $g_{35}=0$	$d_{13}(F_{10}+F_{30})g_{13}=0$ g_{13}(T,P)=0
II-III	Eq.(3.235) for II(i=2) Eq.(3.236) for III(i=3)	$F_2=F_3$	-33<T<-24 1.8<P<3.2	$g_{12}=0$, $g_{25}=0$, $g_{26}=0$, $g_{L3}=0$, $g_{35}=0$	$d_{23}(F_{20}+F_{30})g_{23}=0$ g_{23}(T,P)=0
II-V	Eq.(3.235) for II(i=2) Eq.(3.237) for V(i=5)	$F_2=F_5$	-64<T<-24 3.2≤P<6	$g_{12}=0$, $g_{23}=0$, $g_{26}=0$, $g_{L5}=0$, $g_{35}=0$, $g_{56}=0$	$d_{25}(F_{20}+F_{50})g_{25}=0$ g_{25}(T,P)=0
II-VI	Eq.(3.235) for II(i=2) Eq.(3.238) for VI(i=6)	$F_2=F_6$	-74<T<-64 P=6.2	$g_{12}=0$, $g_{23}=0$, $g_{25}=0$, $g_{L6}=0$, $g_{56}=0$, $g_{67}=0$, $g_{68}=0$	$d_{26}(F_{20}+F_{60})g_{26}=0$ g_{26}(T,P)=0
III-V	Eq.(3.236) for III(i=3) Eq.(3.237) for V(i=5)	$F_3=F_5$	-24<T<-16 P=3.2	$g_{L3}=0$, $g_{13}=0$, $g_{23}=0$, $g_{L5}=0$, $g_{25}=0$, $g_{56}=0$	$d_{35}(F_{30}+F_{50})g_{35}=0$ g_{35}(T,P)=0
V-VI	Eq.(3.237) for V(i=5) Eq.(3.238) for VI(i=6)	$F_5=F_6$	-64<T<0 P=6	$g_{L5}=0$, $g_{35}=0$, $g_{25}=0$, $g_{L6}=0$, $g_{26}=0$, $g_{67}=0$	$d_{56}(F_{50}+F_{60})g_{56}=0$ g_{56}(T,P)=0
VI-VII	Eq.(3.238) for VI(i=6) Eq.(3.239) for VII(i=7)	$F_6=F_7$	1≤T≤83 P=20.8	$g_{L6}=0$, $g_{56}=0$, $g_{26}=0$, $g_{68}=0$, $g_{L7}=0$, $g_{78}=0$	$d_{67}(F_{60}+F_{70})g_{67}=0$ g_{67}(T,P)=0
VI-VIII	Eq.(3.238) for VI(i=6) Eq.(3.240) for VIII(i=8)	$F_6=F_8$	-74≤T≤1 17.6≤T<20.8	$g_{L6}=0$, $g_{56}=0$, $g_{26}=0$, $g_{67}=0$, $g_{78}=0$	$d_{68}(F_{60}+F_{80})g_{68}=0$ g_{68}(T,P)=0
VII-VIII	Eq.(3.239) for VII(i=7) Eq.(3.240) for VIII(i=8)	$F_7=F_8$	T=1 20.8<P<30	$g_{L7}=0$, $g_{67}=0$, $g_{68}=0$	$d_{78}(F_{70}+F_{80})g_{78}=0$ g_{78}(T,P)=0

For the liquid-solid I transition for ice, the phase line equation is F_I=0 since the free energy change for this transition is zero, so that using Eq. (3.229) we obtain the phase line equation for L-I transition as

$$f_1(T,P) = 0 \tag{3.241}$$

Using Eq. (3.234), Eq. (3.241) becomes

$$-d_{L1}g_{L1}(T,P) - d_{13}g_{13}(T,P) + d_{12}g_{12}(T,P) = 0 \tag{3.242}$$

Experimentally, the L-I transition occurs in the region -21<T≤0 ^{0}C and 0≤P≤1.8 kbar (see Fig. 3.19). In this pressure and temperature region g_{12}(T,P)=0 and g_{13}(T,P)=0 (see Table 3.17). Hence, in this region from Eq. (3.242) we obtain the phase line equation for the L-I transition as

$$g_{L1}(T,P) = 0 \tag{3.243}$$

Using this function g_{L1}(T,P), the parameters α_{L11} and α_{L12} (Table 3.16) are obtained from fitting to the experimental data (see Fig. 3.19). The choice for the functions g_{Li}(T,P) is based on the experimental T-P phase diagram of ice (Fig. 3.19). Depending on the phase boundaries observed experimentally among the liquid and ice phases of I, III, V, VI and VII, the temperature and pressure dependence of the function g(T,P) is constructed, as given in Table 3.16.

For the solid I-solid III transition for ice, the phase line equation is F_1=F_3 so that using Eq. (3.229) we obtain the phase line equation for the I-III transition as

$$F_{10}f_1(T,P) = F_{30}f_3(T,P) \tag{3.244}$$

where F_{10} and F_{30} are given by Eq. (3.228). Using Eqs. (3.234) and (3.236), Eq. (3.244) becomes

$$F_{10}\{-d_{L1}g_{L1}(T,P) - d_{13}g_{13}(T,P) + d_{12}g_{12}(T,P)\}$$

$$= F_{30}\{-d_{L3}g_{L3}(T,P) + d_{13}g_{13}(T,P) + d_{23}g_{23}(T,P) - d_{35}g_{35}(T,P)\} \tag{3.245}$$

Experimentally, the I-III transition occurs in the region $-33 \leq T \leq -21\ ^0C$ and P=1.8 kbar (see Fig. 3.19). In this pressure and temperature region $g_{L1}(T,P)=0$, $g_{12}(T,P)=0$, $g_{L3}(T,P)=0$, $g_{23}(T,P)=0$ and $g_{35}(T,P)=0$ (see Table 3.18). Hence, in this region from Eq. (3.245) we get

$$d_{13}(F_{10}+F_{30})g_{13}(T,P)=0 \tag{3.246}$$

Therefore, from Eq. (3.246) we obtain the phase line equation for the I-III transition as

$$g_{13}(T,P)=0 \tag{3.247}$$

Using this function $g_{13}(T,P)$, the parameter α_{131} (Table 3.17) is obtained from fitting the experimental data (see Fig. 3.19).

Using the free energy F_i (Eq. 3.222) for the phases I, II, III, V, VI, VII and VIII of ice,the thermodynamic functions such as the specific heat, order parameter and the susceptibility can be predicted as functions of temperature and pressure for the transitions among the phases indicated. Here, as examples, we predicted the temperature dependence of the specific heat C_p, the order parameter ψ and the inverse susceptibility χ^{-1} for the liquid-solid I and solid I-solid III transitions in ice. This was demonstrated numerically for both transitions.

First, for the liquid-solid I transition the thermodynamic quantities can be calculated. The free energy of the solid I can be written according to Eq. (3.222) as

$$F_I = a_1\psi_1^2 + b_1\psi_1^4 + c_1\psi_1^6 \tag{3.248}$$

By minimizing the free energy F_I with respect to the order parameter ψ_1, we get

$$\frac{\partial F_I}{\partial \psi_I} = a_1 + 2b_1\psi_1^2 + 3c_1\psi_1^4 = 0 \tag{3.249}$$

For the liquid-solid I transition on the phase line, we have the change in free energy as F_I-F_L=0, which gives

$$a_1\psi_1^2 + b_1\psi_1^4 + c_1\psi_1^6 = 0 \tag{3.250}$$

From Eqs. (3.249) and (3.250), the order parameter ψ_1 can be expressed as

$$\psi_1^2 = -\frac{b_1}{2c_1} = -\frac{2a_1}{b_1} \tag{3.251}$$

By substituting Eq. (3.251) into the free energy F_I (Eq. 3.248), we then obtain the F_I in terms of its coefficients as

$$F_I = \frac{2a_1^2}{b_1} - \frac{8a_1^3 c_1}{b_1^3} \tag{3.252}$$

In order to obtain the temperature and pressure dependence of the thermodynamic functions starting from the free energy F_I of solid I (Eq. 3.252), we assume that

$$a_1 = [a_{10}(T - T_t) + a_{11}(P - P_t) + a_{12}(P - P_t)^2]^{1/2} \tag{3.253}$$

and

$$b_1 = b_{10}(T - T_t)^{1/2}, \quad c_1 = 1 \tag{3.254}$$

where T_t and P_t represent the transition temperature and pressure along the phase line, respectively, and a_{10}, a_{11}, a_{12} and b_{10} are constants.

By employing the phase line equation from Eq. (3.251) for the liquid-solid I transition,

$$f_1 = b_1^2 - 4a_1c_1 \tag{3.255}$$

the coefficients in Eqs. (3.253) and (3.254) can be evaluated. This is done by writing our expression g_{L1}(T,P) fitted to the experimental data [62] for the liquid-solid I (Table 3.16) in the form

$$f_1(T,P) = f_0\left\{(T - T_t) - \left[\alpha_{L11}(P - P_t) + \alpha_{L12}(P - P_t)^2\right]\right\} \tag{3.256}$$

where P_t=0 kbar and T_t=0 ^{0}C and f_0 is a constant.

By using the temperature and pressure dependence of the coefficients a_1 and b_1 (Eqs. 3.253 and 3.254) in Eq. (3.255), f_1 can be written as

$$f_1(T,P) = (b_{10}^2 - 4a_{10})(T - T_t) - 4a_{11}(P - P_t) - 4a_{12}(P - P_t)^2 \tag{3.257}$$

By equating Eq. (3.257) to Eq. (3.256), the coefficients a_{11} and a_{12} can be obtained as

$$a_{11} = f_0 \frac{\alpha_{L11}}{4}, \qquad a_{12} = f_0 \frac{\alpha_{L12}}{4} \tag{3.258}$$

Since we calculated the coefficients α_{L11} and α_{L12} (Table 3.16) from fitting $g_{L1}(T,P)$ to the experimental data [76] for the liquid-solid I transition, the coefficients a_{11} and a_{12} can be calculated numerically from Eq. (3.258). By taking f_0=1, we obtained the values of $a_{11} = 1.9792$ ^{0}C/kbar and a_{12}=0.5208 ^{0}C/(kbar)^2. From Eq. (3.257), we also have

$$f_0 = 1 = b_{10}^2 - 4a_{10} \tag{3.259}$$

or by choosing a_{10}=2, we get b_{10}=3.

The temperature dependence of the specific heat C_p can now be predicted by knowing the values of the coefficients. Using the definition $C_p = T(\partial^2 F / \partial T^2)$ and by substituting the temperature and pressure dependence of the coefficients a_1 (Eq. 3.253)and b_1 (Eq. 3.254) into the free energy F_I (Eq. 3.252) of the solid I, the specific heat C_p(I) can be reduced to the form

$$C_p(I) = C_p(L) + \left(\frac{6a_{10}^3}{b_{10}^3} \right) T\left(T - T_t\right)^{-1/2} \tag{3.260}$$

where C_p(L) is the specific heat of the liquid phase close to the liquid-solid I transition. For this form of C_p(I), we neglected the terms such as $(T\text{-}T_t)^{-3/2}$, $(T\text{-}T_t)^{-5/2}$ and $(T\text{-}T_t)^{-7/2}$ since they are weakly divergent close to the melting line for solid I. Using the values of a_{10} and b_{10} given above in Eq. (3.260), the temperature dependence of the specific heat C_p(I) for the liquid-solid I transition is obtained as

$$C_p(I) = C_p(L) + \left(\frac{-16}{9}\right) T\left|T - T_t\right|^{-1/2} \tag{3.261}$$

with the critical exponent α=1/2 according to the power-law formula $C_p \approx \left|T\text{-}T_t\right|^{-\alpha}$ for the critical behaviour of the specific heat. We demonstrated the specific heat $C_p(I)$ as a function of temperature according to Eq. (3.261) where T_t=0 ^{0}C within the temperature range -21 ^{0}C < T < 0 ^{0}C (Table 3.16) for the liquid-solid I transition in ice, as plotted in Fig. 3.20.

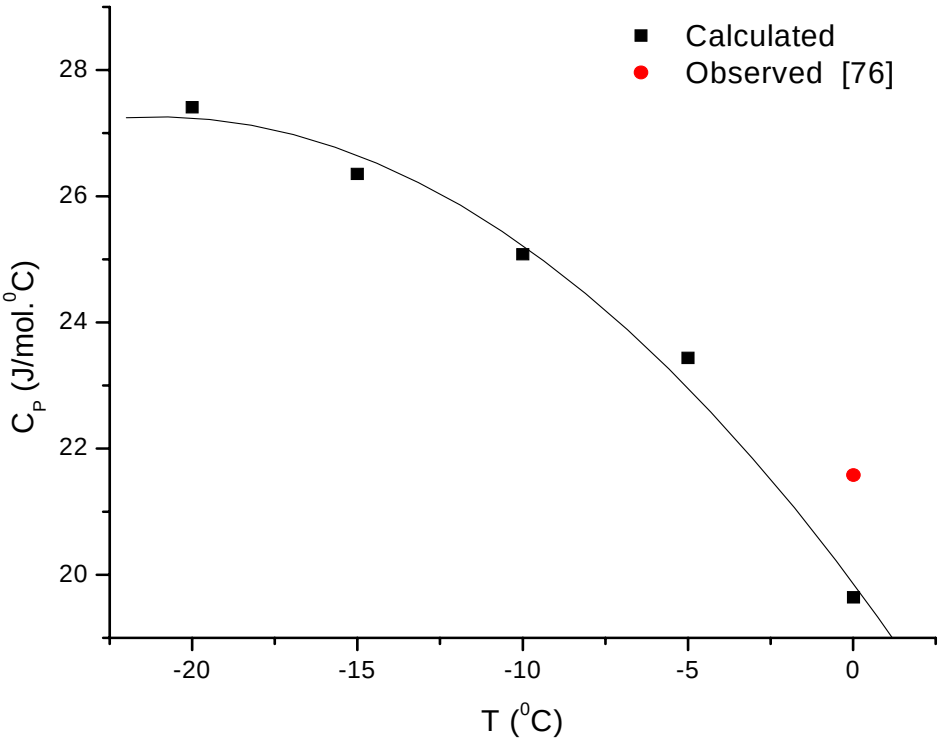

Figure 3.20 Calculated specific heat C_p as a function of temperature for the liquid-solid I transition in ice according to Eq. (3.261). Solid curve represents the best fit to values given here.

The temperature dependence of the order parameter ψ_1 can be predicted for the liquid-solid I transition using Eq. (3.251). By substituting the temperature dependence of a_1 given in Eq. (3.253) and b_1 Eq. (3.254) into Eq. (3.251), we obtain that

$$\psi_1 = \sqrt{\frac{b_{10}}{2}}(T_t - T)^{1/4} \tag{3.262}$$

in the solid I phase of ice. Using b_{10}=3, the order parameter ψ_1 can be calculated as a function of temperature within the temperature interval -21 ^{0}C < T < 0 ^{0}C from Eq. (3.262) with the critical exponent β=1/4 according to the power law formula $\psi \sim |T_t - T|^{-\beta}$ for the order parameter. We plot ψ_1 as a function of temperature for the liquid-solid I transition using Eq. (3.262) where T_t=0 ^{0}C in Fig. 3.21.

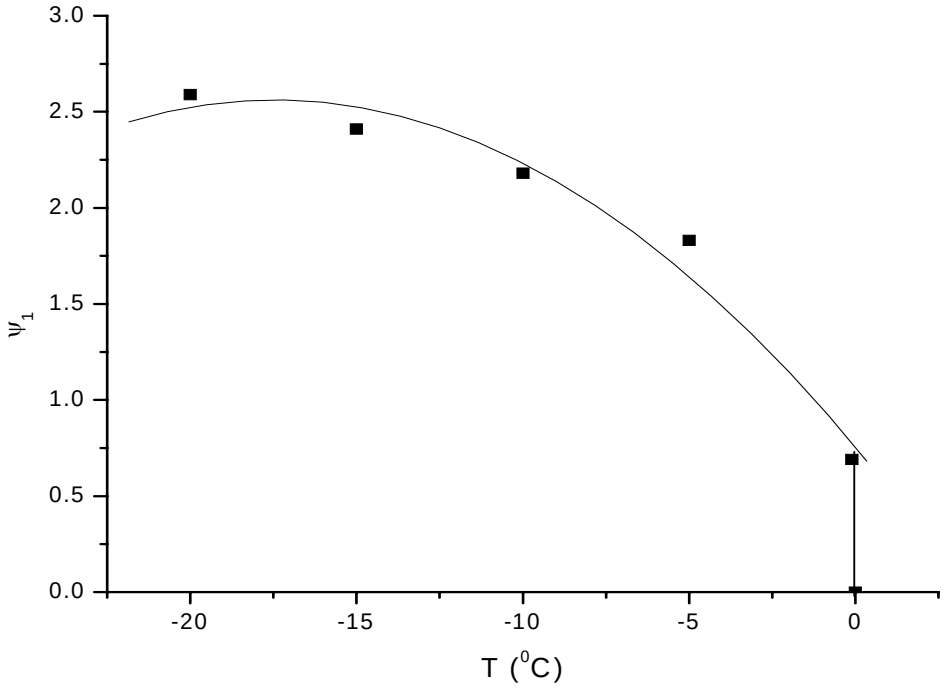

Figure 3.21 Calculated order parameter ψ as a function of temperature for the liquid-solid I transition in ice according to Eq. (3.262). Solid curve represents the best fit to values given here.

The temperature dependence of the susceptibility χ_I can also be predicted for the liquid-solid I transition using the definition $\chi^{-1} = \partial^2 F / \partial \psi^2$. By taking the second derivative of the free energy F_I (Eq. 3.248) with respect to the order parameter ψ_1, the inverse susceptibility can be obtained as

$$\chi_I^{-1} = 2\left(a_1^2 + 6b_1\psi_1^2 + 15c_1\psi_1^4\right) \tag{3.263}$$

By Eq. (3.251), this can be expressed as

$$\chi_I^{-1} = 2\left(a_1^2 + \frac{3}{4}\frac{b_1^2}{c_1}\right) \tag{3.264}$$

Using Eq. (3.253) and Eq. (3.254) in Eq. (3.264), the temperature and pressure dependence of the inverse susceptibility χ_I^{-1} of the solid I can be obtained as

$$\chi_I^{-1} = 2\left[\left(a_{10} + \frac{3b_{10}^2}{4}\right)(T - T_t) + a_{11}(P - P_t) + a_{12}(P - P_t)^2\right] \tag{3.265}$$

By taking $P=P_t=1.8$ kbar and $T_t=0\ ^0$C for the liquid-solid I transition and using the values of a_{10} and b_{10}, the temperature dependence of the inverse susceptibility χ_I^{-1} from Eq. (3.265) can be reduced to

$$\chi_I^{-1} = \frac{35}{2}|T - T_t| \tag{3.266}$$

This represents the critical behaviour of the susceptibility according to the power law $\chi \sim |T\text{-}T_t|^{-\gamma}$ with the critical exponent $\gamma=1$ for the liquid-solid I transition in ice. We demonstrated the temperature dependence of the susceptibility χ_I within the temperature interval $-21\ ^0\text{C} < T < 0\ ^0\text{C}$ at P=1.8 kbar using Eq. (3.266) where $T_t=0\ ^0$C, as plotted in Fig. 3.22.

For solid I-solid III transition, the thermodynamic quantities are also calculated. The free energy of the solid III can be expressed in terms of the order parameter ψ_3 according to Eq. (3.222)

$$F_{III} = a_3\psi_3^2 + b_3\psi_3^4 + c_3\psi_3^6 \tag{3.267}$$

as the free energy of the solid I (Eq. 3.248). Since the solid I-solid III transition is of a first order, we have $F_I=F_{III}$ or,

$$a_1\psi_1^2 + b_1\psi_1^4 + c_1\psi_1^6 - (a_3\psi_3^2 + b_3\psi_3^4 + c_3\psi_3^6) = 0 \tag{3.268}$$

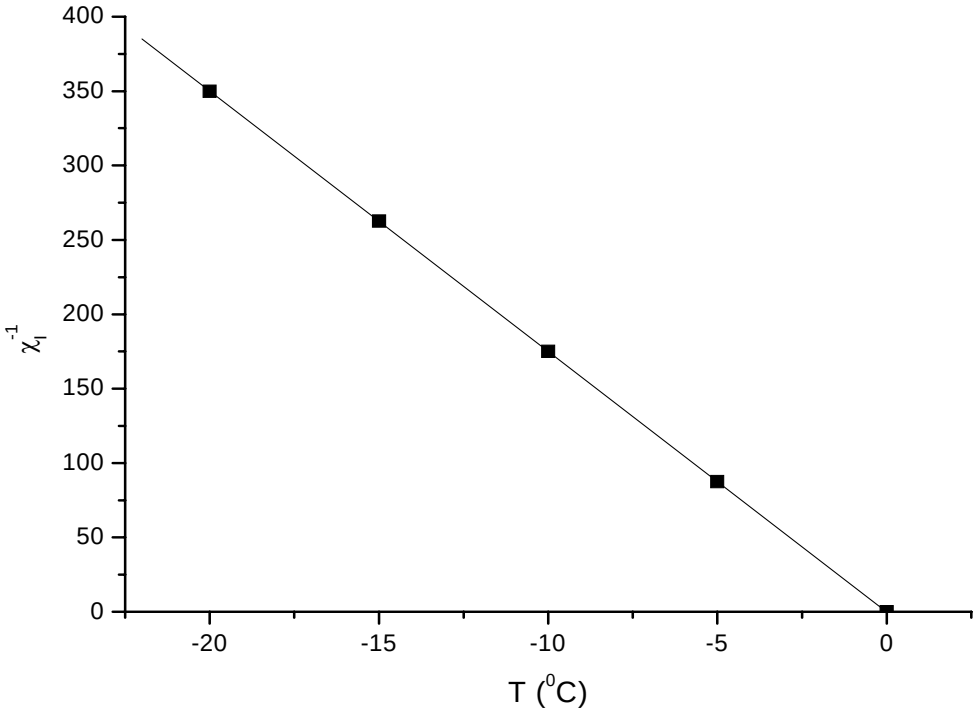

Figure 3.22 Calculated inverse susceptibility χ_I^{-1} as a function of temperature for the liquid-solid I transition in ice according to Eq. (3.266). Straight line represents the best fit to the values given here.

From the liquid-solid I transition ($F_I=F_L=0$), ψ_1 can be solved using Eq. (3.248) as,

$$\psi_1^2 = \left(\frac{1}{3c_1}\right)\left[-b_1 + \left(b_1^2 - 3a_1c_1\right)^{1/2}\right] \tag{3.269}$$

which gives a positive value for ψ_1^2. Similarly, from the liquid-solid III transition ($F_{III}=F_L=0$), ψ_3 can be solved using Eq. (3.267) as

$$\psi_3^2 = \left(\frac{1}{3c_3}\right)\left[-b_3 + \left(b_3^2 - 3a_3c_3\right)^{1/2}\right] \tag{3.270}$$

which is also the solution for a positive ψ_3^2. By defining the functions f_1 (Eq. 3.255) and f_3 as

$$f_3 = b_3^2 - 4a_3c_3 \tag{3.271}$$

ψ_1^2 (Eq. 3.269) and ψ_3^2 (Eq. 3.270) can be expressed as

$$\psi_1^2 = -\frac{2b_1 + (b_1^2 + 3f_1)^{1/2}}{6c_1} \tag{3.272}$$

and

$$\psi_3^2 = -\frac{2b_3 + (b_3^2 + 3f_3)^{1/2}}{6c_3} \tag{3.273}$$

By substituting ψ_1^2 (Eq. 3.272) into the F_I (Eq. 3.248), one gets

$$F_I = \frac{g}{c_1^2} \tag{3.274}$$

where

$$g = \frac{1}{54}\left[-b_1^3 + 9b_1f_1 + (b_1^2 + 3f_1)^{3/2}\right] \tag{3.275}$$

Also, by substituting ψ_3^2 (Eq. 3.273) into the F_{III} (Eq. 3.267), we have

$$F_3 = \frac{d}{c_3^2} \tag{3.276}$$

where

$$d = \frac{1}{54}\left[-b_3^3 + 9b_3 f_3 + (b_3^2 + 3f_3)^{3/2}\right] \tag{3.277}$$

By writing F_I=F_{III}, the phase line equation for the solid I-solid III transition can be established. This gives

$$\frac{g}{c_1^2} - \frac{d}{c_3^2} = h$$

(3.278) By choosing c_1= c_3=c, the phase line equation for the solid I-solid III transition then becomes

$$c = \left(\frac{g-d}{h}\right)^{1/2} \tag{3.279}$$

The temperature dependence of the specific heat C_p for the solid I-solid III transition, can be obtained from the free energies F_I (Eq. 3.274) and F_{III} (Eq. 3.276). Using the temperature and pressure dependence of a_1 and b_1 (Eqs. 3.253 and 3.254) in F_I (Eq. 3.274) through Eqs. (3.255) and (3.275), the specific heat C_p for the solid I phase can be obtained as a function of temperature

$$C_p(I) = \frac{1}{18}\left[b_{10}(2b_{10}^2 - 9a_{10}) + 2(b_{10}^2 - 3a_{10})^{-1/2} T(T-T_t)^{-1/2}\right] \tag{3.280}$$

Similarly, by assuming the temperature and pressure dependence of the coefficients a_3 , b_3 and c_3 as

$$a_3 = a_{30}(T-T_t) + a_{31}(P-P_t) + a_{32}(P-P_t)^2 \tag{3.281}$$

and

$$b_3 = b_{30}(T-T_t)^{1/2}, \quad c_3 = 1 \tag{3.282}$$

the temperature dependence of the specific heat C_p for the solid III phase can be obtained as a function of temperature

$$C_p(III) = \frac{1}{18}\left[b_{30}(2b_{30}^2 - 9a_{30}) + 2(b_{30}^2 - 3a_{30})^{-1/2}\right] T(T-T_t)^{-1/2} \tag{3.283}$$

Eq. (3.283) is obtained by substituting Eqs. (3.281) and (3.282) into Eq. (3.276) by means of Eqs. (3.271) and (3.277).

The temperature dependence of the specific heat C_p(I) and C_p(III) for the solid I (Eq. 3.280) and solid III (Eq. 3.283) can be demonstrated numerically using the values of $a_{10} = a_{30} = 2$ and $b_{10} = b_{30} = 3$, which reduces to

$$C_p(I) = C_p(III) = \frac{1}{9\sqrt{3}} T(T - T_t)^{-1/2}$$

(3.284)

We plot C_p(I) or C_p(III) as a function of temperature in Fig. 3.23 within the temperature interval -33 ^{0}C < T < -21 ^{0}C for P=1.8 kbar (Table 3.17) according to Eq. (3.284) where T_t= -21 ^{0}C.

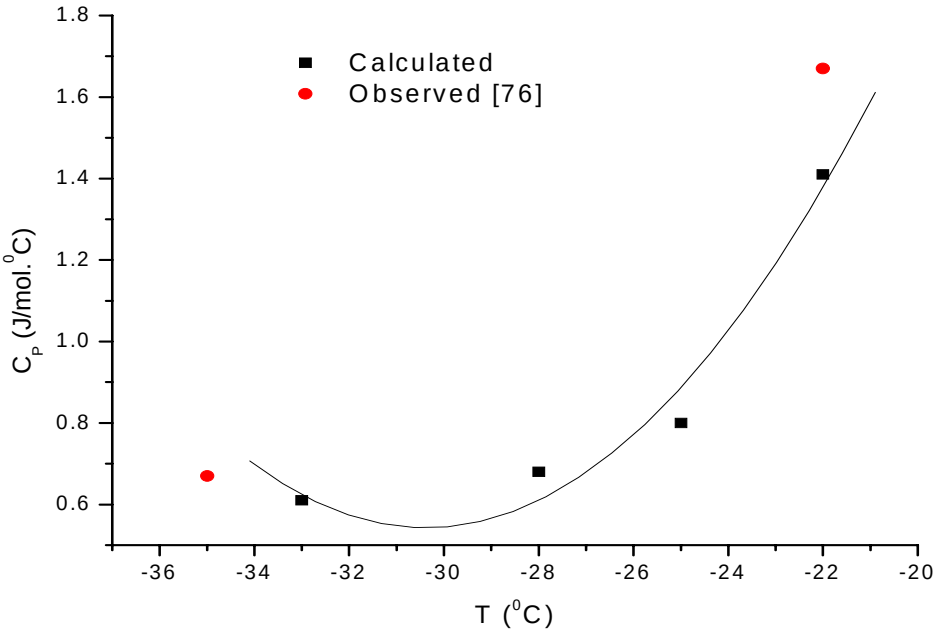

Figure 3.23 Calculated specific heat C_p as a function of temperature for the solid I-solid III transition in ice at 1.8 kbar according to Eq. (3.284). Solid curve represents the best fit to values given here.

The order parameter ψ can be obtained at various temperatures for the solid I-solid III transition within the temperature interval -33 ^{0}C < T < -21 ^{0}C at 1.8 kbar in ice. Using Eqs. (3.253) and (3.254) at P=P_t=1.8 kbar in Eq. (3.269) for ψ_1 of the solid I phase, one gets

$$\psi_1^2 = \frac{1}{3}\left[(b_{10}^2 - 3a_{10})^{1/2} - b_{10}\right](T - T_t)^{1/2} \tag{3.285}$$

or below the transition temperature (T_t= -21 ^{0}C)

$$\psi_1 = -\frac{1}{\sqrt{3}}\left[(b_{10}^2 - 3a_{10})^{1/2} - b_{10}\right]^{1/2}(T_t - T)^{1/4} \tag{3.286}$$

Similarly, using Eqs. (3.281) and (3.282) at P=P_t=1.8 kbar in Eq. (3.270), we get for the solid III phase

$$\psi_3 = -\frac{1}{\sqrt{3}}\left[(b_{30}^2 - 3a_{30})^{1/2} - b_{30}\right]^{1/2}(T_t - T)^{1/4} \tag{3.287}$$

By using the above values of $a_{10} = a_{30}$ and $b_{10} = b_{30}$ in Eqs. (3.286) and (3.287), the temperature dependence of the order parameters ψ_1 and ψ_3 can be expressed as

$$\psi_1 = \psi_3 = \left(1 - \frac{\sqrt{3}}{3}\right)^{1/2}(T_t - T)^{1/4} \tag{3.288}$$

We plot the order parameter ($\psi_1 = \psi_3$) as a function of temperature for the solid I-solid III transition of ice in Fig. 3.24.

Finally, the temperature dependence of the susceptibility can be predicted for the solid I-solid III transition in ice from the free energies of F_I (Eq. 3.248) and F_{III} (Eq. 3.267). By taking the second derivative of F_I with respect to the ψ_1 and using the temperature and pressure dependence of the coefficients a_1 and b_1 (Eqs. 3.253 and 3.254) as we performed for the liquid-solid I transition, we obtain the inverse susceptibility χ_I^{-1} by Eq. (3.265). At P=P_t=1.8 kbar, it will depend on the

temperature as given by Eq. (3.266) where T_t= -21 ^{0}C. Similarly, for the solid III we have the same temperature dependence of the inverse susceptibility χ_{III}^{-1}, as given by Eq. (3.266). We plot the temperature dependence of the inverse susceptibility $\chi_I^{-1} = \chi_{III}^{-1}$ within the same temperature interval (-33 ^{0}C < T < -21 ^{0}C) at P=1.8 kbar for the solid I-solid III transition of ice in Fig. 3.25.

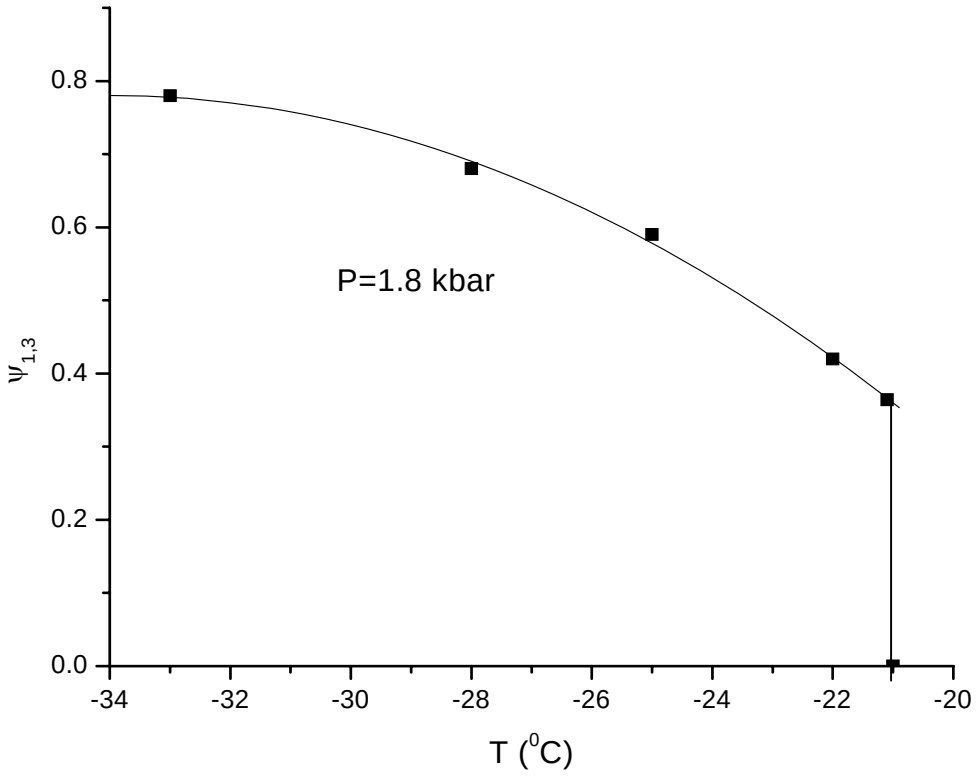

Figure 3.24 Calculated order parameter ψ as a function of temperature for the solid I-solid III transition in ice at 1.8 kbar according to Eq. (3.288). Solid curve represents the best fit to values given here.

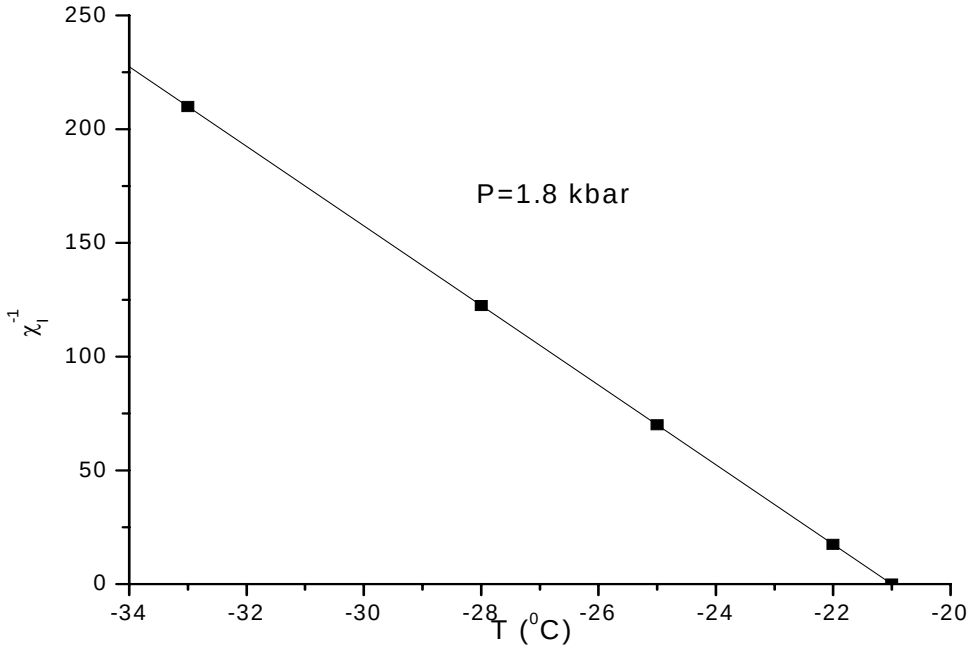

Figure 3.25 Calculated inverse susceptibility χ_I^{-1} as a function of temperature for the solid I-solid III transition in ice at 1.8 kbar according to Eq. (3.266). Straight line represents the best fit to the values given here.

3.3 Calculation of the Spontaneous Polarization and the dielectric Constant Using a Mean Field Model Close to the Paraelectric-Ferroelectric Phase Transition in Ammonium Sulphate

In section 2.5 we have described the ferroelectric properties of crystals in terms of polarization and the dielectric constant. In this section we calculate the spontaneous polarization and the dielectric constant close to the paraelectric-ferroelectric phase transition in ammonium sulfate.

We give here a mean field model which can describe the ferroelectric-paraelectric phase transition for ferroelectric materials. We expand the free energy in terms of the spontaneous polarization P (order parameter),

$$F = a_0 + a_2P^2 + a_4P^4 + a_6P^6 \tag{3.289}$$

where we assume that a_0 and a_6 are constants, a_2 and a_4 depend on temperature. We give the temperature dependencies of the coefficients a_2 and a_4 for the ferroelectric and paraelectric phases, separately below. Eq. (3.289) describes a first order phase transition with $a_4 < 0$ and $a_6 > 0$. By minimizing the free energy with respect to the spontaneous polarization, we get

$$P(2a_2 + 4a_4P^2 + 6a_6P^4) = 0 \tag{3.290}$$

The above equation can be solved for the spontaneous polarization P. The P=0 solution defines the paraelectric phase. The quadratic solution gives

$$P^2 = \frac{-a_4 \pm (a_4^2 - 3a_2a_6)^{1/2}}{3a_6} \tag{3.291}$$

which describes the ferroelectric phase. By using the temperature dependencies of the coefficients a_2 and a_4, the spontaneous polarization can be calculated as a function of temperature according to Eq. (3.291).

The temperature dependence of the electric susceptibility χ can also be derived from the free energy (Eq. 3.289). By taking the second derivative of the free energy with respect to the polarization, $\chi^{-1} = \left(\frac{\partial^2 F}{\partial P^2}\right)_T$ or the first derivative of the electric field defined as $E = \left(\frac{\partial F}{\partial P}\right)_T$ with respect to the polarization, we get the temperature dependence of the electric susceptibility as

$$\frac{1}{\chi} = 2a_2 + 12a_4P^2 + 30a_6P^4 \tag{3.292}$$

By taking the spontaneous polarization being zero (P=0) in the paraelectric phase,

$$\frac{1}{\chi} = \frac{1}{\varepsilon - 1} = 2a_2 \tag{3.293}$$

represents the temperature dependence of the electric susceptibility or equivalently, the dielectric constant ε in the paraelectric phase ($T > T_C$), whereas Eq. (3.292) is the χ relation in the ferroelectric phase ($T < T_C$).

Eq. (3.291) can be represented in terms of the coefficients a_2, a_4 and a_6 by substituting Eq. (3.290), the P^2 solution (with the minus sign in root square) into

Eq. (3.291). Using the ansatz $\frac{a_2 a_6}{a_4^2} \langle\langle 1$ and by expanding the root square term in Eq. (3.291) as

$$(a_4^2 - 3a_2 a_6)^{1/2} \cong a_4 - \frac{3}{2}\frac{a_2 a_6}{a_4} \tag{3.294}$$

By inserting Eq. (3.294) into Eq. (3.291), we obtain the spontaneous polarization as

$$P^2 = -\frac{2}{3}\frac{a_4}{a_6} + \frac{a_2}{2a_4} \tag{3.295}$$

Inserting Eq. (3.295) into Eq. (3.292) and aftersome algebra, the reciprocal electric susceptibility (Eq. 3.292) becomes

$$\frac{1}{\chi} = \frac{1}{\varepsilon - 1} = -12a_2 + \frac{16}{3}\frac{a_4^2}{a_6} \tag{3.296}$$

Thus, Eq. (3.296) represents the temperature dependence of the dielectric constant in the ferroelectric phase.

We calculate here the temperature dependence of the spontaneous polarization P and the electric susceptibility χ or the dielectric constant ε for the ferroelectric-paraelectric phase transition in $(NH_4)_2SO_4$. This calculation was performed for the three different frequencies, namely, 100, 500 and 2000 Hz on the basis of the experimental data for $(NH_4)_2SO_4$ [78]. We fitted the expressions for the dielectric constant (Eqs. 3.293 and 3.296) which we derived from the mean field model, to the experimental data for $(NH_4)_2SO_4$ [78]. For our fits, we assumed the temperature dependence of the coefficients as

$$a_2 = a_{20} + a_{21}(T - T_C) + a_{22}(T - T_C)^2 \tag{3.297}$$

for the paraelectric phase ($T > T_C$) according to Eq. (3.293).

For the ferroelectric phase, we assumed the temperature dependencies of the coefficients a_2 and a_4 for our fits as

$$a_2 = a_{20}(T - T_C) \tag{3.298}$$

$$a_4 = a_{40} + a_{41}(T - T_C) \tag{3.299}$$

and

$$a_6 = a_{60} \tag{3.300}$$

On the basis of the temperature dependence of the coefficient a_2 (Eq. 3.297), the dielectric constant ε (Eq. 3.293) can be written as

$$\frac{1}{\varepsilon-1} = 2a_{20} + 2a_{21}(T - T_C) + 2a_{22}(T - T_C)^2 \tag{3.301}$$

in the paraelectric phase.

Similarly, using the temperature dependencies of the coefficients a_2 (Eq. 3.298) and a_4 (Eq. 3.299) and a_6 (Eq. 3.300), the dielectric constant ε (Eq. 3.296) can be written as

$$\frac{1}{\varepsilon-1} = \frac{16}{3}\frac{a_{40}^2}{a_{60}} + \left[\frac{32}{3}\frac{a_{40}a_{41}}{a_{60}} - 12a_{20}\right](T - T_C) + \frac{16}{3}\frac{a_{41}^2}{a_{60}}(T - T_C)^2 \tag{3.302}$$

in the ferroelectric phase.

Finally, the temperature dependence of the spontaneous polarization (Eq. 3.295) can be written in terms of the temperature-dependent a_2, a_4 and a_6 terms as

$$P^2 = -\frac{2}{3a_{60}}[a_{40} + a_{41}(T - T_C)] + \frac{a_{20}(T-T_C)}{2[a_{40}-a_{41}(T-T_C)]} \tag{3.303}$$

Thus, we fitted first Eq. (3.302) to the experimental data for the dielectric constant [79] and determined the coefficients a_{20}, a_{40} and a_{41} at the frequency of 100 Hz for $(NH_4)_2SO_4$ in the ferroelectric phase ($T<T_C$). We chose here $a_{60} = 1$. Our fitted values of a_{20}, a_{40} and a_{41} are tabulated within the temperature interval in Table 3.19. We plot 1/(ε-1) as a function of T_C-T at 100 Hz for $(NH_4)_2SO_4$ in the ferroelectric phase ($T<T_C$) in Fig. 3.26 with the observed data [79]. We then fitted Eq. (3.301) to the experimental data [78] for $(NH_4)_2SO_4$ at 100 Hz and calculated the coefficients a_{20}, a_{21} and a_{22}, as given in Table 3.20 for the paraelectric phase ($T>T_C$). Fig. 3.27 gives 1/(ε-1) at various T-T_C values. Observed data for 100 Hz [78] are also given in Fig. 3.27.

Table 3.19 Values of the parameters calculated according to Eq.(3.302) within the temperature interval given for the frequencies indicated in the ferroelectric phase ($T<T_c$) of $(NH_4)SO_4$. The figure numbers are also given here to indicate the parameters used for each frequency.

Frequency(Hz)	a_{20} x10^{-4}/^{o}C	$-a_{40}$	$-a_{41}$ x10^{-3}/^{o}C	ΔT (K)= T_c-T	Figs.
100	1.80	0.0498	2.252	0< ΔT < 16	3.26
500	5.3118	0.07452	4.2575	0< ΔT < 20	3.28
2000	16.268	0.1174	7.963	0< ΔT < 20	3.31

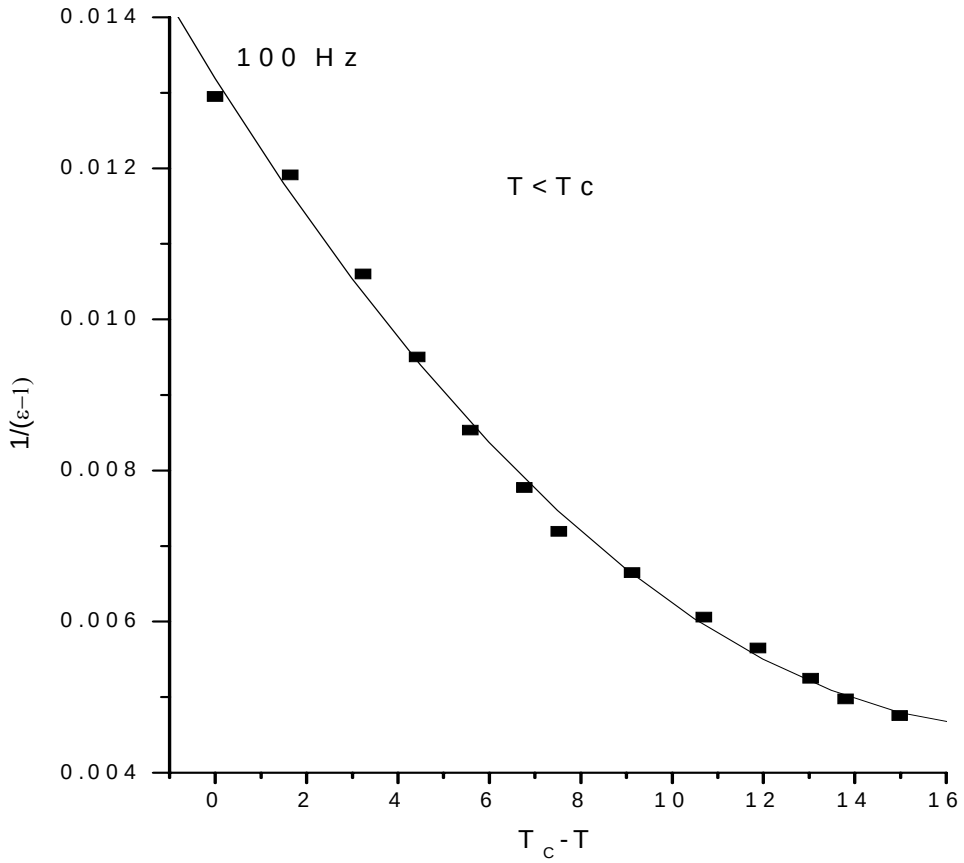

Figure 3.26 Inverse susceptibility $\chi^{-1}=1/(\epsilon-1)$, ϵ is the dielectric constant, calculated from Eq. (3.302) as a function of T_c-T in the ferroelectric phase ($T<T_c$) of $(NH_4)_2SO_4$ at the frequency of 100 Hz. (■) represents the observed data [78].

Table 3.20 Values of the parameters calculated according to Eq.(3.301) within the temperature interval given for the frequencies indicated in the paraelectric phase ($T>T_c$) of $(NH_4)SO_4$. The figure numbers are also given here to indicate the parameters used for each frequency.

Frequency(Hz)	a_{20}	$-a_{21}$ x10^{-4}/^oC	a_{22} x10^{-6}/$^oC^2$	ΔT (K)= $T-T_c$	Figs.
100	0.00642	1.183	1.288	$0<\Delta T<55$	3.27
500	0.01444	6.85	24.55	$0<\Delta T<18$	3.29
500	0.01023	0.5967	0.4158	$20<\Delta T<85$	3.30
2000	0.02039	2.1988	2.002	$0<\Delta T<80$	3.32

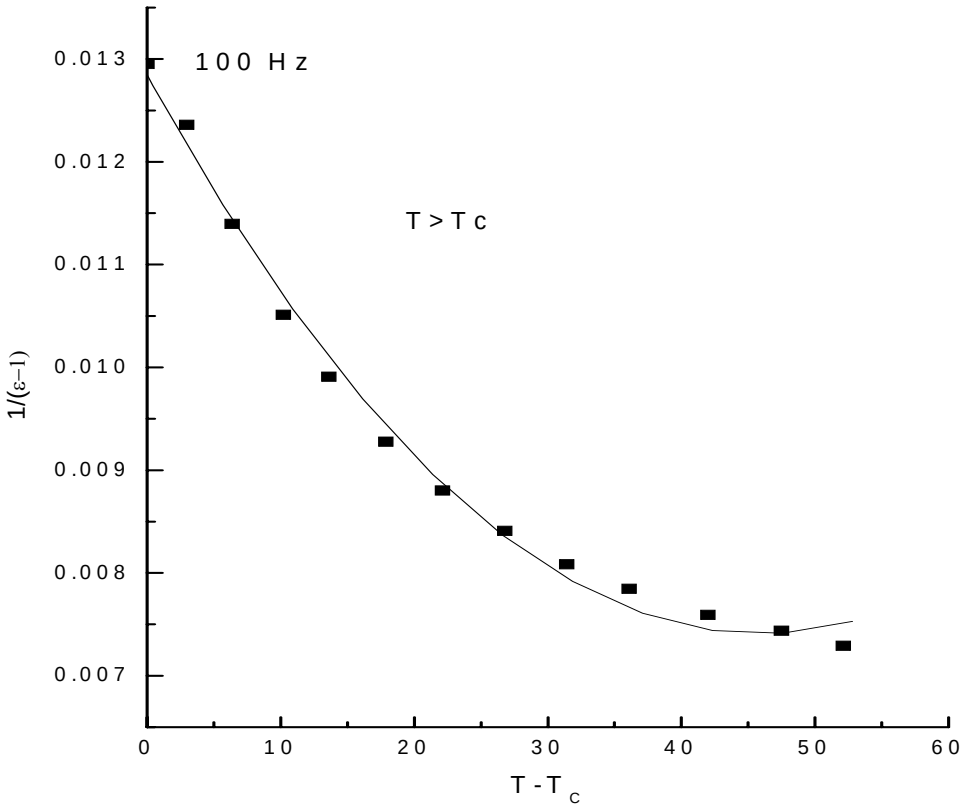

Figure 3.27 Inverse susceptibility $\chi^{-1}=1/(\epsilon-1)$, ϵ is the dielectric constant, calculated from Eq.(3.301) as a function of $T-T_c$ in the paraelectric phase ($T>T_c$) of $(NH_4)_2SO_4$ at the frequency of 100 Hz. (■) represents the observed data [78].

Similar calculation was also carried out at the frequencies of 500 and 2000 Hz for the ferroelectric and paraelectric phases of $(NH_4)_2SO_4$. By fitting Eq. (3.302) to the observed data at the frequencies of 500 and 2000 Hz [78], the coefficients a_{20}, a_{40} and a_{41} were determined within the temperature intervals in the ferroelectric phase, as given in Table 3.19. Also, by fitting Eq. (3.301) to the observed data [78], the coefficients a_{20}, a_{21} and a_{22} were determined within the temperature interval in the paraelectric phase, as tabulated in Table 3.20. Fig. 3.28 represents our calculated (Eq. 3.302) 1/(ε-1) against T_C-T in the ferroelectric phase ($T<T_C$) with the observed data [78]. Figs. 3.29 and 3.30 give our fits in the temperature intervals, as indicated in Table 3.20, for 1/(ε-1) against T-T_C in the paraelectric phase. The observed data [78] are also shown there. We plot in Figs. 3.31 and 3.32 our calculated values of 1/(ε-1) according to Eqs. (3.302) and (3.301), respectively against T_C-T (T-T_C) at the frequency of 2000 Hz in $(NH_4)_2SO_4$.

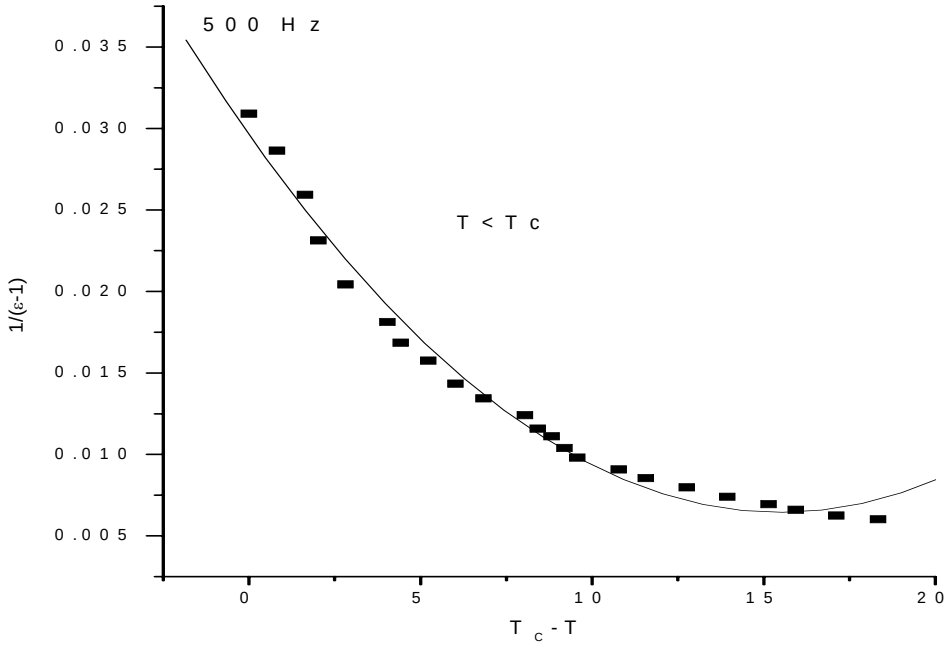

Figure 3.28 Inverse susceptibility $\chi^{-1}=1/(\epsilon-1)$, ϵ is the dielectric constant, calculated from Eq.(3.302) as a function of T_c-T in the ferroelectric phase ($T<T_c$) of $(NH_4)_2SO_4$ at the frequency of 500 Hz. (■) represents the observed data [78].

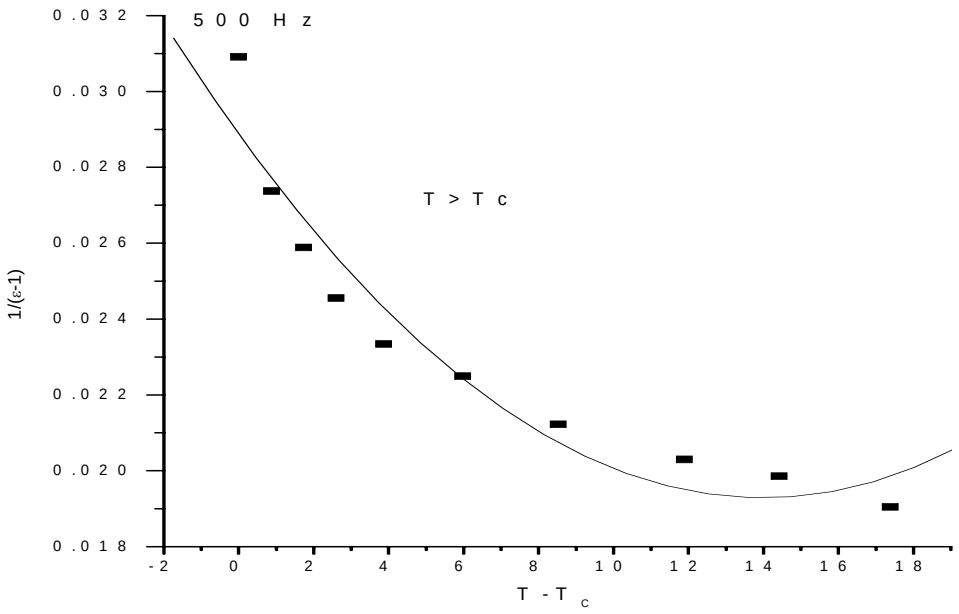

Figure 3.29 Inverse susceptibility $\chi^{-1}=1/(\epsilon-1)$, ϵ is the dielectric constant, calculated from Eq.(3.301) as a function of T-T_c in the paraelectric phase ($T>T_c$) within the temperature interval indicated for $(NH_4)_2SO_4$ at the frequency of 500 Hz. (■) represents the observed data [78].

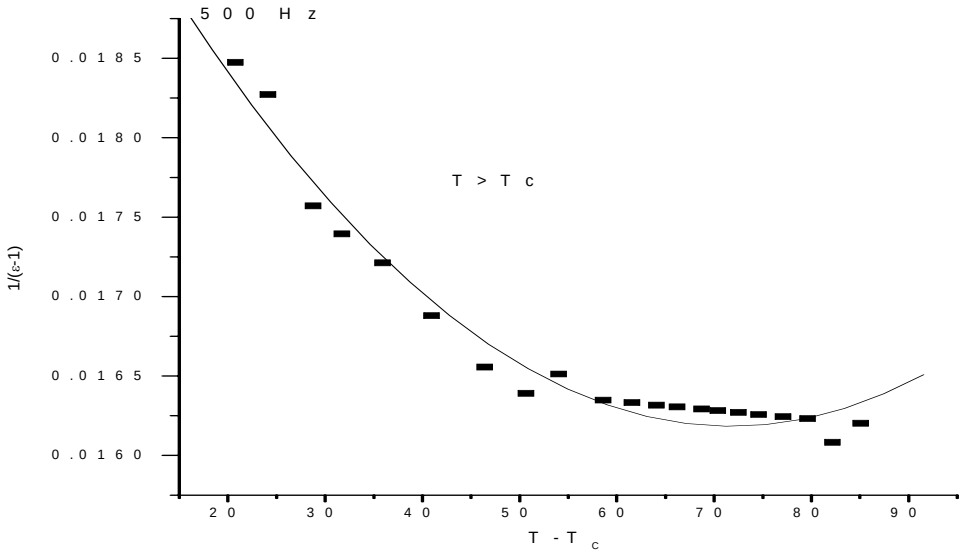

Figure 3.30 Inverse susceptibility $\chi^{-1}=1/(\epsilon-1)$, ϵ is the dielectric constant, calculated from Eq.(3.301) as a function of T-T_c in the paraelectric phase ($T>T_c$) within the temperature interval indicated for $(NH_4)_2SO_4$ at the frequency of 500 Hz. (■) represents the observed data [78].

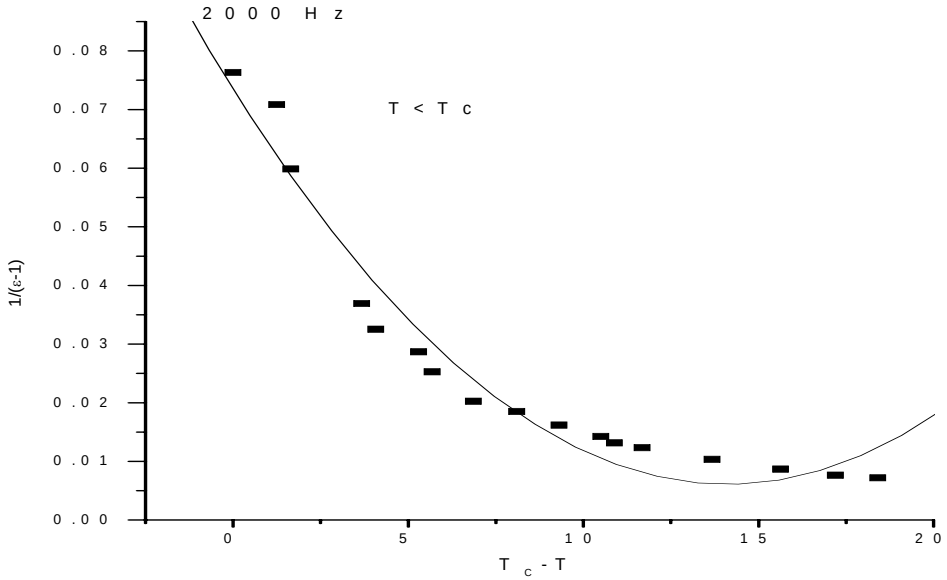

Figure 3.31 Inverse susceptibility $\chi^{-1}=1/(\epsilon-1)$, ϵ is the dielectric constant, calculated from Eq. (3.302) as a function of T_c-T in the ferroelectric phase ($T<T_c$) within the temperature interval indicated for $(NH_4)_2SO_4$ at the frequency of 2000 Hz. (■) represents the observed data [78].

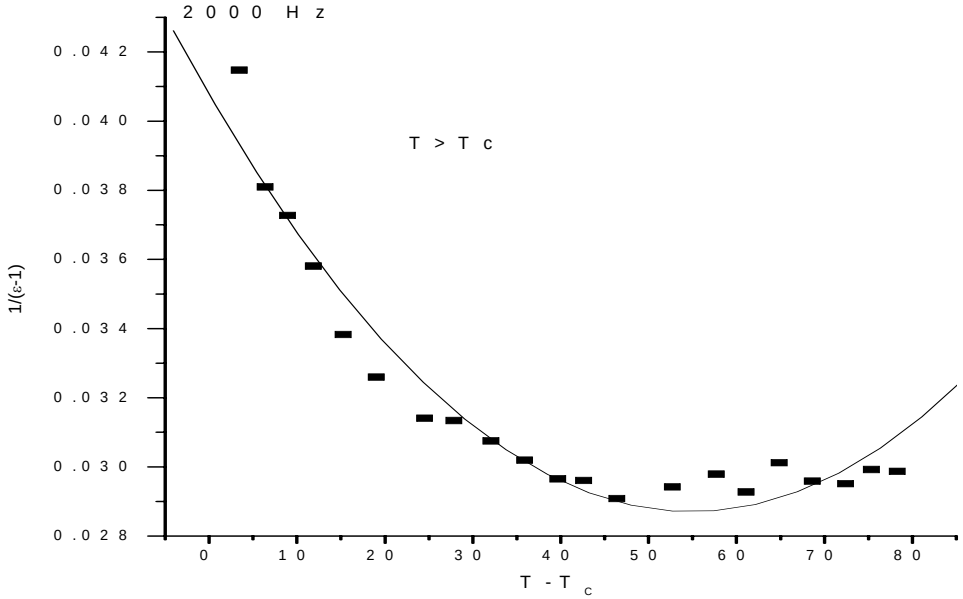

Figure 3.32 Inverse susceptibility $\chi^{-1}=1/(\epsilon-1)$, ϵ is the dielectric constant, calculated from Eq. (3.301) as a function of T-T_c in the paraelectric phase ($T>T_c$) within the temperature interval indicated for $(NH_4)_2SO_4$ at the frequency of 2000 Hz. (■) represents the observed data [78].

Since we determined the coefficients a_{20}, a_{40} and a_{41} for the ferroelectric phase at the frequencies of 100, 500 and 2000 Hz (Table 3.19), we were able to evaluate the spontaneous polarization as a function of temperature according to Eq. (3.303) for $(NH_4)_2SO_4$. Figs. (3.33-3.35) give our calculated polarization at various temperatures at the frequencies of 100, 500 and 2000 Hz, respectively.

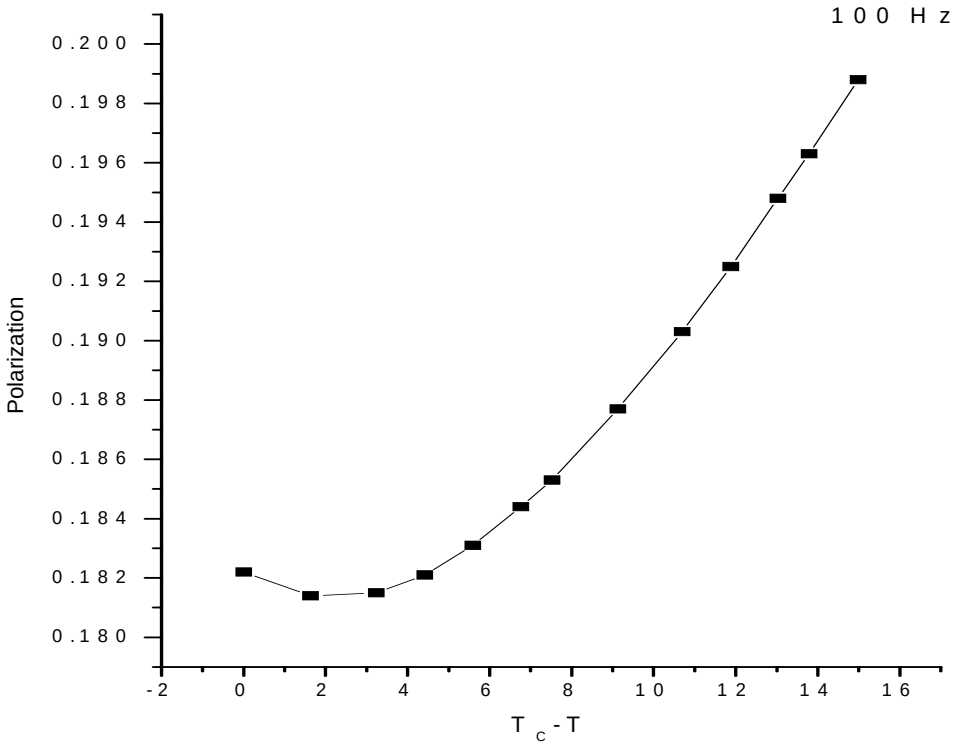

Figure 3.33 Polarization calculated from Eq. (3.303) as a function of T_c-T for $(NH_4)_2SO_4$ at the frequency of 100 Hz. (■) represents our calculated values of the polarization at various temperatures and the solid line is the best fit (Eq. 3.303).

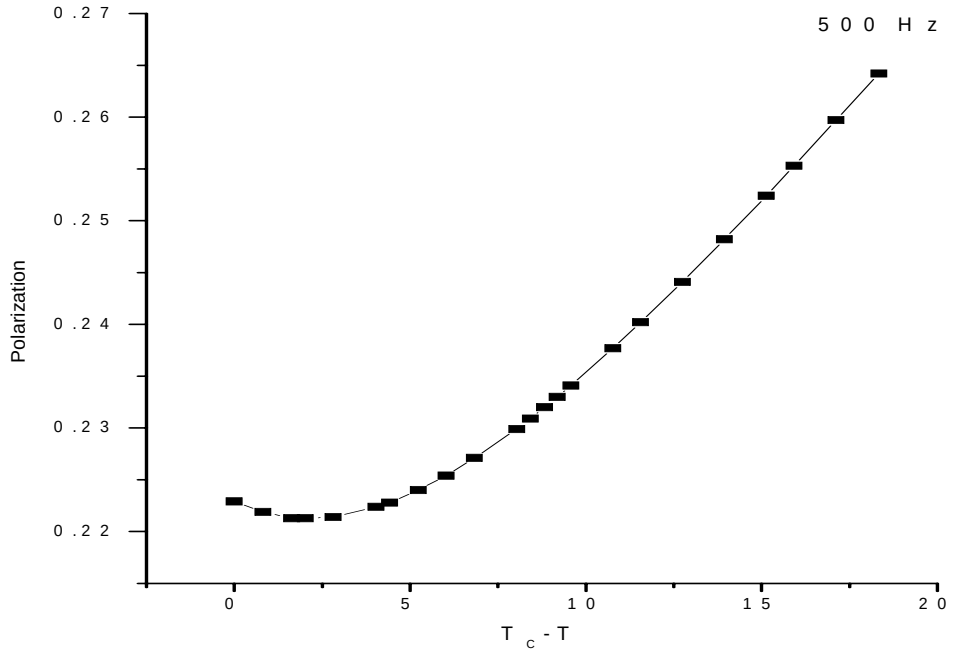

Figure 3.34 Polarization calculated from Eq. (3.303) as a function of T_c-T for $(NH_4)_2SO_4$ at the frequency of 500 Hz. (■) represents our calculated values of the polarization at various temperatures and the solid line is the best fit (Eq. 3.303).

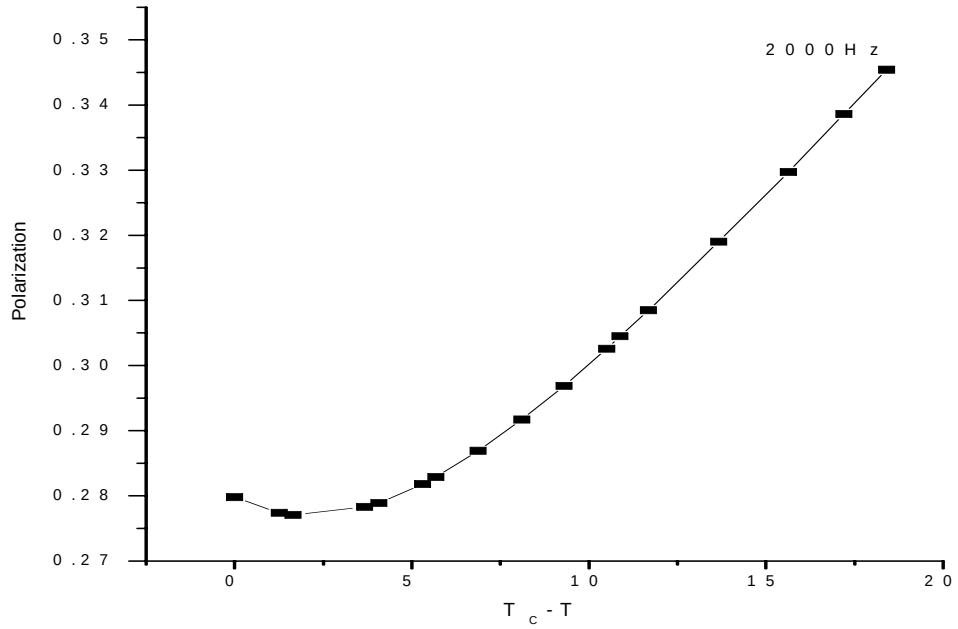

Figure 3.35 Polarization calculated from Eq. (3.303) as a function of T_c-T for $(NH_4)_2SO_4$ at the frequency of 2000 Hz. (■) represents our calculated values of the polarization at various temperatures and the solid line is the best fit (Eq. 3.303).

CHAPTER 4

DISCUSSION

For the λ-phase transition, we first calculated the critical exponent and by using the values of the critical exponent, we plotted the specific heat against the temperature for the ν_7 (56 cm^{-1}) and ν_2 (1684 cm^{-1}) Raman modes. For the disordered β-antiferro-ordered γ phase transition which is a second order phase transition in NH_4Br, the values of the critical exponent α which we deduced from the Raman frequencies of the ν_7 (56 cm^{-1}) and ν_2 (1684 cm^{-1}) modes, can be compared with the predictions of an Ising model. Our value of α=0.19 (below and above T_λ) due to the ν_7 (56 cm^{-1}) mode is close to the critical exponent value of 0.125 (=1/8) for the specific heat C_P predicted from a three dimensional Ising model. However, our values of α=0.45 ($T< T_\lambda$) and α=0.57 ($T> T_\lambda$) due to the ν_2 (1684 cm^{-1}) mode in NH_4Br, are very large compared to the Ising value. Those values can be reasonably compared with the value of α'≈0.67 obtained from the analysis of the experimental measurements of C_P data for NH_4Cl [3].

According to Figs. 3.4 and 3.5, there are discrepancies that occur close to the transition temperature T_λ. These discrepancies may be due to the fact that we compared our calculated C_{VI} with the observed C_P instead of C_V which is not accessible experimentally. Although there are discrepancies, our calculated values of the specific heat C_{VI} are reasonably in good agreement with the observed C_P for NH_4Br. There are also some discrepancies for ν_7 (56 cm^{-1}) above T_λ. This discrepancy can be explained on the basis of the pseudospin-phonon coupling in an Ising model due to Yamada *et al.* [62]. If the critical behaviour of the frequency shifts for the ν_7 (56 cm^{-1}) Raman mode is not the same in the β and γ phases, in other words, the temperature dependence of the frequency shifts is accompanied

with a different value of the critical exponent α above T_λ, this may affect our calculated values of C_{VI} in the β phase. As a result of this, our calculated C_{VI} values can possibly agree better with the observed C_P [3] above T_λ, as we obtained for the ν_2 (1684 cm^{-1}) mode using two different values of the critical exponent below and above T_λ [54].

After this calculation, we calculated a linear variation between the specific heat and the frequency shifts according to the Pippard relation by using the calculated critical exponent values for both ν_7 (56 cm^{-1}) and ν_2 (1684 cm^{-1}) Raman modes below and above T_λ (=234 K). By using this linear variation, we obtained the values of the $(dP/dT)_\lambda$ for two seperate temperature regions and from the slope values, we see that $(dP/dT)_\lambda$ varies considerably, depending on entirely the temperature interval where the analysis was performed.

The values of the slope $(dP/dT)_\lambda$ which we deduced using the Raman frequencies of the ν_7 (56 cm^{-1}) and ν_2 (1684 cm^{-1}) modes, can be compared with the previous values of 62.1 bar/K for the ν_5 (134 cm^{-1}) and 90.1 bar/K for the ν_5 (177 cm^{-1}) Raman modes in NH_4Br [79]. All our values obtained in this study and also those given in the earlier study [79] for the $(dP/dT)_\lambda$, can be compared with the $(dP/dT)_\lambda$ value of 58.68 bar/K which is the value of Garland and Young [80] from their plot of C_P against αV for NH_4Br. Our slope values given here for NH_4Br can also be compared with the earlier values of 105.5 bar/K for the lattice mode of ν_5 (174 cm^{-1}) [52] and 94.9 bar/K for the internal mode of ν_2 (1708 cm^{-1}) [81] in NH_4Cl (T_λ=241.5 K). Another comparison can be made between our $(dP/dT)_\lambda$ values for the ν_7 (56 cm^{-1}) mode (Table 3.4) and ν_2 (1684 cm^{-1}) mode (Table 3.5) in NH_4Br (P=0), and those $(dP/dT)_C$ values which have been obtained recently [82] for the ν_7 (93 cm^{-1}) and ν_5 (144 cm^{-1}) disorder-induced modes of NH_4Cl close to its tricritical phase transition (P≅1.6 kbar). As has been reported in the previous study [83], the $(dP/dT)_C$ values are 151 bar/K for the ν_7 (93 cm^{-1}) mode ($T>T_C$)and 93.9 bar/K ($T< T_C$), and 129.5 bar/K ($T>T_C$) for the ν_5 (144 cm^{-1}) mode in NH_4Cl (P≅1.6 kbar, T_C=257.17K). We also note here that the values of the intercept $T(dS/dT)_\lambda$ for the lattice mode of ν_7 (56 cm^{-1}) (Table 3.4), are considerably lower

than those given for the internal mode of ν_2 (1684 cm^{-1}) (Table 3.5) in NH_4Br at the λ point.

By knowing the values of $(1/\nu)(\partial\nu/\partial P)_T$ and γ_T, we can calculate the isothermal compressibility κ_T using Eq. (2.4). Thus, the thermodynamic quantities such as the specific heat C_P, the thermal expansivity α_P and the isothermal compressibility κ_T can be calculated by means of our spectroscopically modified Pippard relations (Eqs. 2.1 and 2.2). This then provides us to obtain the thermodynamic data from the frequencies measured accurately for NH_4Br close to its λ-transition line. Also, a linear variation of the thermal expansivity α_p with the frequency shifts $(1/\nu)(\partial\nu/\partial P)_T$ can be tested close to the λ-transition line for NH_4Br. Thus, the thermal expansivity and isothermal compressibility can be calculated from the frequencies measured as a function of pressure in NH_4Br [64].

In section 3.2, we calculated the phase diagrams using the mean field theory for NH_4Cl, ND_4Cl, $(NH_4)_2SO_4/H_2O$, $LiK_{1-x}Rb_xSO_4$, $K_2S_2O_7$-$KHSO_4$, CnM-CrM, CnM-CO, C_6H_6 and ice. By fitting the phase diagrams for these nine structures, we calculated the temperature and pressure or concentration dependence of the coefficients. This gave us the temperature and pressure or concentration dependence of the free energies and the order parameters of these materials. Furthermore, this led us to predict the temperature and pressure dependence of some other thermodynamic quantities such as the specific heat, isothermal compressibility and thermal expansivity. Our mean field models studied here do not only predict the phase line equations for the T-P (or X) phase diagram, but also they predict the temperature and pressure (or concentration) dependencies of the free energy, order parameter and the relevant thermodynamic quantities. Furthermore, since the Raman intensity is proportional to the order parameter, from the temperature dependence of the order parameters ψ, the Raman intensity can be calculated and compared with the experimentally measured intensities of those modes involved in the mechanism of the λ-phase transitions. Also, by taking the temperature derivative of the order parameter, the specific heat can be calculated. As examples, the specific heat C_P, the order parameter ψ and the inverse susceptibility χ^{-1} were calculated as functions of temperature at 1.8 kbar for the

solid I-solid III transition in ice, as shown in Figs. (3.23-3.25), respectively. This was done by calculating the coefficients in the free energy expansion, which were used in the expressions of C_P, ψ and χ^{-1} for ice. Similar treatment can be performed for the other materials studied here. The temperature dependence of some thermodynamic quantities close to phase transitions in benzene (C_6H_6) by using the coefficients obtained in the free energy, is in progress and this work will be published elsewhere.

We calculated in section 3.3 the temperature dependence of the dielectric constant by the relations derived from our mean field model for the ferroelectric and paraelectric phases of $(NH_4)_2SO_4$. This calculation was carried out at the frequencies of 100, 500 and 2000 Hz for $(NH_4)_2SO_4$. By fitting the equations to the experimental data [78], we deduced the values of the coefficients (Tables 3.19 and 3.20). As we see from our plots (Figs. 3.26-3.32), the quadratic fits are reasonably good and they can be compared well with the observed data [78]. In particular, at the frequency of 100 Hz (Figs. 3.26 and 3.27), the observed data is very well represented by the predictions of our mean field model. At higher frequencies (500 and 2000 Hz) our fits (Figs. 3.28-3.32) are not as good as that for 100 Hz because of some scattered data which is not well represented by a quadratic function according to our mean field model. At the frequency of 500 Hz, we fitted the equation to the experimental data [78] in the paralectric phase ($T>T_C$) for two different temperature intervals (Figs. 3.29 and 3.30). This was due to the fact that the experimental measurements were ranged from 0 to 90 K ($T-T_C$).

By knowing the values of the coefficients (Table 3.21) from the fits of the dielectric constant ε, we were then able to evaluate the spontaneous polarization for various temperatures at the frequencies of 100, 500 and 2000 Hz in $(NH_4)_2SO_4$. As shown in Figs. (3.33-3.35), our calculated values of the spontaneous polarization exhibit usual critical behaviour in the ferroelectric phase. As the temperature increases, the spontaneous polarization grows which indicates the ordering due to the reorientation of the NH_4^+ ions. As shown in Figs. (3.33-3.35), the spontaneous polarization exhibits almost the same critical behaviour within the temperature interval in the ferroelectric phase. Our values of the spontaneous polarization

calculated at the frequencies of 100, 500 and 2000 Hz, can be compared with the experimental measurements.

CHAPTER 5

CONCLUSIONS

Using the mean field models, the T-P and T-X phase diagrams of various physical systems such as NH_4Cl, ND_4Cl, $(NH_4)_2SO_4/H_2O$, $LiK_{1-x}Rb_xSO_4$, $K_2S_2O_7$-$KHSO_4$, cholesteric systems (CnM-CrM, CnM-CO), benzene (C_6H_6) and ice, were calculated in this study. By fitting the phase line equations derived from the mean field models to the experimental data for these systems, the T-P and T-X phase diagrams were obtained. This was done by assuming the temperature and pressure (or concentration) dependence of the coefficients in the phase line equations. These dependences were chosen in the simplest form and the phase line equations were fitted to the experimental data by means of the quadratic polynomials.

By expressing the thermodynamic quantities such as the order parameter, specific heat and the susceptibility in terms of the coefficients expanded in the free energies of those systems studied here, their critical behaviour has been predicted, as examplified for ice. For the liquid-solid I and solid I-solid III transitions in ice, the temperature dependences of the specific heat C_P, the order parameter ψ and the inverse susceptibility χ^{-1} were obtained. The critical behaviour of C_P, ψ and χ was described with the values of the critical exponents $\alpha= 1/2$, $\beta=1/4$ and $\gamma=1$, respectively from the mean field models. According to the universal scaling law $\alpha+2\beta+\gamma \geq 2$, summation of our exponent values gives the value of 2. In fact, the exponent value for the order parameter ψ should be equal to 1/2 for a second order transition in the mean field theory. Our value of $\beta=1/4$ which is the tricritical value in the mean field theory indicates that the transitions of the liquid-solid I and solid I-solid III in ice are not of a second order type, but instead, most likely they are nearly second order or weakly first order. Also, the mean field theory gives for a

second order transition the value of α=0 for the specific heat. Our value of the α=1/2 is the tricritical value in the mean field theory. This is also another indication that ice exhibits a weakly first order or nearly second order transition regarding liquid-solid I and solid I-solid III transitions since the tricritical behaviour is just the transition between the first order and the second order. As performed for ice, by deriving the temperature dependence of the order parameter, specific heat and the susceptibility from the free energy, the values of the critical expoonents can be extracted for all the physical systems studied here. Thus, the type of phase transitions can be determined for those systems whose T-P or T-X phase diagrams were obtained using the mean field theory. Experimental measurements for the order parameter, heat capacity and the susceptibility close to phase transitions as given in the T-P or T-X phase diagrams of the physical systems studied here, can examine our predictions on the basis of the mean field models.

In this study, spontaneous polarization and the dielectric constant were calculated as a function of temperature for constant frequencies from a mean field model of ammonium sulphate. By expanding the free energy in terms of the spontaneous polarization up to the sixth order term, spontaneous polarization and the dielectric constant (or dielectric susceptibility) were calculated at various temperatures for fixed frequencies of 100, 500 and 2000 Hz, as stated above. This was done by assuming the temperature dependence of the coefficients in the free energy of the mean field model. The calculated inverse susceptibility in the quadratic form was fitted to the experimental data for the fixed frequencies studied for $(NH_4)_2SO_4$. This mean field model given here is the simplest one since the sublattice structure of $(NH_4)_2SO_4$ has not been considered here. According to the two sublattice model for this molecular crystal, the free energy has been expanded in terms of two polarizations P_1 and P_2 with the linear coupling P_1P_2 [83]. Another sublattice model up to P_1^4 (P_2^4) with the linear coupling term P_1P_2 which considers dipole-dipole interactions has also been introduced [84]. The critical behaviour of spontaneous polarization and the dielectric susceptibility has been studied using the experimental data for both sublattice models [83, 84]. In a more recent study [85] by considering a quadratic coupling term $P_1^2P_2^2$ which describes the quadrupole-quadrupole interactions, a two sublattice model has been introduced to calculate the

temperature dependence of dielectric susceptibility using the experimental data for the dielectric constant of $(NH_4)_2SO_4$ [83, 84]. In general, polarization and dielectric susceptibility are the frequency dependent and it should be of interest to study the dynamical properties of ammonium sulfate close to the paraelectric-ferroelectric phase transition in this system.

In this study, the critical behaviour of the specific heat was predicted on the basis of and Ising model by analyzing the Raman frequency shifts for the lattice and internal modes of NH_4Br close to the λ-transition point. The specific heat C_P was related linearly to the Raman frequency shifts $(1/\nu)(\partial\nu/\partial T)_P$ for the λ-phase transition of NH_4Br.

Calculations of the phase diagrams and predictions for the critical behaviour of the thermodynamic quantities from the mean field models studied here indicate that our methods given are adequate to investigate the mechanism of phase transitions for the physical systems of interest.

REFERENCES

[1] Wikipedia, http://en.wikipedia.org/wiki/Phase_transition, visited on February 2009

[2] Wikipedia, http://en.wikipedia.org/wiki/Ammonium_bromide, visited on February 2009

[3] K. J. Lushington, C. W. Garland, J. Chem. Phys. **72**, 5752 (1980)

[4] H. A. Levy and S. W. Peterson, Phys. Rev. **86**, 766 (1952)

[5] Wikipedia, http://en.wikipedia.org/wiki/Ammonium_chloride, visited on February 2009.

[6] B. B. Weiner and C. W. Garland, J. Chem. Phys. **56**, 155 (1972)

[7] C. W. Garland, D. E. Bruins and T. J. Greytak, Phys. Rev. **B12**, 2759 (1975)

[8] C. W. Garland and J. D. Baloga, Phys. Rev. **B16**, 331 (1977)

[9] C. W. Garland and B. B. Weiner, Phys. Rev. **B3**, 1634 (1971)

[10] L. Benguigui, Solid State Comm. **20**, 173 (1976)

[11] W. B. Yelon, D. E. Cox, P. J. Kortman and W. B. Daniels, Phys. Rev. **B9**, 4843 (1974)

[12] C. Zahradnik and C. W. Garland, J. Chem. Phys. **70**, 1011 (1979)

[13] Wikipedia, http://en.wikipedia.org/wiki/Ammonium_sulphate, visited on February 2009.

[14] B. T. Mathias and J. P. Reneika, Phys. Rev. **103**, 262 (1956)

[15] E. O. Schlenger and W. C. Hamilton, J. Chem. Phys. **44**, 4498 (1966)

[16] V. A. Piragas and V. E. Schneider, Sov. Phys. Solid State **20**, 990 (1978)

[17] L. E. O'Reilly and T. Tsang, J. Chem. Phys. **46**, 1291 (1967)

[18] R. Sawada, Y. Takagi and Y. Ishibashi, J. Phys. Soc. Jpn. **34**, 748 (1973)

[19] J. Xu, D. Imre, R. McGraw and I. Tang, J. Phys. Chem. B **102**, 7462 (1998)

[20] H. Yurtseven, Y. Enginer, S. Şen and S. Salihoğlu, Journal of the Indian Chemical Society **84**, 350 (2007)

[21] Y.Y. Li, Solid State Commun. **51**, 355 (1984)

[22] J. Chung and T. Hahn, Acta Crysttallogr. Sect A **28**, 557 (1972)

[23] H. Sankaran, S. M. Sharma, and S. K. Sikka, Solid State Commun. **66**, 7 (1988)

[24] D.R. Ventura, N. L. Spezialli, and M.A. Pimenta, Phys. Rev. B **54**, 11869 (1996)

[25] A. Righi, P. Bourson, A. P. Ayala, R. L. Moreira, P. Galez, and J. L. Soubeyroux, Solid State Commun. **107**, 193 (1998)

[26] P. L. Zhang, Q. W. Yan, and J. X. Boucherle, Acta Crysttallogr. Sect B **43**, 147 (1987)

[27] A. J. Bradley, Philos. Mag. **49**, 1225 (1925)

[28] H. Schulz, U. Zucker, and R. French, Acta Crysttallogr. Sect B **41**, 21 (1985)

[29] M. L. Bansal, S. K. Deb, A. P. Roy, and V. C. Sahni, Solid State Commun. **36**, 1047 (1985)

[30] W. Kleemann, F.G. Schafer, and A. S. Chaves, Solid State Commun. **64**, 189 (1986)

[31] S.Bhakay-Tamhane, A. Sequeira, and R. Chidambaram, Phase Transitions **35**, 75 (1991)

[32] J. Mendes Filho, J. E. Moreira, F. E. A. Melo, F. A. Germano, and A. S. B. Sombra, Solid State Commun. **60**, 189 (1986)

[33] K. Stahl, T. Balic-Zunic, F. da Silva, K.M. Eriksen, R.W. Berg and R. Fehrmann, J. Solid State Chem. **178**, 1697 (2005)

[34] Wikipedia, http://en.wikipedia.org/wiki/Potassium_pyrosulfate, visited on February 2009

[35] K.M. Eriksen, R. Fehrmann, G. Hatem, M. Gaune-Escard, O.B. Lapina and V.M. Mastikhin, J. Phys. Chem. **B100**, 10771 (1996)

[36] B.E. North, G.G. Shipley and D.M. Small, Biochem. Biophys. Acta **424**, 376 (1976)

[37] D. M. Small *M. Blank, Ed., Plenum Press, Newyork, N.Y.,* 55-83 (1970)

[38] G.J. Davis, R.S. Porter, J.W.Steiner and D.M. Small, Mol. Cryst. Liq. Cryst. **10**, 331 (1970)

[39] Wikipedia, http://en.wikipedia.org/wiki/Benzene, visited on February 2009

[40] M. M. Thiery and J. M. Leger, J. Chem. Phys. **89**, 4255 (1988).

[41] E. G. Cox, Rev. Mod. Phys. **30**, 159 (1958)

[42] E. G. Cox, D. W. J. Cruickshank and J. A. S. Smith, Proc. R. Soc. London Ser: A **247**, 1 (1958)

[43] G. E. Bacon, N. A. Curry and S. A. Wilson, Proc. R. Soc. London Ser: A **279**, 98 (1964)

[44] G. J. Piermarini, A. D. Mighell, C. E. Weir and S. Block, Science **169**,1250 (1969)

[45] J. Akella and G. J. Kennedy, J. Chem. Phys. **55**, 793 (1971)

[46] Ph. Pruzan, J. C. Chervin, M. M. Thiery, J. P. Itie, J. M. Besson, J. P. Forgerit and M. Revault, J. Chem. Phys. **92**, 6910 (1990)

[47] S. Block, C. E. Weir and G. J. Piermarini, Science **169**, 586 (1970)

[48] F. Cansell, D. Fabre and J. P. Petitet, J. Chem. Phys. **99**, 7300 (1993)

[49] R. M. Klein, M. Nourbakhsh and P. N. Adler, J. Mater. Sci. **3**, 657 (1968)

[50] Wikipedia, http://en.wikipedia.org/wiki/Ice, visited on February 2009

[51] A. B. Pippard, The Elements of Classical Thermodynamics (Cambridge University Press, New York) 1957

[52] H. Yurtseven and W.F. Sherman, J. Mol. Struc. **115**, 169 (1984).

[53] ETH-PNM Education, http://www.pnm.ethz.ch/education/advancedssp/Exercise1 , visited on February 2009

[54] S. Şen and H. Yurtseven, J. Mol. Struc. **834-836**, 561 (2007)

[55] Wikipedia, http://en.wikipedia.org/wiki/Mean_Field_Theory, visited on February 2009

[56] University of Prince Edward Island Department of Physics http://www.upei.ca/~physics/sbo/Teaching/StatPhysII/StatPhysII_Notes/Phys402_L12.pdf , visited on February 2009

[57] NationMaster Encyclopedia, http://www.natinmaster.com/encyclopedia/Polarization-density, visited on February 2009

[58] C. Kittell *Seventh Ed., John Wiley and Sons Inc., Newyork, N.Y.,* 381-405 (1996)

[59] NationMaster Encyclopedia, http://www.natinmaster.com/encyclopedia/Ferroelectric, visited on February 2009

[60] NationMaster Encyclopedia, http://www.natinmaster.com/encyclopedia/

Hysteresis, visited on February 2009

[61] NationMaster Encyclopedia, http://www.natinmaster.com/encyclopedia/Paraelectricity, visited on February 2009

[62] Y. Yamada, M. Mori, Y. Noda, J. Phys. Soc. Jpn. **32**, 1565 (1972)

[63] P. Schwartz, Phys. Rev. **B 4**, 920 (1971)

[64] H. Yurtseven, A. Yanık, S. Şen, Spectrochim Acta **A 71**, 105 (2008)

[65] K. J. Lushington and C. W. Garland, J. Chem. Phys. **72**, 5752 (1980)

[66] H. Yurtseven, M. Güleç and W.F. Sherman, Phase Trans. **56**, 137 (1996)

[67] Phase Changes: Phase Diagram, http://www. Chm.davidson.edu/ ChemistryApplets/PhaseChanges/PhaseDiagram.html, visited on February 2009

[68] Phase Diagrams, http://www.brocku.ca/earthsciences/people/gfinn/petrology/ phase.htm, visited on February 2009

[69] C. W. F. T. Pistorius, J. Chem. Phys., **50**, 1436 (1969)

[70] H. Yurtseven, S. Salihoğlu, S. Şen, Phys. Stat. Sol. B, **244**, 2589 (2007)

[71] H. Yurtseven and S. Şen, Jpn. J. Appl. Phys., **47**, 2217 (2008)

[72] S. Şen and H. Yurtseven, "Calculation of the Phase Diagram Using the Mean Field Theory for $K_2S_2O_7$-$KHSO_4$", J. Mol. Liq. (in print) 2009

[73] H. Yurtseven and S. Şen "Calculation of the T-X Phase Diagram of Binary Mixtures of Cholestanyl Myristate (CnM)-Cholesteryl Myristate (CrM) and Cholestanyl Myristate (CnM)-Cholesteryl Oleate (CO)", Annals of NYAS (in print) 2009

[74] B.E. North and D.M. Small, J. Phys. Chem., **81**, 723 (1977).

[75] S. Şen and H. Yurtseven "T-P Phase Diagram of Benzene", J. Optoelectronics and Adv. Mater. (in print) 2008

[76] H. Yurtseven, S. Salihoğlu, Y. Enginer and S. Şen, Il Nuovo Cimento B, **123**, 533 (2008)

[77] N. N. Fletcher, The Chemical Physics of Ice (Cambridge University Press), 1970.

[78] Y. A. Badr and S. Awad, J. Phys. Chem. Solids, **45**, 351 (1984)

[79] H. Yurtseven and W. F. Sherman, J. Mol. Struc. **435**, 143 (1997).

[80] C. W. Garland and R. A. Young, J. Chem. Phys. **49**, 5282 (1968).

[81] H. Yurtseven and W. F. Sherman, J. Mol. Struc. **323**, 243 (1994).

[82] H. Yurtseven and F. Eraslan, J. Quan. Spec. and Rad. Trans. **102**, 513 (2006).

[83] A. Onodera, Y. Sugata and Y. Shiozaki, Solid State Comm. **27**, 243 (1978).

[84] A. Onodera, O. Cynshi and Y. Shiozaki, J. Phys. C: Solid State Phys. **18**, 2831 (1985).

[85] Y. Enginer, S. Salihoğlu and H. Yurtseven, Chin. J. Phys. **41**, 399 (2003)

CIRRICULUM VITAE

PERSONEL INFORMATION

Surname, Name: Şen Sema

Nationality: Turkish (TC)

Date and Place of Birth: 1 August 1976, Çanakkale

Marital Status: Married

Phone: 0(312)8154300

email: sema.sen@taek.gov.tr

EDUCATION

Degree	Institution	Year of Graduation
MS	METU Physics	2002
BS	METU Physics	2000
High School	Ezine Lisesi, Çanakkale	1993

WORK EXPERIENCE

Year	Place	Enrollment
2007- Present	Turkish Atomic Energy Agency (TAEK)	Physicist
2000-2007	METU Department of Physics	Research Assistant

PUBLICATIONS

1. H. Yurtseven, Y. Enginer, S. Şen and S. Salihoğlu, Journal of the Indian Chemical Society **84**, 350 (2007)
2. S. Şen and H. Yurtseven, J. Mol. Struc. **834-836**, 561 (2007)
3. H. Yurtseven, A. Yanık, S. Şen, Spectrochim Acta **A 71**, 105 (2008)
4. H. Yurtseven, S. Salihoğlu, S. Şen, Phys. Stat. Sol. B, **244**, 2589 (2007)
5. H. Yurtseven and S. Şen, Jpn. J. Appl. Phys., **47**, 2217 (2008)
6. H. Yurtseven, S. Salihoğlu, Y. Enginer and S. Şen, Il Nuovo Cimento B, **123**, 533 (2008)

7. S. Şen and H. Yurtseven, J. Mol. Liq., **145**, 48 (2009)
8. H. Yurtseven and S. Şen "Calculation of the T-X Phase Diagram of Binary Mixtures of Cholestanyl Myristate (CnM)-Cholesteryl Myristate (CrM) and Cholestanyl Myristate (CnM)-Cholesteryl Oleate (CO)", Annals of NYAS (in print) 2009
9. S. Şen and H. Yurtseven "T-P Phase Diagram of Benzene", J. Optoelectronics and Adv. Mater. (in print) 2008